E.T.S. de Ingeniería Industrial,
Informática y de Telecomunicación

CONTACT OPTIMIZATION ON CRYSTALLINE SILICON SOLAR CELLS

Degree in Industrial Engineering

Final Degree Project

Iranzu Oyarzábal Oquiñena

Director: Andoni Urtasun Erburu (UPNA)

Eugenia Zugasti Rosende (CENER)

Pamplona, 28/06/2017

Final Degree Project
Contact optimization on crystalline silicon solar cells

ABSTRACT

The present Final Degree Project has been developed in CENER (National Renewable Energy Centre), in particular in the Photovoltaic Solar Energy department.

Nowadays, photovoltaic technologies' main challenge is to increase solar cells' efficiency while reducing cost. In crystalline silicon, standard Al-BSF (Aluminium Back Surface Field) structure does not constitute an optimal architecture in terms of efficiency. In order to achieve higher conversion efficiency, PERC (Passivated Emitter and Rear Contact) architecture has been developed and started to be used in the industry. It is expected to reach in the following years values of efficiency of up to 23.5 %, never attainable with the standard Al-BSF structure, with which the highest efficiency reached is around 20 %.

During the Project, firstly solar cells are processed according to Al-BSF structure and characterized to fix a baseline process. Once this finished, the main focus is to process solar cells with the new PERC architecture. Different experiments varying rear solar cell contact - in particular laser parameters to perform localized contacts and their design - are carried out and characterized in order to find the optimal parameters of this process.

KEYWORDS: Photovoltaic energy, solar cell, metallic contact, Al-BSF structure, PERC, efficiency, recombination.

GENERAL INDEX

FIGURE INDEX

TABLE INDEX

1.- PROJECT SCOPE AND OBJECTIVE

The present Final Degree Project belongs to the area of knowledge involving the development of production processes for solar cells. In particular, it is focused on improving their efficiency. The main objective is to modify the rear side electrodes of the solar cell aiming to achieve a more efficient crystalline silicon solar cell with a modified architecture.

Firstly, solar cells will be processed according to Al-BSF structure, which is the standard way used nowadays in the industry to fix a baseline process. To form the contacts, screen-printing technique will be performed using aluminum (Al) for the back contact and silver (Ag) for the front contact. The final performance of these cells will be characterized through IV curve, electroluminescence and thermography. Furthermore, the morphology and formation of the contacts will be studied in depth by using optical microscopy and scanning electron microscope (SEM) techniques.

Once this finished, solar cells will be processed according to PERC (Passivated Emitter and Rear Contact) structure, an improved architecture able to collect broader light spectral range and in a more efficient way. First of all, a state of the art study of PERC solar cells will be performed based on scientific publications, to know critical parameters of the layers involved. Then, new screens will be designed to form front and back contacts in PERC structure. These screens should be able to work with new screen-printing pastes that have been purchased to manufacture the PERC structure. Once this step finished, printing process parameters will be optimize to process PERC solar cells. Finally, experiments' results will be evaluated using the same characterization tools as with standard solar cells, and both results will be compared.

2.- CONCEPTUAL FRAMEWORK OF PHOTOVOLTAIC SOLAR ENERGY

Solar photovoltaic energy uses light to generate electricity thanks to the electronic characteristics of the used materials (semiconductors). It is based on the transformation of the solar radiation into direct current – by the Photovoltaic Effect – in a clean and quiet way, when the sun's photons enter the semiconductor materials of the solar cells.

PHOTOVOLTAIC TECHNOLOGIES

The photovoltaic solar energy is one the most growing industries in the world, principally due to the need of evolving to a cleaner and more sustainable energetic system. During the last years, new developments have been carried out regarding device design, material involved and production technologies, as well as new concepts to enhance the global efficiency of the cell.

A wide range of photovoltaic cell technologies are available in the marketplace categorized depending on the raw material used and their commercial maturity [1].

- **First generation**. Systems that use crystalline silicon (c-Si) both in its monocrystalline and multicrystalline forms. Silicon based solar cells count for more than 93% of the worldwide production in 2015 (Figure 1). Its success is due to its abundancy, its stability and non-toxicity. This technology is mature and in mass production.
- **Second generation**. Systems that are based on thin film technologies, including amorphous silicon (*a*-Si), cadmium telluride (CdTe) and copper indium selenide (CIS). Thin-film solar cells require much less semiconductor material, less than 3 µm compared to around 180 µm of c-Si technologies, to absorb sunlight. Its main challenge is to increase the market share by increasing yield at its competitive cost.
- **Third generation**. Systems that include emerging photovoltaic technologies: organics, perovskites... This type of semiconductors is considered to be the least expensive way of electricity generation by PV means, but there are still some issues that must be solved regarding stability and durability. These technologies are still under development.

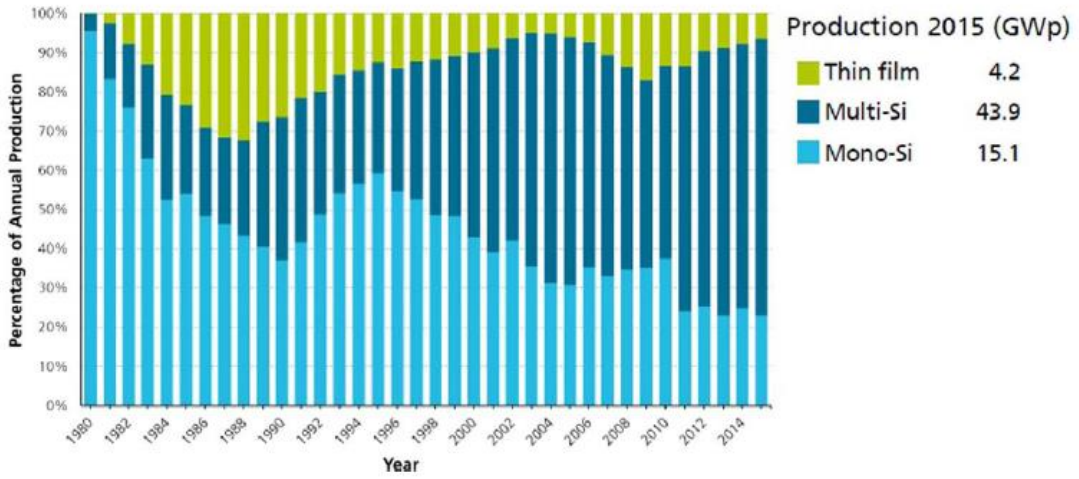

Figure 1. Annual production distribution by technology [1]

The efficiency values reached by each technology are different, being the maximum for III-V multi-junction high concentration solar cells. This technology has experienced the highest increase in efficiency during the last 15 years, as shown in Figure 2. These solar cells reach efficiencies of 46% in laboratory in high light or sunlight concentration. With respect to crystalline silicon technology, the highest efficiencies are reached by Kaneka heterojunction solar cells, with values up to 26.6 % under one-sun illumination.

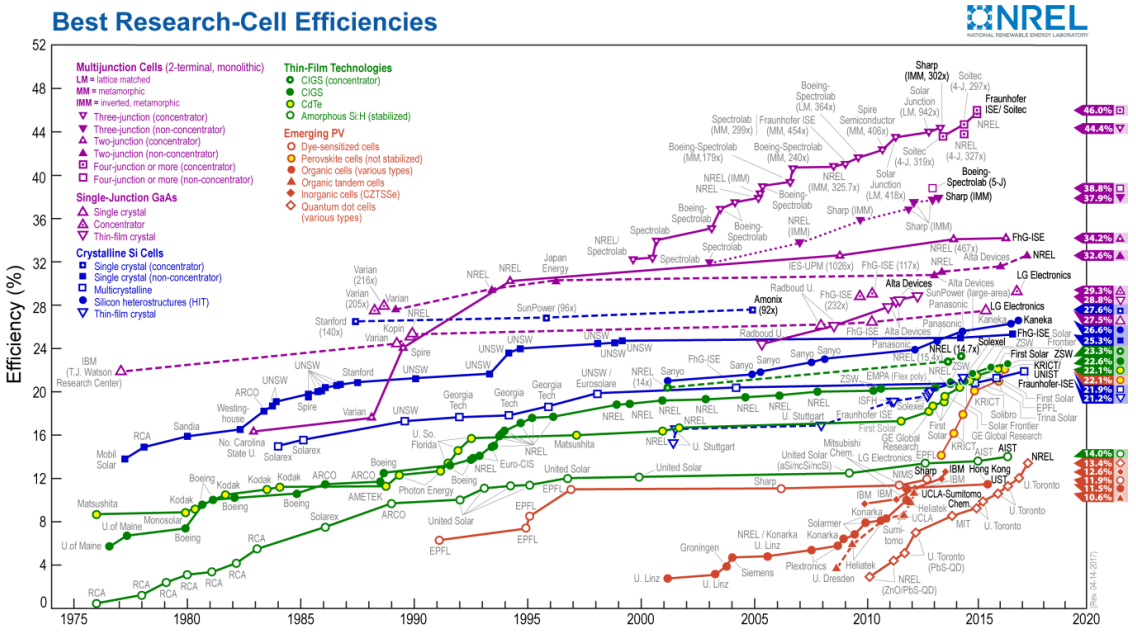

Figure 2. Best Research-Cell Efficiencies of solar cell technologies [2]

ELEMENTS OF A PHOTOVOLTAIC SYSTEM

The cells, independently of the technology used for their manufacturing, are interconnected in series and parallel to form a module. Apart from it, an inverter, a battery and a charge controller (not always) are needed (**Figure 3**). The inverter is responsible for converting the direct current generated (DC) into alternating current (AC). The charge controller has the function of preserving the battery from being charged or discharged completely.

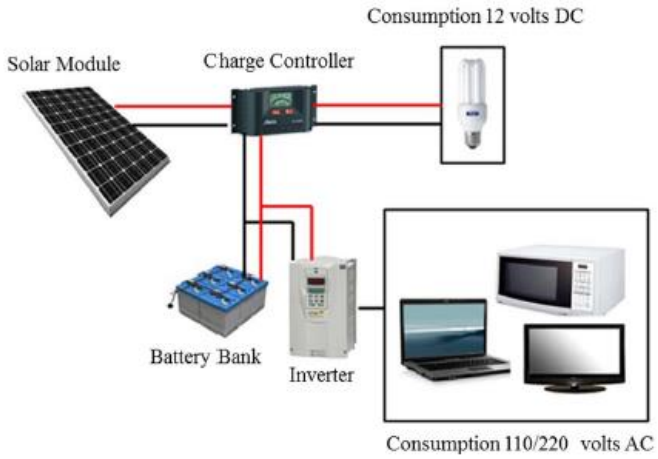

Figure 3. Schematic of a typical photovoltaic system [1]

3.- CRYSTALLINE SILICON SOLAR CELL TECHNOLOGY

3.1.- BASICS OF SOLAR CELLS

Solar cells, which are the principal energy conversion device, are made of semiconductor materials. Semiconductors are materials in which the range of excitation energies is interrupted by an energy gap of width E_G (**Figure 4**). The energy range below the gap, called the valence band, is nearly completely occupied with electrons. The energy range above the gap, called the conduction band is, however, nearly empty. Semiconductors absorb photons having at least the energy E_G. Photons with smaller energies cannot excite electrons from the valence band to the conduction band, and they are not absorbed. They are transmitted, reflected or absorbed by phonons, impurities or free charge carriers. For this reason, only a specific range of the solar spectrum is absorbed depending on the band gap of the semiconductor [3].

The basic classification used to define the different semiconductor types are the following:

- **Intrinsic material.**

It is a material to which impurities have not been added, has a certain level of carrier concentration at a given temperature. Carrier concentration is the number of electrons in the conduction band or the number of holes in the valence band, since both are present in the same quantity (Figure 4). Intrinsic carrier concentration increases exponentially with temperature.

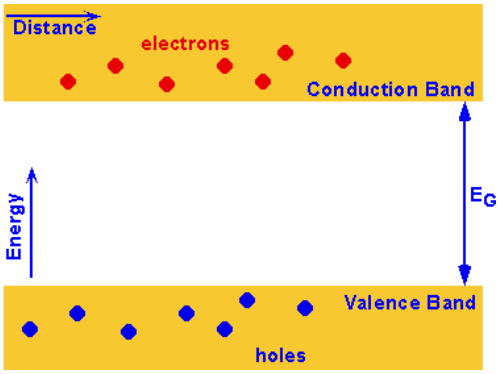

Figure 4. Intrinsic carrier concentration in a semiconductor [4]

- **Extrinsic material.**

An intrinsic structure can be changed to shift the balance between electrons and holes. This new situation can be observed in Figure 5. This shifting in the carrier balance is done by adding impurities and the effect is called doping. By applying it, two types of semiconductors are obtained:

- P-type semiconductor. Holes constitute the majority carriers and electrons the minority ones.

- N-type semiconductor. In this case, electrons are the majority carriers of the material, being holes the minority ones.

Once the doping takes place, the new carrier concentration can be calculated. The equilibrium carrier concentration for majority carriers is equal to the intrinsic carrier concentration plus the number of free carriers added by the dopant.

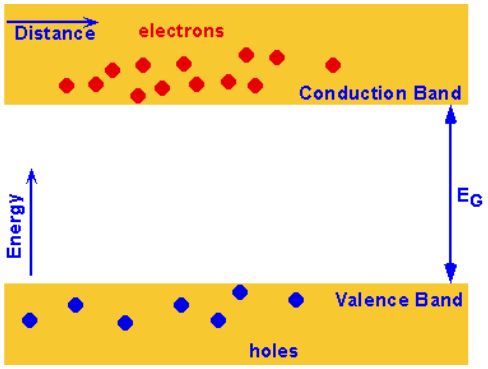

Figure 5. Equilibrium carrier concentration for n-type material and low doping [4]

Among semiconductor materials described before, silicon is the most widely used type for the manufacturing of solar cells. Silicon is an element from group IV of the periodic table [4]. Silicon crystals are composed of atoms bonded together in a regular structure, as can be observed in Figure 6. It has 4 electrons in the valence band that can be promoted to the conduction band when reaching the necessary energy level.

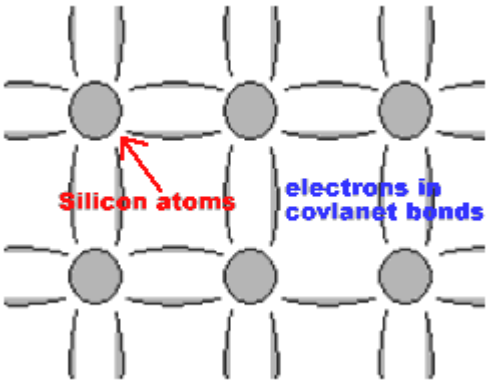

Figure 6. Representation of the silicon crystal lattice with its covalent bonds [4]

3.2.- OPERATION PRINCIPLE: THE PHOTOVOLTAIC EFFECT

As mentioned before, the electricity generation in a solar cell is based on the Photovoltaic Effect.

The generation of current in a solar cell starts with the absorption of the incident photons by the semiconductor to promote the valence electrons to the conduction band. The promotion of an electron to the conduction band leaves an empty space, which can be occupied by an electron from a neighboring atom. This phenomenon can be seen as the movement of an empty space (“positively charged particle”), called “hole”, from one place to

another. Both, electrons and holes are called “carriers” and participate in conduction in PV devices.

In the absence of an external circuit, the free generated carriers recombine and no current or power is generated. To prevent this recombination is what the p-n junction is used for. A silicon wafer doped with phosphorus and boron creates an n-type and p-type semiconductor, respectively. This union of two semiconductors with complementary doping is called p-n junction. Electrons move—on their way towards the electron contact—through regions with a large electron conductivity, while the current of the holes in that direction is suppressed by a very small hole conductivity. The opposite happens for holes and electrons on the way towards the hole contact. For the p-n junction, different conductivities are achieved by doping. This leads to an electric potential difference, the so-called “built-in voltage”, between the contacts. The difference in conductivities of electrons and holes on the way to “their” contact is the decisive condition for selective transport [5].

However, not all the electrons are extracted generating current. Some of the free electrons recombine with free holes, reducing the conversion efficiency of the solar cell.

A graphical representation of the energy generation process is captured in **Figure 7** [1].

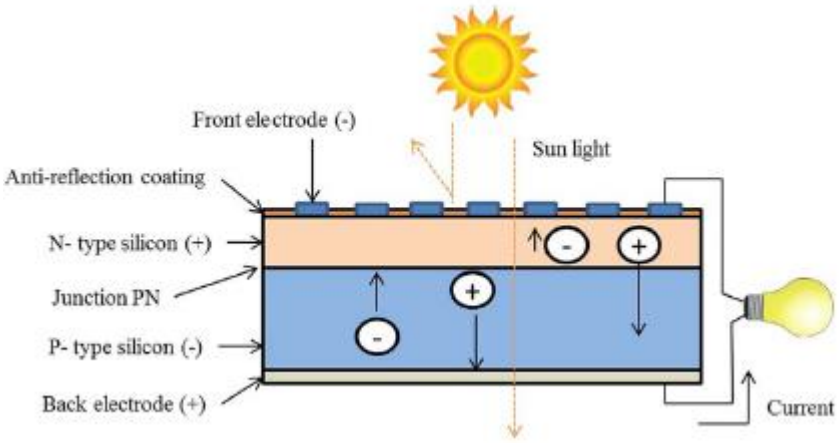

Figure 7. Representation of the process of electricity generation [1]

3.3.- ELECTRICAL PARAMETERS

The electrical parameters that characterize a solar cell (**Figure 8**) are the following:

➔ **Short-circuit current (Isc)**.

It is the current that flows through the solar cell when the applied voltage is zero. It is a magnitude that depends on the active area of the cell, its optical properties and the spectrum of the incident light among others.

➔ **Open-circuit voltage (Voc)**.

It is the voltage of a solar cell when there is zero current flow. That is, the maximum voltage available from the cell. It is due to the polarization of the junction because of the current generated by radiation. The final value depends strongly on the cell recombination, as well as on the operating temperature.

➔ **Maximum power point (Pmp)**.

It is the operation point in which the power generated reaches the highest value (P_{max}). The maximum power voltage and current correspond to this operation point. Therefore, the following relationship is hold:

$$P_{max} = V_{mp} I_{mp}$$

➔ **Fill factor (FF)**.

It is the parameter that, in conjuction with V_{oc} and I_{sc}, determines the maximum power from a solar cell. Theoretically, the maximum value is obtained by differentiating the product of current and voltage with respect to voltage, and making it equal to zero. Graphically, the fill factor is the area of the largest rectangle than can fit in the IV curve**.** It is an indicator of the quality of the solar cell.

The fill factor is obtained with the following formula:

$$FF = \frac{V_{mp}\, I_{mp}}{V_{oc}\, I_{sc}}$$

➔ **Efficiency (η).**

It is determined as the fraction of incident power which is converted to electricity. It depends on the spectrum and intensity of the incident sunlight and the temperature of the cell.

As $P_{max} = V_{oc}\, I_{sc}\, FF$,

$$\eta = \frac{V_{oc}\, I_{sc}\, FF}{P_{in}}$$

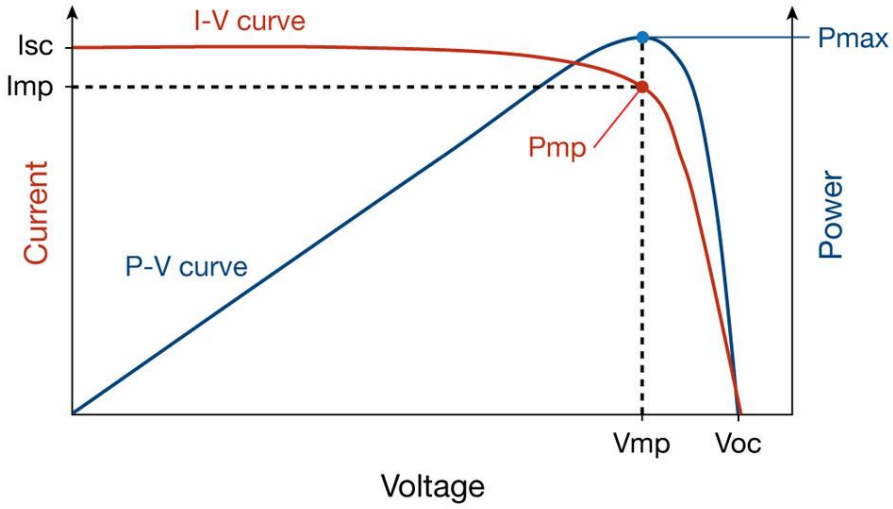

Figure 8. Electrical parameters of a solar cell [3]

3.4.- LIMITATION OF SOLAR CELL PERFORMANCE

3.4.1.- Recombination losses

Recombination is the process in which electrons and hole are annihilated. From the energy set free in this reaction, photons or phonons are produced. There are two main types of recombination losses depending on the region of the cell in which they occur: at the surface or in the bulk.

Bulk recombination

There are three types of recombination taking place in the bulk.

- Radiative recombination. In this process, a hole reacts with an electron and produces a photon.
- Recombination through defect levels. Defect levels with energies in the forbidden zone of the band gap capture electrons and holes over a series of excited states with successive dissipation of energy.
- Auger recombination. The energy set free during this recombination is transferred to an electron of a hole as kinetic energy that is subsequently lost to the lattice through collisions with phonons.

Surface recombination

This type of recombination is caused by defects at the semiconductor surface or impurities within the surface interfaces. This region constitutes a severe disruption of the crystal lattice, causing dangling bonds. The surface recombination velocity is defined as the rate at which carriers move towards the surface, and it is used to specify the recombination at a surface. The reduction of this type of recombination is achieved by depositing a passivation layer on top of the semiconductor and/or limiting the concentration of one type of carriers, electrons or holes, to avoid recombination.

Recombination affects both the short-circuit current and the open-circuit voltage.

3.4.2.- Optical losses

This type of losses are mainly due to light that could have generated an electron-hole pair but it does not, it could be because light is reflected from the front surface or because it is not absorbed by the solar cell.

In order to reduce this type of losses, several improvements can be done:

- Top contact coverage minimization.
- Anti-reflection coating deposition on the top surface. (*See 4.1.4.- Silicon nitride deposition*.)
- Surface texturing to reduce reflection. (See
- *4.1.1.- Cleaning of organic particles, saw damage removal and* texturing**.**)
- Thicker solar cell to increase absorption.
- Increase of the optical path length in the solar cell.

Optical losses affect the power from a solar cell by lowering the short-circuit current.

3.4.3.- Series resistance losses

Series resistance, in conjunction with shunt resistance, dissipates power of the cell reducing its efficiency. The principal impact is the reduction of the fill factor. The causes of this effect are the following, which are graphically represented in **Figure 9**.

- The movement of current through the emitter and base of the solar cell.
- The contact resistance between the metal contact and the silicon.
- The resistance of the top and rear metallic contacts.

Therefore, it can be extracted that series resistance is principally caused by the use of non-optimally-out contact design or problems during contact formation.

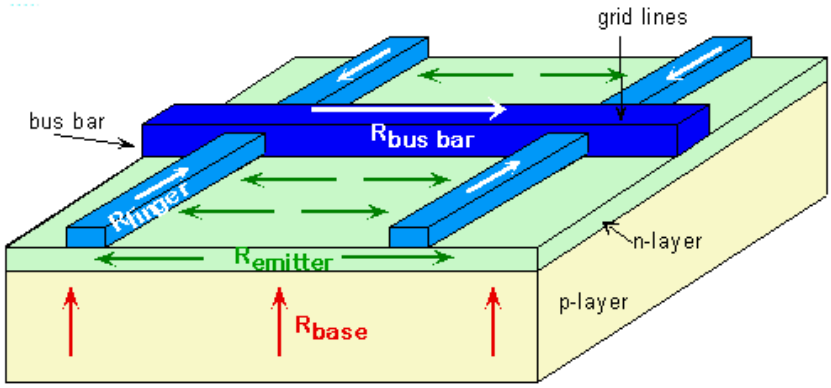

Figure 9. Graphical representation of the terms of series resistance [4]

3.4.4.- Shunt resistance losses

Shunt resistance causes power losses in solar cells by providing an alternative current path for the light-generated current. The effect is particularly visible at low light levels, where there is less light-generated current. These types of losses are typically caused by manufacturing defects on the solar cell.

3.5.- HIGH EFFICIENCY SOLAR CELL ARCHITECTURES: PERC

Nowadays, photovoltaic technologies main challenge is to increase solar cells' efficiency while reducing cost. With respect to silicon-based solar cells, the standard Al-BSF structure does not constitute an optimal structure in terms of efficiency. Solar cells featuring a full area aluminum back-surface field (Al-BSF) on the rear surface experiment a high rear-surface recombination velocity and low internal reflectance [7]. Due to these two loss mechanisms the maximum efficiency of today's industrial silicon solar cells with full area Al-BSF has been stuck to around 20 % in the last few years.

In order to overcome these problems and to achieve higher conversion efficiency, a better quality of the rear-surface passivation and reflectance is needed. An alternative to the standard Al-BSF structure is the PERC (Passivated Emitter and Rear Contact) structure, which is expected to reach in the following years values of efficiency of up to 23.5 %, never attainable with the standard Al-BSF structure, as can be observed in **Figure 10** [8].

In a PERC solar cell, the full area aluminum layer is substituted by a passivation layer with local openings where there is contact between the Al layer and the rear silicon surface (Figure 11), minimizing the recombination of free carriers at the rear surface and increasing, at the same time, the internal rear reflectivity, and hence enhancing efficiency.

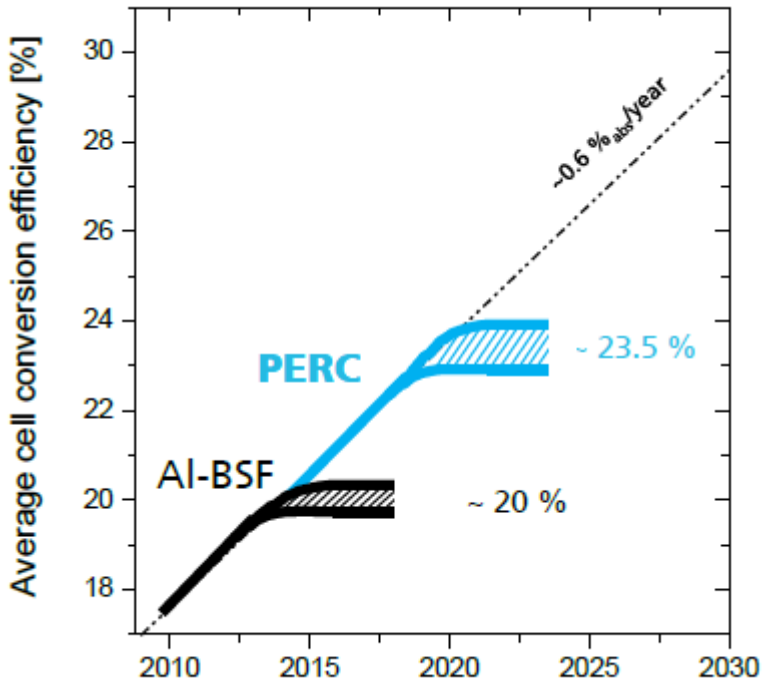

Figure 10. Expectations of efficiency by silicon structure in the following years [8]

The continuous increase in efficiency of this type of cells is possible by both, improving the lifetime of the minority carriers to a higher value than 1 ms and tending to the design of smaller fingers.

In PERC solar cells processing, two process steps are added. On the one hand, a passivation layer is deposited on the rear surface. On the other hand, for the fabrication of the metal contacts, local areas of the passivation layer are removed before the metallization of the aluminum electrode. This removal is typically accomplished by laser ablation.

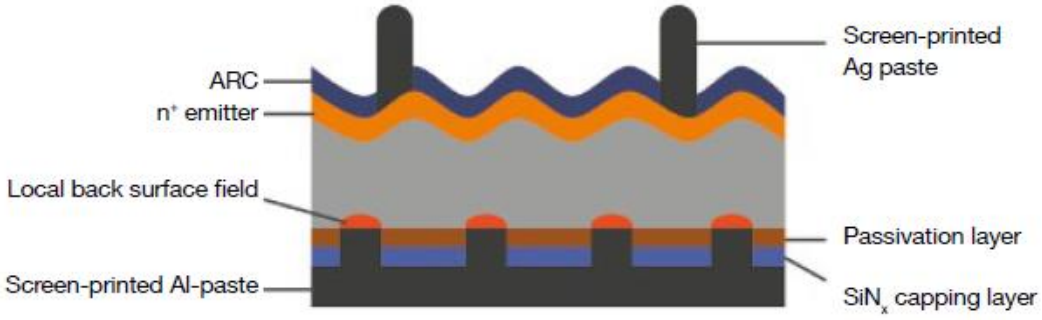

Figure 11. Schematic of PERC solar cell [9]

Passivation layer parameters

For p-type solar cells, rear surface recombination is minimized by means of a silicon oxide layer [10] or an aluminum oxide layer [9] grown over the silicon surface. Then, normally, silicon nitride is deposited onto it as capping layer.

The silicon nitride layer improves the optical reflectivity of the rear surface. Its typical thickness is in the range up to 100 nm for a 180 µm wafer thickness [11, 12, 13].The silicon oxide layer thickness is in the range of 10 nm, also for a 180 µm wafer thickness [13].

Laser ablation parameters

In order to create selective openings on the rear dielectric layers, laser is the most popular technique. To form the contact, an aluminum layer is printed and a high temperature process is performed after laser ablation. Then, local Al-BSF contacts are produced only on the openings of the rear dielectric layers formed by the laser.

As it is described in [7], the contact shape and the thickness of Al-BSF layer were found to be heavily dependent on the laser ablation pattern and contact area.

With respect to the contact area, it is necessary to look for a compromise between series resistance and surface recombination. The more number of laser points and hence, the bigger the contact surface, the less the series resistance but the greater the surface recombination.

According to R. Hendel [14], dots or lines can be used for the dielectric ablation. The typical total area to be laser opened falls in the range of 3-5 %. In case of line openings, the typical line spacing requirement is between 0.5 and 2 mm. However, in case of dot opening, the spacing range is a bit smaller, between 0.2 and 1 mm.

M. Gebhardt [12] states that separation distance between individual dots on the rear surface of the cell are between 0.4 and 1 mm. Line separation distance should fall in the range from 0.7 to 1.5 mm.

Depending on the distance selected and the diameter of the laser beam, the contact area can be computed.

With respect to the laser ablation pattern, as mentioned before, the process can be performed with lines or dots pattern. If choosing dots, different geometries can be found depending on the disposition of the dots. There are three possible contact lattices disposed in regular patterns: triangular, square and hexagonal.

4.- METHODOLOGY APPLIED DURING THE PROJECT

4.1.- SOLAR CELL FABRICATION PROCESS

As the project belongs to the area of knowledge involving the development of production processes of solar cells, the explanation of the fabrication process steps applied becomes crucial.

In the first place, solar cells are processed according to Al-BSF structure, which is represented in Figure 12.

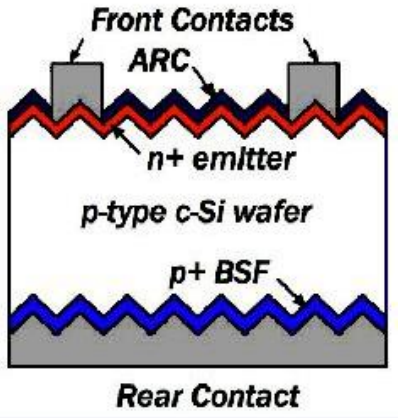

Figure 12. Representation of the main layers of a processed p-type crystalline Al-BSF standard silicon solar cell

The fabrication sequence for screen-printed p-type crystalline silicon solar cells with Al-BSF structure consists of several steps depicted sequentially in Figure 13 [15].

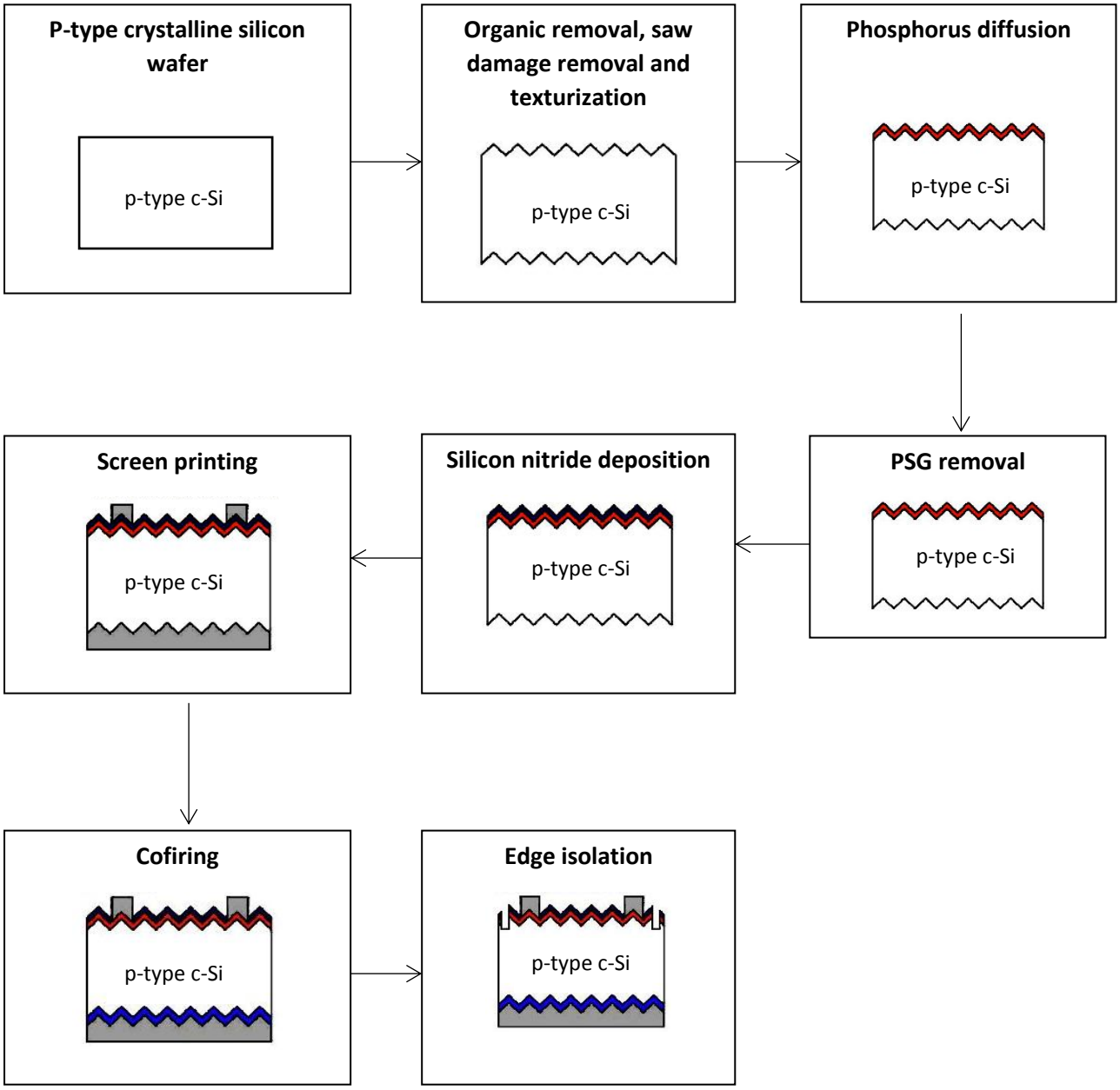

Figure 13. Process sequence of fabrication of solar cells

4.1.1.- Cleaning of organic particles, saw damage removal and texturing.

When cutting silicon ingots into wafers by wire sawing, small cracks are formed on the surface of the wafer. These cracks penetrate around 10 µm deep into the surface, reducing the mechanical strength of the wafer and increasing recombination in the surface. Hence, this

damage needs to be removed from the wafer. However, before this step, organic contaminants need to be removed from the wafer surface. Otherwise, they would cause an increase of surface and bulk recombination when being subjected to high-temperature in the following process steps.

Then, in order to remove saw damage, there are 3 processes that can be used: Alkaline etching, acidic texturing and plasma etching.

Each of the processes previously stated forms a different surface texture, but all of them help to reduce the total light reflection of the wafer.

- Alkaline etching.

  It is an anisotropic process and therefore has different etch rates for different crystallographic orientations. This makes the method more suitable for monocrystalline silicon wafers. Pyramids with a square base are formed randomly distributed over the surface, as can be observed in **Figure 14**. To improve uniformity, isopropyl alcohol (IPA) is added to the solution.

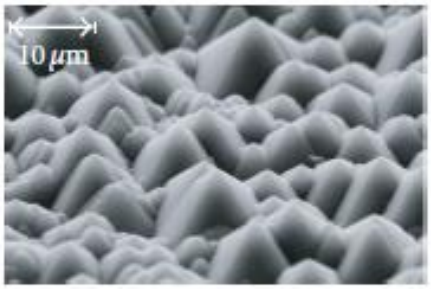

Figure 14. SEM image of the alkaline-textured surfaces [15]

- Acidic texturing

  The treatment is not dependent on the crystallographic orientation since it is an isotropic process. This makes it suitable for multicrystalline silicon (**Figure 15**).

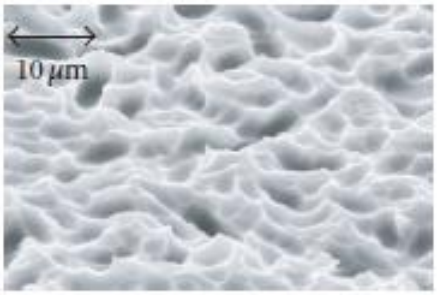

Figure 15. SEM image of the top view of an acidic-textured silicon wafer [15]

To clean the wafers after texturization, they are cleaned in subsequent cycles of ozone (O_3), hydrochloric acid (HCl), and hydrofluoric acid (HF) and finally dried in nitrogen. Deionized water is used for rinsing after each chemical step. O_3 is also used to oxidize the silicon surface. HCl is useful to remove alkal and metal impurities from the surface, while HF etches the silicon dioxide off and forms a hydrophobic surface.

4.1.2.- Diffusion

The thermal diffusion of phosphorus leads to the creation of an emitter to the wafer, for p-n junction formation.

The equipment used for this process is called $POCl_3$ tube furnace (**Figure 16**).

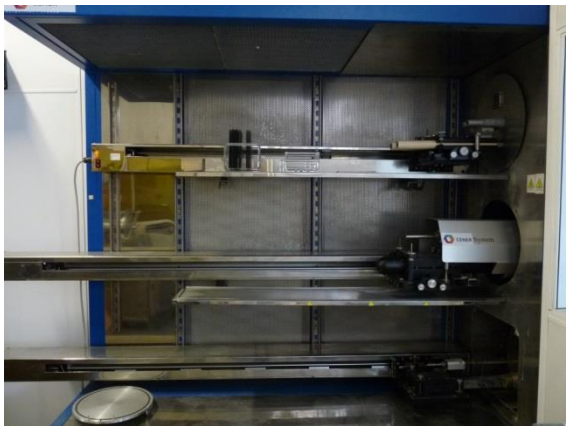

Figure 16. Tube furnace [CENER]

To start the process of phosphorous diffusion, the wafers are put into the tube furnace and heated up to around 800 °C in an O_2 ambient. Nitrogen is used as a carrier gas through a bubbler filled with liquid phosphorus oxide ($POCl_3$) which is the source of phosphorus. From that reaction, P_2O_5 deposits onto the wafer surfaces in a thin layer during pre-deposition step. This layer is called a phosphor-silicate glass (PSG) and it is compounded by SiO_2 and P_2O_5.

Then, a drive-in process step diffuses phosphorus into the p-type silicon wafer due to the high temperature, forming the needed p-n junction.

The dopant surface concentration therefore decreases with time, since the dopant moves into the semiconductor as time increases. Curve a) from **Figure 17** represents the case of low surface concentration, while curve d) corresponds to a high concentration case [16].

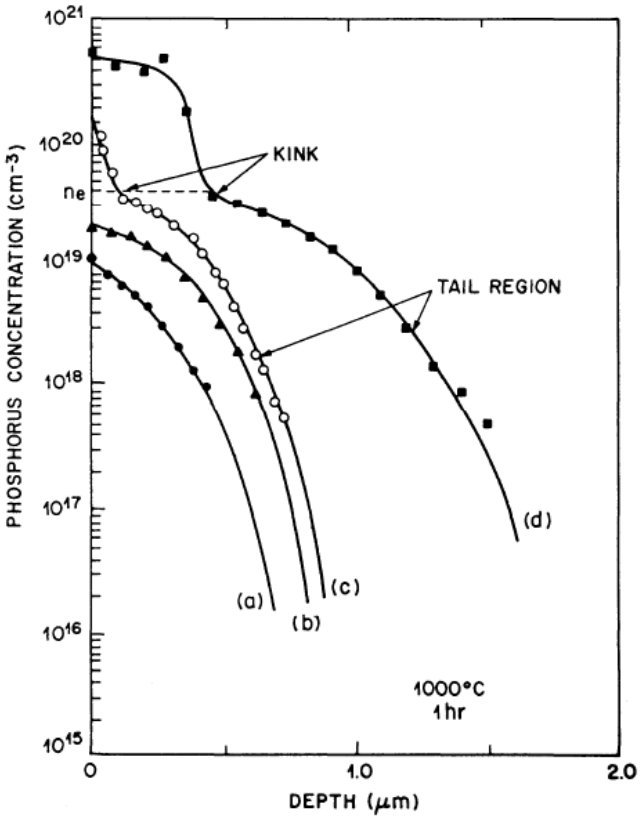

Figure 17. Dopant profile of a phosphorus diffusion for various surface concentrations after diffusion into silicon for 1 hour at 1000 °C [16]

4.1.3.- Phosphorus silicate glass (PSG) removal

Hydrofluoric acid (HF) is used to etch off phosphorus silicate glass on the wafer surface.

4.1.4.- Silicon nitride deposition

In this process step, a layer of silicon nitride is deposited onto the front side of the solar cell. The layer has two main functions: on the one hand, it is used as an antireflection coating, and on the other hand, it serves as a good surface passivation to reduce recombination losses of the surface.

The objective is that the wave reflected from the anti-reflection coating top surface is out of phase with the wave reflected from the semiconductor surfaces. The destructive interference results in zero net reflected energy. The thickness of the coating is chosen so that

the wavelength in the dielectric material is one quarter the wavelength of the incoming wave, and it is obtained by applying the following formula:

$$d = \frac{\lambda}{4\,n}$$

where,

d = coating thickness

λ = free-space wavelength

n = refractive index

For silicon nitride with a refractive index of approximately 2 and in order to minimize optical reflection at 600 nm - where the absorption of silicon is maximum - the silicon nitride film should have a thickness of around 75 nm [4].

There are several ways of depositing this layer. However, the most widely used system is the plasma-enhanced chemical vapor deposition (PEVCD). The machine used for the deposition is shown in **Figure 18**. During this process, the SiNx:H film is formed in a reaction of silane (SiH_4) and ammonia (NH_3). The conditions of temperature and pressure are in the ranges of 200-450 °C and 0.01-0.1 mbar, respectively.

Figure 18. PECVD equipment for silicon nitride deposition [CENER]

4.1.5.- Screen printing of the contacts

In order to extract the electrons from a solar cell, it is necessary to deposit metallic contacts on the front and rear surfaces. As metals are opaque to light, to maximize optical power the front metallized area should cover the smallest area of the surface cell and extract

the maximum number of electrons. However, contacts cannot be too small in order to avoid electrical power losses. A compromise should be found. On the rear side, the shadowing problem is not critical since light is not incident directly on this surface.

The front usual configuration is composed by a few big contacts, called *busbars*, between 2 and 5 depending on the cell surface, and a higher number of thin contacts, called *fingers*, on a direction perpendicular to busbars (Figure 19).

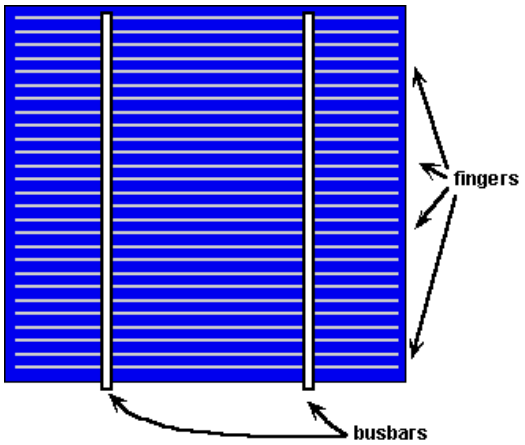

Figure 19. Schematic of a standard design of front contacts.

The equipment used to fulfill the screen-printing process step (Figure 20) consists mainly on screens and pastes as well as a screen printing machine. The screen used is mounted with a certain tension into an aluminium frame and has areas that are blocked off with an emulsion, and opened areas where the paste can go through. The screen is positioned on the machine just above the front side of the wafer, existing a small and defined distance between both, which is called snap-off distance.

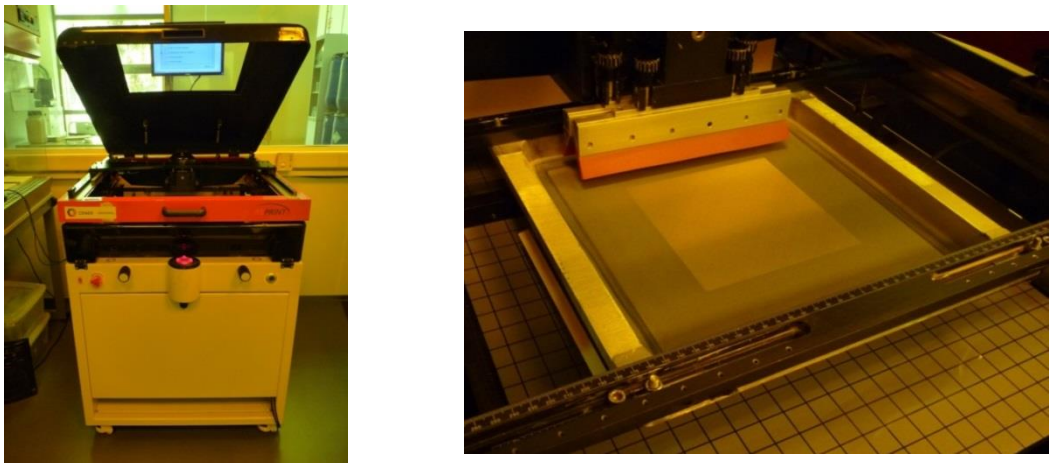

Figure 20. Picture of the screen-printing machine (left) and its inside with the screen and the squeegees used (right) [CENER]

Two squeegees, each of them located against the other, are responsible for the printing process. Depending on the direction of the printing, one or the other squeegee moves. The main steps of this process are illustrated in Figure 21.

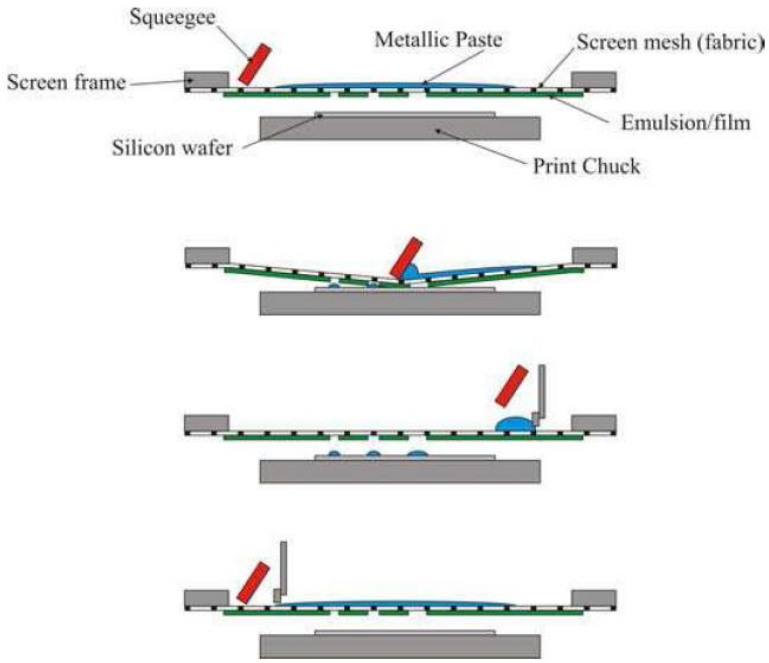

Figure 21. Main steps of the screen-printing cycle [17]

Front contacts

It consists on the deposition of the silver metallic paste on the front side of the wafer and above the silicon nitride layer. Buses and fingers are formed, whose width and distance between them depend on the design of the screen.

Silver paste is used as a conductive metal because of its good contact properties, conductivity and excellent solderability.

To start the process, one of the squeegees is moved without pressure over the screen. This way, the screen openings are uniformly filled with Ag paste, which is called flooding of the screen. Then, the squeegee is moved with a previously defined pressure, pressing the screen locally against the wafer surface and pushing the silver metallic paste through the opened areas of the screen onto the wafer surface.

After finishing this process of printing, the wafer is transported to a drying oven.

The main components of the front paste are the following [17]:

- Silver powder. Represents a 70-85% in weight. It is mixed with particles of different shapes, responsible for the paste conductivity and the cohesion of the contact.

The rest of the components are sensitive to the device surface that is wanted to be contacted as well as to temperature profiles and processing times.

- Powder of glass frits. Constitutes up to the 5% in weight of the paste. Glass frits are metal oxides. Their function is to melt the dielectric layers by forming eutectic alloys of lower melting point. These are deposited on the silicon nitride layer, allowing the metal particles to reach the silicon emitter.
- Organic compounds. To transport the suspended silver and glass particles. Inside this group we find organic solvents to allow the mixture be used as a paint, and organic binders to maintain the particles joined.
- Other additives to change the rheological properties of the mixture. They are found in proportions lower than 2 % in weight.

Rear busbars

It is an optional step that only takes place when series interconnection of cells is wanted to be done to form modules. This step is necessary since it is not possible to solder onto the screen-printed Al contact. To print these busbars, a silver and aluminium (Ag/Al) paste is used, so that they can be easily soldered to tabbing ribbons. According to the geometry, they need to be large to allow certain misalignments in the process, and small to reduce efficiency losses (there is no Al-BSF underneath the busbars).

After printing, the wafer is transported to a drying oven, in order to evaporate the solvents that screen-printing pastes contain.

Rear contact

In this step, the aluminum paste to form the rear contact is printed in the rear side of the wafer.

The pattern of the screen used for this printing has a different geometry from the one used for the front contact, it covers the whole back surface of the wafer.

Comparing this paste with the silver one, apart from the different metal particles, the rest of the components are of similar chemistry.

After printing, a drying process in an oven is needed as in the other screen-printing steps.

4.1.6.- Firing

Once the printing process is finished, both front and rear sides' contacts are fired simultaneously in a firing furnace, shown in **Figure 22**, which is called cofiring process. For that purpose, a RTP (Rapid Thermal Processing) equipment is used. Pastes are designed in order to follow a common thermal final treatment to create the contact at the same time in both sides of the cell.

It is important to dry each of the contacts after printing and before firing to avoid metallic contamination that would cause a shunting problem of the p-n junction.

During firing, the wafer is subjected to changes in temperature during a period of time (**Figure 23**). This results on chemical and structural changes inside the printing pastes and substrate surfaces.

Figure 22. RTP equipment [CENER]

At the beginning of the process, at the front side and at temperatures below 600 °C, the organic compounds that keep the dried metallic pastes attached to the surfaces are burned out. At the same time, the hydrogen contained in the silicon nitride layer is released into the bulk of the wafer to passivate electrical defects [17].

In the second step, the firing peak, higher temperatures are reached and the formation of the contacts takes place. Glass frits melt the silicon nitride and silver particles suffer a sintering process that creates a conductive film. Previously, during the chemical reaction liquid Pb etches the surface in some places, where then, during cooling, silver crystallites form the ohmic contact with the emitter. Then, a conductive contact is formed during the solidification of the silver and the glass frits mixture. This contact is a combination of a direct contact between the sintered silver and the silver crystallites, a tunneling contact through frits, and regions without electrical contact.

With respect to the rear side, aluminium paste follows the same burn out of organic components. During the firing step, the aluminium melts and can go through the oxide of the particles, reaching the silicon surface. In the next step, cooling down, silicon is rejected from the melt, and recrystallizes as the epitaxial Al-doped layer called Back Surface Field (BSF).

One problem of firing is the bowing. It is produced when temperature gets below 577 °C, because of the differences of thermal expansion coefficients between the Al contact and the silicon. It is created when the melted alloy solidifies with the eutectic composition. This bowing problem is larger when reducing silicon wafer thickness, so this limits the possible reduction of thickness of the cell.

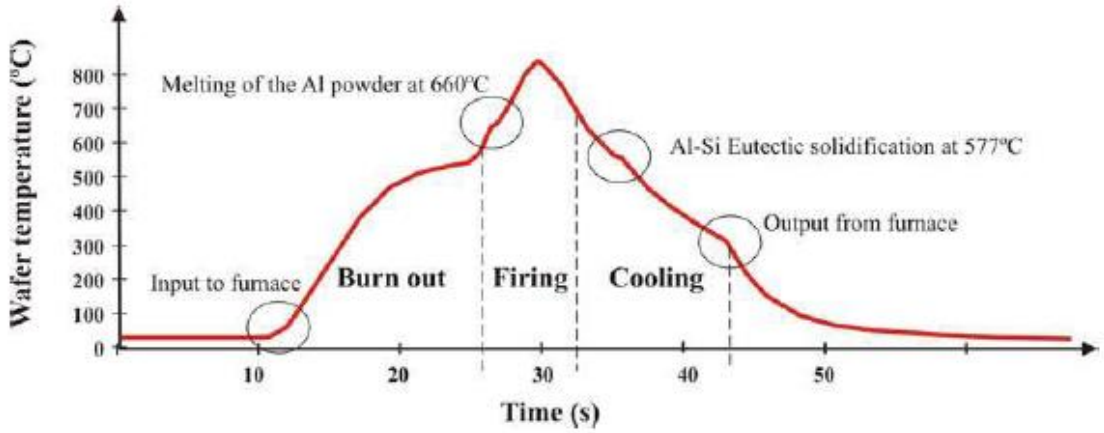

Figure 23. Temperature profile of the cofiring process in the furnace [17]

4.1.7.- Edge isolation

This step consists on the removal of doping around the edge of the solar cell. During emitter diffusion process, phosphorus diffused also takes place over the edges and rear side of the wafer. This creates shunt paths between the front (n-type) and back (p-type) surface [18]. The removal of the phosphorus diffusion around the edge isolates electrically the front emitter from the rear cell, as can be seen in **Figure 24** b). This way, shunt resistance is increased and the efficiency of the solar cell increases.

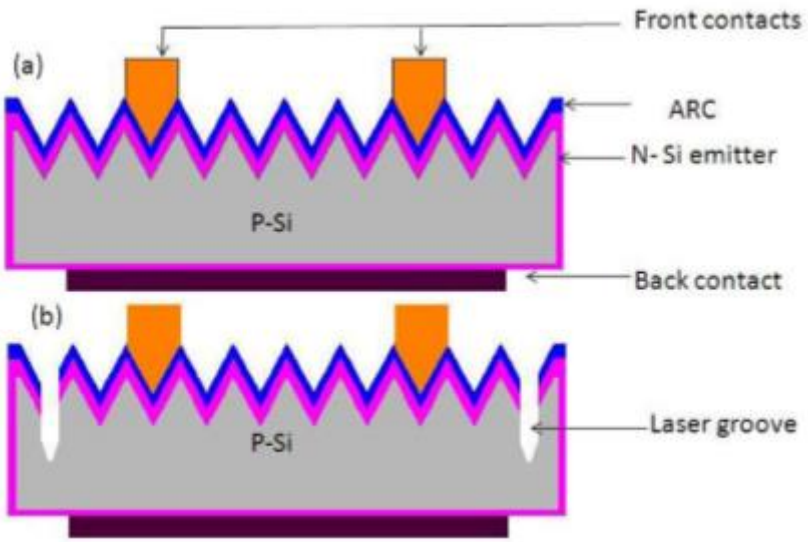

Figure 24. Comparison of (a) a cell with no edge isolation, where front and back side are linked, and (b) a cell with front edge isolation [18]

Laser edge isolation is one of the most used techniques because of the high speed and precision of its beam. According to S.R. Reddy [18], laser edge isolation processes shows an increase of average output power of solar cells by 3.45% compared to the plasma edge isolation process. The process can be performed by scribing a groove by laser (**Figure 25**) on either front or back side of the solar cell.

Figure 25. Picture of the laser equipment [CENER]

4.2.- SOLAR CELL CHARACTERIZATION

4.2.1.- IV Curve measurement

The IV curve represents the operation points of a solar cell, so any alteration on its operation is reflected on this curve.

It can be traced with natural radiation of the sun or by using a solar simulator. In any case, measurements should be corrected to Standard Test Conditions or STC (1000 W/m^2, 25°C and AM1.5G spectrum). By the measurement of the curve, all electrical parameters described in section *3.1.- BASICS OF SOLAR CELLS* are obtained.

The curve follows the shape shown in **Figure 8**. From that measurement, series and parallel resistance values can be approximately obtained.

A big value of series resistance can be due to bad metallic contact. It makes the slope of the curve around the open circuit voltage decrease, as can be observed in **Figure 26 (left)**, and it has also a big impact on the fill factor.

A reduction on the value of parallel resistance is linked to fabrication defects and therefore, indicates the presence of shunts in the solar cell. It causes an important reduction on the current generated, since it finds "alternative paths" to flow through. Its main effect on the curve is a decrease on its slope near the short circuit current point (**Figure 26 (right)**). As it occurs with the series resistance, it has a big influence on the fill factor.

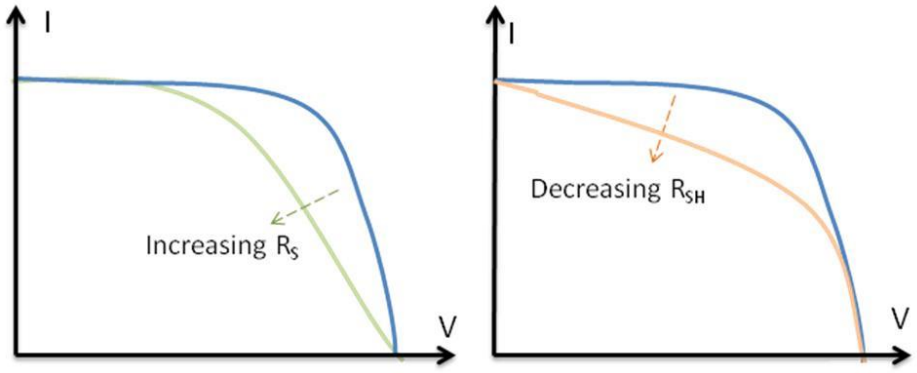

Figure 26. Effect of series and parallel resistance on the IV curve.

For the measurement of the curve, a solar simulator is used. This system uses calibrated light source and a temperature controller, since a solar cell is sensitive to both.

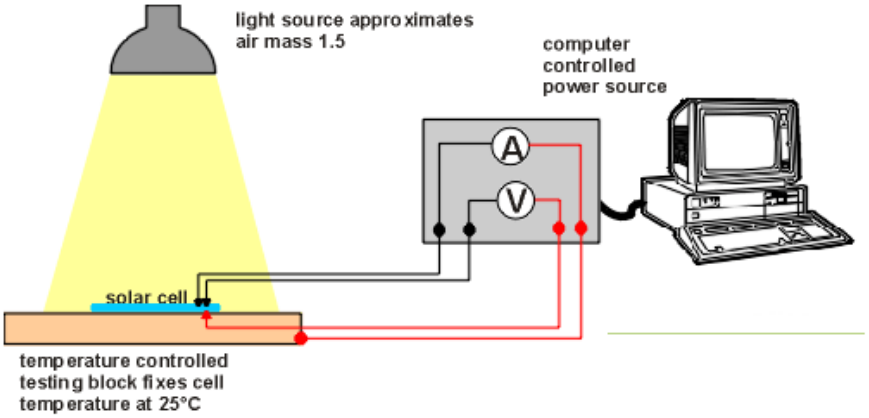

Figure 27. Configuration of the equipment for the measurement of the IV curve [4]

For routine measurements, a reference cell is used to calibrate the light source. A reference cell is a cell previously measured and certified, and should be electrically and optically as close as possible to the cell under test.

To control temperature, the cell test block is cooled to keep the temperature of the cell fixed to 25 ◦C, as shown in Figure 27.

During data acquisition, a load resistor is varied from zero to infinity. The variables that are directly obtained from this test are open-circuit voltage, short-circuit current density, and voltage and current density at maximum power point. From these ones, others as fill factor or efficiency previously mentioned can be obtained.

4.2.2.- Electroluminescence

It is a characterization technique based on the picture capturing of solar cells in order to study their quality. Solar cells transform electromagnetic radiation emitted by the sun into electric energy. This technique consists on reversing the process, making current flow through the cell so that it emits radiation. This radiation is captured by a remotely-controlled camera.

The emission range of silicon solar cells falls in the range of 1000-1200 nm, range in which Si-chip cameras have a lower response. Some filters limit the camera response to the emission range of solar cells. However, this range is relatively small so high capture times are used.

The method is based on the capture of two complementary images. The first one, called the high polarity one, is taken by flowing a value of current similar to the short-circuit one through the cell. For capturing the second one, the low polarity one, a value of current of a 10% of the applied previously is applied.

This technique allows detecting cracks and defects on the cell, as well as information of the quality of the material and series resistance values.

4.2.3.- Thermography

Thermography is a technique used for characterizing solar cells in an easy and non-destructive way. It is based on the identification of defects with a thermal camera that identifies the cell temperature differences. For characterization in laboratory, Lock-in thermography is used.

This technique consists in the application of a pulsed-current of fixed frequency and amplitude. Two images are captured during each current period: one during the cycle of highest current and the other during the cycle of lowest current. The resulting image is the difference of both of them.

This technique allows detecting hot spots caused by shunts of the cell.

4.2.4.- Lifetime carrier measurement

For measuring carrier lifetime, a μ-PCD system is used. A laser pulse of a certain wavelength is used for generation of the photo carriers. It is possible to make different measurements at various stages of the process and with a considerable precision [15]. By selecting a certain area of the cell, it is also possible to build a carrier lifetime map, showing different colors which are traduced into values through a color scale.

This technique allows evaluating the quality of the material and passivation properties of the passivation layers, as well as problems in the manufacturing that could degrade minority carrier lifetime of the solar cells.

4.2.5.- Optical microscopy

This type of microscope constitutes an easy way to perform optical inspection of the samples, when the size of what wants to be seen falls in the magnification range of the microscope. It has different values of magnification (5x, 10x, 20x…). In addition to this, there exists the possibility of performing measurements on the inspection's pictures to increase the quantity of information obtained.

This technique allows inspecting laser formation of the localized back openings as well as front contact morphology.

4.2.6.- Spectral response measurement

Spectral response refers to the ratio between the current generated by the solar cell and the power incident on it. It has the shape represented on the following graph.

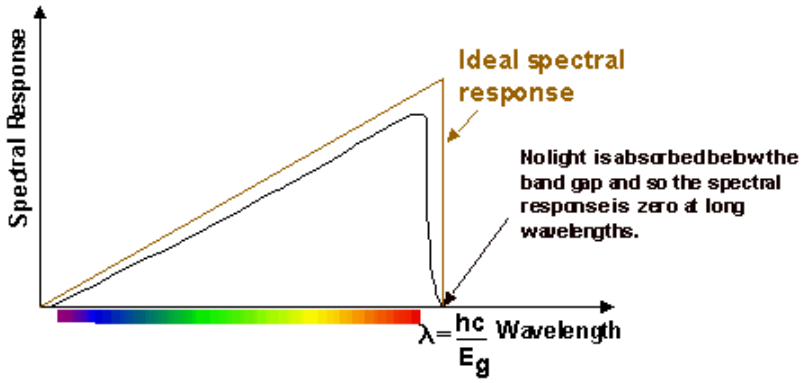

Figure 28. Shape of the spectral response of a solar cell, that is, for different wavelengths [4]

The response is limited at both long and short wavelengths, as shown in Figure 28. At long wavelengths the semiconductor has no capacity of absorbing photons with energies below the band gap. At small wavelengths, the spectral response decreases, since each photon has a large energy and the ratio of photons to power is reduced. Energies above the band gap are neither utilized, and go to heating the solar cell.

The spectral response of a solar cell is measured with the spectrophotometer.

4.2.7.- SEM (Scanning Electron Microscopy)

In this microscope (Figure 29), the signal generating system and the signal processing system are separated. There is no optical path between the specimen and the SEM image and therefore, provides indirect images. The image obtained is in fact synthetic of the interaction between electrons and the specimen surface.

Figure 29. SEM [CENER]

During the present project, it was used for examining the morphology of the rear contacts, both in case of the standard Al-BSF structure and for PERC structure.

5.- EXPERIMENTAL PROCEDURE, RESULTS AND DISCUSSION

5.1.- BASELINE: Al-BSF STANDARD SOLAR CELL

In a first step, solar cells were processed according to Al-BSF structure, which is the standard used nowadays in the industry, in order to fix a baseline. For getting that structure, p-type or n-type silicon substrates can be used. In this case, p-type silicon substrates were chosen to perform the first experiments.

In a first stage, two p-type monocrystalline substrates were taken; in particular the ones named *Only-25* and *Iris-08,* and processed into solar cells.

After this stage, the following objective was to manufacture 4 substrates with the same structure, but offering the possibility of joining different cells to build a module. However, the main purpose was not to evaluate the performance of the module, but the one of the individual solar cells. This way, they could be compared with the previously processed ones. The processed substrates were named *Only-12*, *Only-13*, *Only-26* and *Only-27*.

5.1.1.-Fabrication process and design

The whole fabrication process previously explained in section *4.1.- SOLAR CELL FABRICATION PROCESS* was performed to transform the substrates into solar cells.

For the two stages recently mentioned, after removing the saw damage, the wafers were subjected to alkaline texturization. Then, a cleaning step was applied, followed by the phosphorus diffusion process. P-type wafers have an excess of holes and therefore, need the addition of an n-type dopant. Hence, with the thermal diffusion of phosphorus, a thin n+ emitter, and so, the p-n junction, was created. In the next step of the fabrication process, a silicon nitride layer was deposited by PECVD above the n+ emitter, playing the role of antireflection coating and passivation coating, to increase the efficiency of the solar cell.

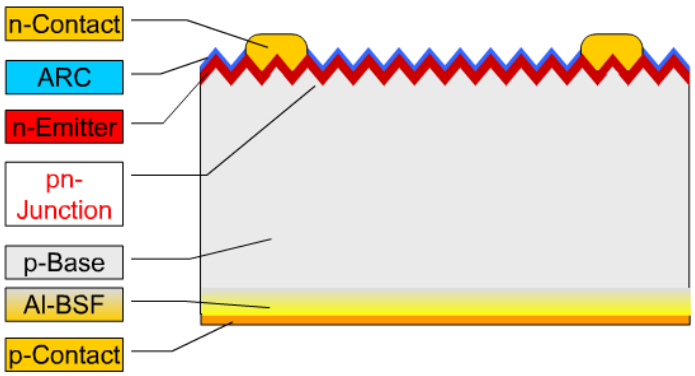

Figure 30. Structure of a Al-BSF standard p-type crystalline silicon solar cell [4]

The next step in the process was the screen-printing of the contacts, being this one the point in which we focus the most in the present project.

In general, for developing the metallization process, the equipment needed is mainly:

- A screen-printing machine.
- A screen. The screen used is particular of the type of metallization (front or rear), and it changes if we desire to have a different geometry such as thinner fingers or a higher number of buses.
- A metallization paste. The characteristics of the paste with respect to size of silver particles and so on, need to be compatible with the specifications of the screen used. Because of that, before the process, it is necessary to match a metallization paste with the screen suitable for it.

5.1.1.1.- Front contact formation

Front contacts need to be n-type (**Figure 30**). That is, negative pole electrodes that collect electrons. These contacts are metallized over the surface in which the sunlight is incident, and the surface they occupied becomes not productive. This occurs because the light can only be absorbed in the area where no contacts exist. Therefore, printed contact structure leads to shading losses. However, at the same time cross section area must be sufficient for minimizing resistance losses. It is important to optimize the geometry in order to find between both facts the equilibrium point in which we obtain the maximum efficiency of the solar cell.

Design of the front contact screen

In order to optimize the design of the front contact, the electrical power loss and the shading power loss must be taken into account. Basically, the electrical power loss is dependent of the series resistance and the shading power loss is dependent of the fraction of solar cell shadowed by the front contact.

The total series resistance of a solar cell is the sum of the contributions from the following components, which are graphically represented in **Figure 9**.

- Resistance due to the base (R_{base})
- Resistance due to the emitter ($R_{emitter}$)
- Resistance due to busbars (R_{busbar})
- Resistance due to fingers (R_{finger})
- Resistance due to contact of metal with the emitter (R_c)

Front metal coverage is responsible of the fraction of solar cell shadowed by the front contact. The aspects of the geometry of the front contact that may be varied are:

- The number of busbars of the contact grid. They are nowadays in the range from 2 to 5, although the most common ones have 3 busbars.
- The busbars' fired width.
- The amount of fingers and hence, the distance between them.
- The fingers' fired width.

Introducing the formulas to simulate these power losses in a MATLAB code, the best design for the front contact can be found:

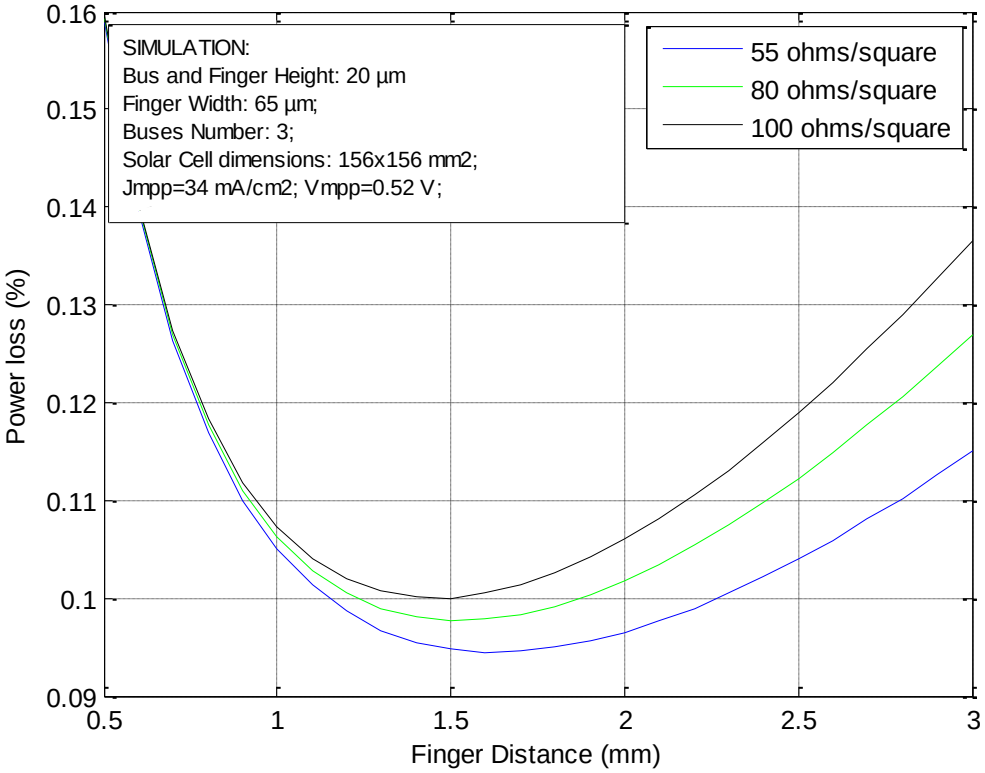

Figure 31. Simulation of the power loss as a function of finger distance at different emitter sheet resistances

As it can be seen in Figure 31, for a fixed finger width, 65 µm, defined mainly by the paste characteristics, and emitter sheet resistance, 80 Ω/□, the optimum finger spacing is found where the sum of electrical power loss and shading power loss is minimized. This finger spacing is approximately 1.5 mm.

In CENER, there was already a screen designed according to the specifications of the metallization silver paste, and with this optimized geometry of fingers and busbars. The matching between both screen and paste was verified by looking at the specifications of each of them.

As it can be seen in the appendix attached to the present project (*APPENDIX II. PV17F METALLIZATION PASTE. DATA SHEET*), the chosen metallization paste was Dupont PV17F. The screen types recommended to use with it are summarized in Table 1.

	(I)	(II)	(III)
Mesh (stainless steel)	290	325	400
Wire Diameter (µm)	20	23	18
Emulsion Thickness (µm)	20–25		
Mesh Angle (degrees)	22–30		

Table 1. Specifications of screen type for PV17F metallization paste

With respect to the screen, shown in Figure 32, the main characteristics are the following (Table 2):

Harvey Summer Ag	
Mesh (mesh/wire)	300-320
Wire diameter (um)	18
Emulsion thickness (um)	18
Angle (degree)	≈22.5

Table 2. Characteristics "Harvey Summer Ag" screen.

As it can be observed, the parameters of both screen and screen type specifications of the paste have similar values. The existing small difference is not crucial, so we can say they can be used together.

It is important to remark that exactly the same front contact formation process was applied to standard solar cells with and without rear busbars.

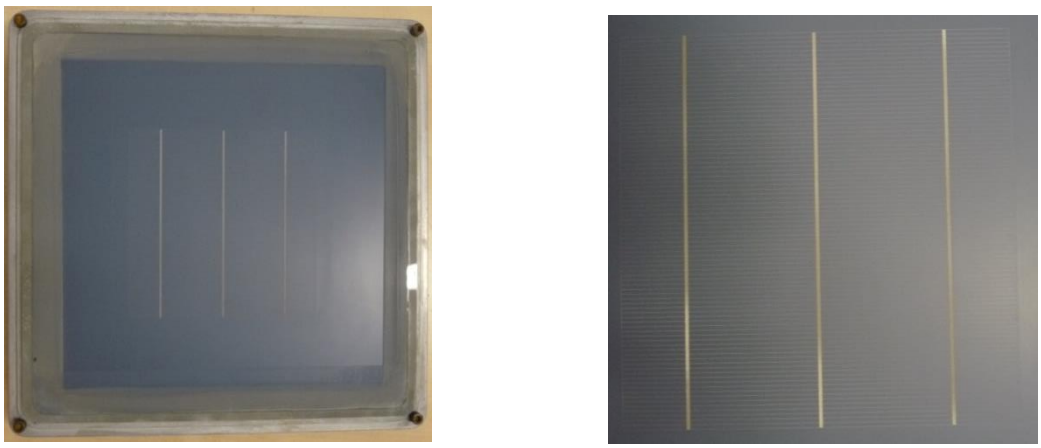

Figure 32. (a) Screen used for the silver metallization, and (b) detail of the contact geometry [CENER]

Once all parameters and equipment were decided, the printing process took place. For both stages (with and without rear busbars), temperature control and stirring of the paste were important (see *APPENDIX I. OPERATION PROTOCOL*).

The results obtained are represented in the following figure (**Figure 33**).

Figure 33. Results of front side metallization of standard Al-BSF solar cells with and without rear soldering pads

5.1.1.2.- Rear contact formation

As it can be observed in **Figure 30** representing the structure, rear contacts are positive pole electrodes, which are responsible for collecting the holes. As the rear side of the cell is not illuminated, a full rear side contact is printed. Its main functions are to reduce recombination by passivating through Back Surface Field (BSF), and to compensate the n-emitter on rear side.

At this point it is important to remark that the screens used and the morphology of the rear contact was different for the case of standard solar cells with and without rear soldering pads.

Al-BSF standard solar cells without soldering tabs

As in the case of front contact metallization, there was already a screen particularly designed for this process, as well as a metallization paste suitable for it. However, before starting the process, the match between both was verified.

The metallization paste to be used for the rear side is Al 5132, while the screen suitable for it was decided to be “Harvey Summer Al”. According to the information contained in the appendix of the metallization paste at the end of the present document (*APPENDIX III. Al5132 METALLIZATION PASTE. DATA SHEET*), the recommended values of mesh/wire diameter/emulsion thickness are: 200/40/5, 250/30/5, 280/35/5 and 325/23/10. It is said that an increase in the mesh count over these values decreases the quantity of paste deposited.

With respect to the characteristics of the screen, they are collected in the following table (Table 3).

Harvey Summer Al	
Mesh (mesh/wire)	250-236
Wire diameter (um)	18
Emulsion thickness (um)	6
Angle (degree)	45º

Table 3. Characteristics "Harvey Summer Al" screen.

Although the value of the wire diameter does not match with the specifications of the paste, the rest of the parameters, that is, the mesh and the emulsion thickness, coincide.

An image of the screen used for back contact deposition is shown in Figure 34.

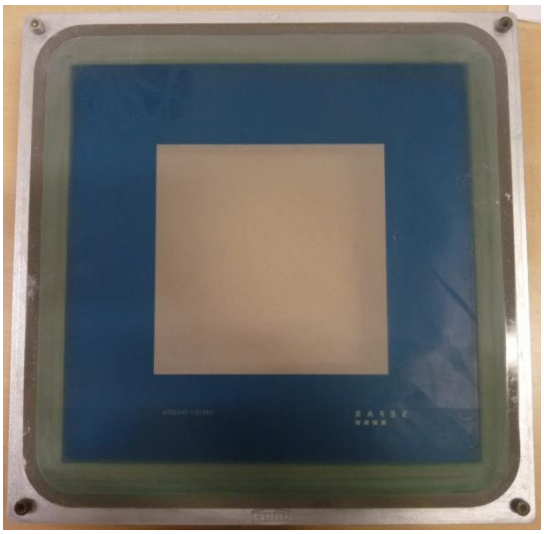

Figure 34. Screen used for the deposition of aluminium on the substrate in cells without rear busbars [CENER]

The result of the process can be observed in Figure 35.

Figure 35. Result of rear side metallization of standard Al-BSF solar cells without soldering pads

Al-BSF standard solar cells with soldering tabs

In this case, the aluminium layer needed to have a different geometry, leaving space for the soldering pads. Hence, a new screen had to be chosen for the printing of the aluminium contact.

The characteristics of this one (Figure 36) are 250 mesh, and a space of 3 mm for each of the soldering pads. This way, we make more probable that the silver paste of the pads goes inside the space left for it in the wafer, despite misalignments.

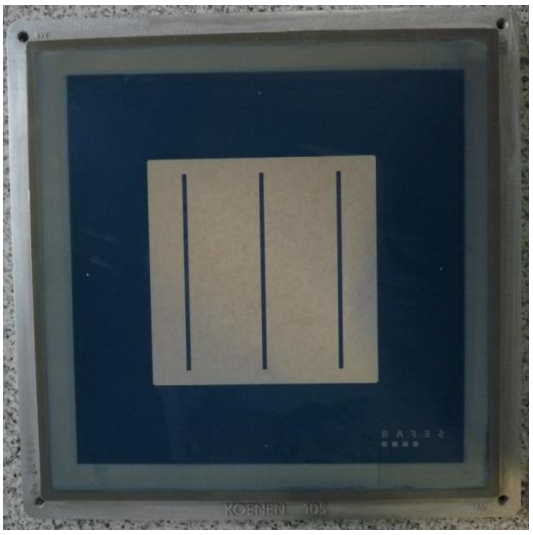

Figure 36. Screen used for the deposition of the aluminium layer on a cell with rear busbars [CENER]

This process was performed before the tabs definition since it was a lot easier to center the substrate with respect to this screen, called “00222 29/30 “, than to the other one, as it can be observed in **Figure 37**.

Figure 37. Result of screen printing of the aluminium layer on standard Al-BSF solar cells with soldering pads

5.1.1.3.- Rear soldering pads definition

This new metallization step is added to the process after rear contact screen-printing, but only in the second stage where possibility of interconnecting cells is incorporated. Busbars, called soldering pads, are printed with a silver-aluminium (Ag/Al) containing paste. Without these rear busbars, aluminium’s solderability problems make impossible the connection between cells.

In the present case, the paste used was PV52A, having highly conductive solderable silver as main component. A suitable screen for it had to be chosen, being this the one represented in **Figure 38**. According to *APPENDIX IV. PV52A METALLIZATION PASTE. DATA SHEET*, the mesh of the screen should be in the range of 150-280 with 5-15 µm emulsion. Among the available screens in the laboratory, the one chosen had reference “00279/0 38/54”, with mesh 250, 3 buses and 5 mm of width of each soldering pad. With this equipment and once again following the steps developed in *APPENDIX I. OPERATION PROTOCOL*, the result of **Figure 39** is obtained.

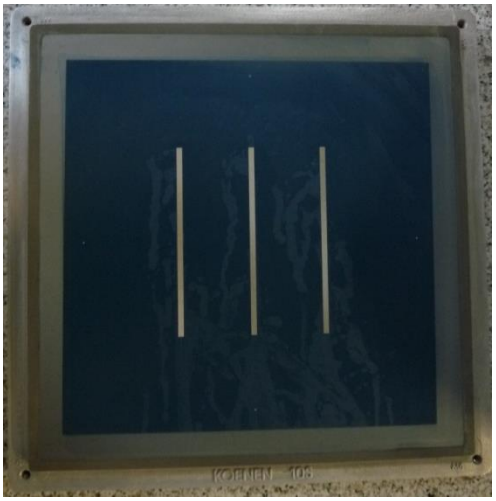

Figure 38. Screen used for the screen-printing of the rear soldering pads [CENER]

Figure 39. Picture of the rear side of one of the metallized wafers after having the rear busbars printed

The following figures summarize the screens and pastes used to print all contacts of the cells with Al-BSF structure. Figure 40 corresponds to standard solar cells without soldering pads, while Figure 41 represents the same for cells with pads included.

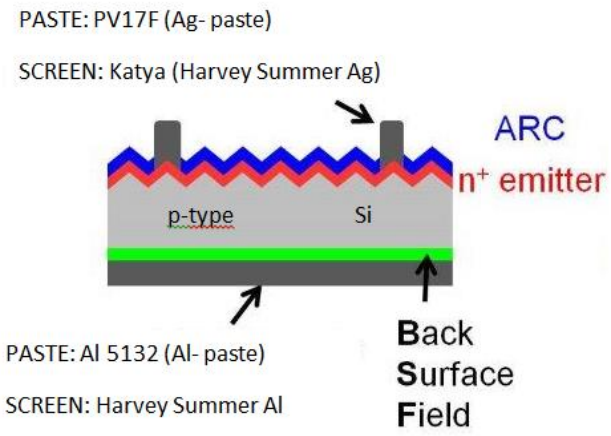

Figure 40. Representation of the screens and pastes used for processing the standard solar cells without rear soldering pads

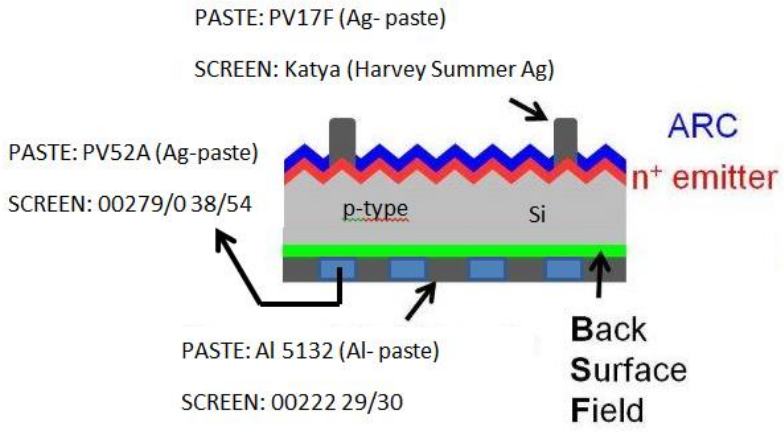

Figure 41. Representation of the screens and pastes used for processing the standard solar cells with rear soldering pads

After each of the metallization processes and before the next one, the substrates were transported to a convection dryer for 10 minutes, at a temperature of 180 °C for the rear side metallization processes and at 200 °C for the front side.

When finishing the printing, cofiring was the next step, necessary to create the contact on both sides of the cell at the same time. To avoid humidity present in the contact, substrates were also dried for about 20 minutes before firing. Once inside the RTP (Rapid Thermal Processing) furnace, the wafer was subjected to changes in temperature, following a profile, with a peak temperature of around 800 ◦C during 1 second. The two silver pastes and the aluminium one used have similar firing parameters, so that they can be fired at the same time.

This is specified in *APPENDIX IV. PV52A METALLIZATION PASTE. DATA SHEET* of the present project.

The final process step was the edge isolation (**Figure 42**). Solar cells were transported to the laser room. Using this equipment and a previously designed template on a computer program, both front and rear side of the cells were isolated.

Figure 42. Detail of the laser edge isolation process performed for the solar cells

This way, the solar cells processed according to Al-BSF structure were ready for the characterization step, described in depth in section *5.1.2.-Performance characterization.*

5.1.2.-Performance characterization

The processed solar cells were characterized using some of the techniques introduced in section *4.2.- SOLAR CELL CHARACTERIZATION*. The objective was to evaluate their performance and also to obtain additional information about morphology of the contacts or characteristics of the cells that could explain that performance.

Al-BSF standard solar cells without soldering tabs

Processed solar cells: Iris-08 and Only-25.

Iris-08 was broken during processing so only spectral response and SEM analysis could be carried out.

➔ IV curve

The IV curve of *Only-25* solar cell was measured following the procedure explained in section *4.2.1.- IV Curve measurement*. Its main electrical parameters were summarized in a table, and its performance compared with the one of previously processed solar cells in CENER (*Only-39*, *Only-51* and *Only-48*).

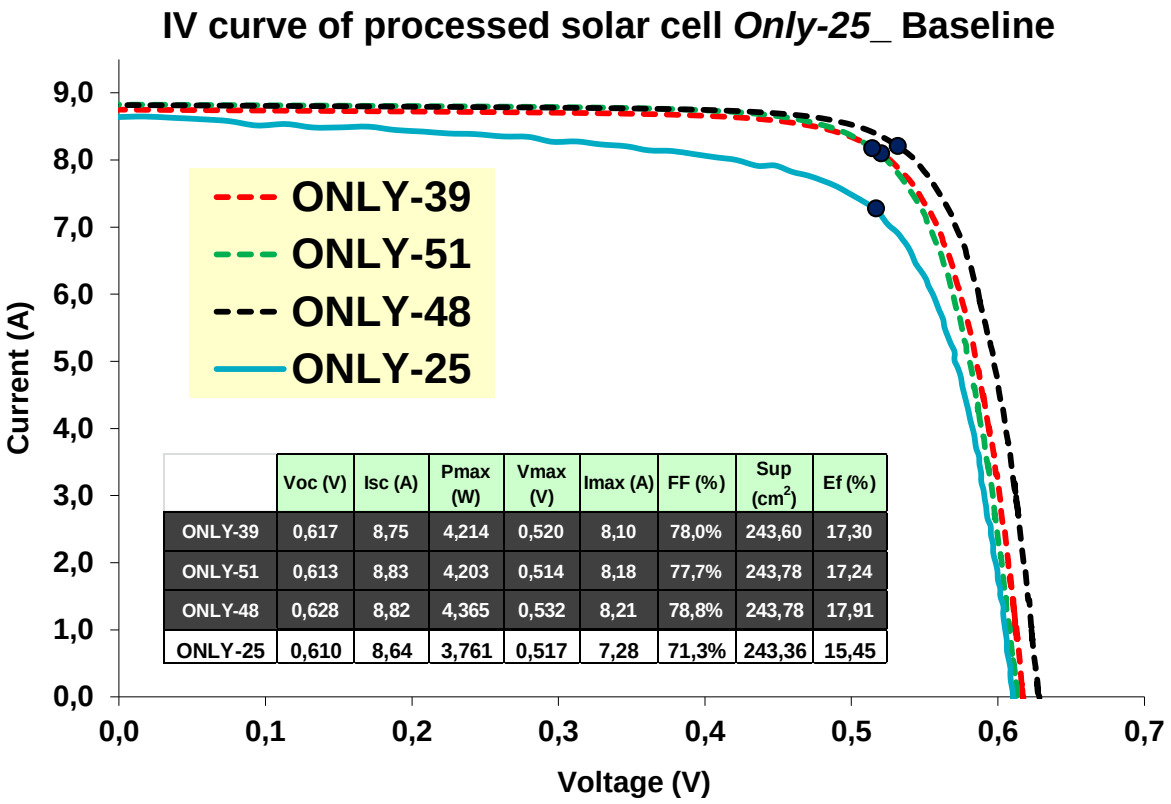

	Voc (V)	Isc (A)	Pmax (W)	Vmax (V)	Imax (A)	FF (%)	Sup (cm^2)	Ef (%)
ONLY-39	0,617	8,75	4,214	0,520	8,10	78,0%	243,60	17,30
ONLY-51	0,613	8,83	4,203	0,514	8,18	77,7%	243,78	17,24
ONLY-48	0,628	8,82	4,365	0,532	8,21	78,8%	243,78	17,91
ONLY-25	0,610	8,64	3,761	0,517	7,28	71,3%	243,36	15,45

Figure 43. IV curve of standard Al-BSF solar cell without soldering pads (*Only-25*)

Compared to the other solar cells considered, the IV curve of *Only-25* does not follow the same shape, showing a worse behavior than on the other cases. The point is to identify the parameters that take a lower value than the one reached in previous solar cell processing, and to find the reasons for this lowering.

By simple inspection of the curve shown in **Figure 43** it is observed that its slope is reduced around the short-circuit current point. This slope reduction is directly linked to a decrease on the parallel resistance of the solar cell. Therefore, a low value of parallel resistance is found to be one of the main problems of the processed *Only-25* solar cell.

As stated in section *3.3.- ELECTRICAL PARAMETERS*, the lowering of the parallel resistance has a direct influence on the fill factor, reducing its value. In fact, on the table that summarizes the parameters, it can be observed that the fill factor took a value of 71.3 %, compared to around 78 % reached in previous processing.

The value of the fill factor determines the maximum power point of the curve, as well as its efficiency. The relationship followed is such that a decrease on the fill factor makes a decrease on the maximum power point (P_{max}) and on the efficiency of the cell (Ef).

➔ Spectral response

A piece of broken *Iris-8* was taken to analyze its spectral response, in particular its external quantum efficiency, with the use of the spectrophotometer.

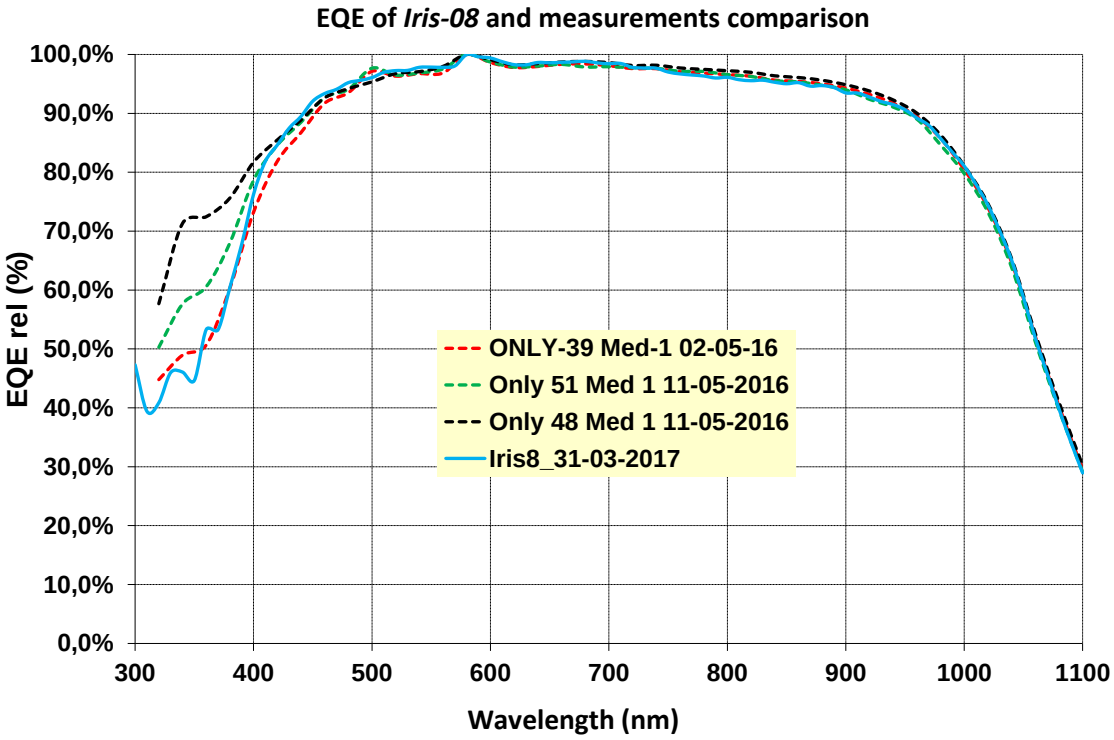

Figure 44. Spectral response of standard Al-BSF solar cell without soldering pads (*Iris-08*)

In the previous figure (Figure 44), it is observed that the spectral current generated by the solar cell *Iris-08* (what is called spectral response) is similar to the ones generated by the previously processed solar cells in CENER.

It follows the same shape, being its response limited at both long and short wavelengths, where photons with energies below and above the band gap, respectively, are found. This coincides with the behavior explained in section *4.2.6.- Spectral response measurement.*

➔ Electroluminescence

Electroluminescence technique was also used to study the quality of the solar cell.

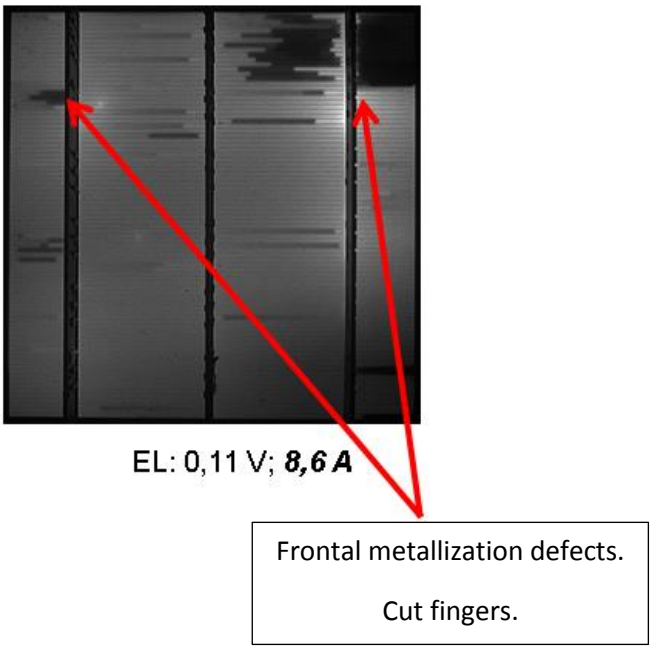

Figure 45. Results of front side view of high polarity electroluminescence test

Observing the pictures from the high polarity electroluminescence test shown in Figure 45 which is performed by applying to the cell its value of short-circuit current, it is clear that there are cut fingers on the front metallization. This is due to a problem on the screen-printing process step. Some of those cuts affect only to a region of the finger, but there are also "dark" regions in which there are a lot of damaged fingers and the contact is not well created.

The electrons of these regions are not collected and hence, efficiency of the solar cell decreases. This problem explains in some way the results observed for the electrical parameters of the IV curve.

To fix the problem of definition of the fingers, the suggestion is to increase in next processing the stabilization time of the metallization paste to 25 ◦C before the process, and to stir for a longer time to reduce its viscosity.

➔ Thermography

Thermography is used for the identification of other type of defects, not the ones related to metallization defects or cracks of the cell, but more related to problems that generate shunts on the electricity generating devices.

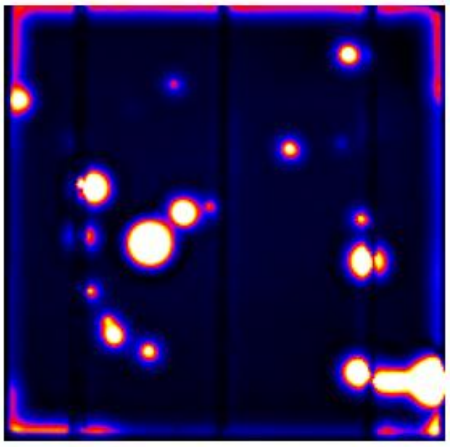

Figure 46. Picture from the thermography test.

On the thermography test results for *Only-25,* illuminated areas can be observed both on the edges of the cell and on the front surface. These lighted up areas indicate the presence of shunts. A high quantity of current flows through the defect points and that the temperature on those points reaches high values, shown by the thermal camera in the form of illuminated areas.

With respect to the edges, it was stated before that phosphorus diffusion also spreads over the edges and rear side of the wafer. This way, the front emitter and the rear cell are connected, and shunt paths are created between the front (n-type) and back (p-type) surface. Edge isolation was performed by laser scribing a groove on the front side of the wafer. However, by looking at **Figure 46,** it can be extracted that the number of times the laser beam scribed the surface were not sufficient to completely isolate front and back sides. That is the reason why a shunt is appreciated on the edges in the form of an illuminated square.

With respect to the rest of lighted up areas around the front surface of the cell, they indicate the presence of shunts due to metallic contaminations, since it means that a high quantity of current is going through those points. Exhaustive cleaning of the tools used during screen-printing process is suggested to solve this problem.

➔ SEM

A small piece of *Iris-08* solar cell was taken to be introduced in the SEM to study the morphology of the rear Al-BSF contact, after decorating interfaces in an acidic solution. From **Figure 47**, it can be extracted that Al-BSF layer, that is, the epitaxial Al-doped silicon layer, has an average width of 1 µm. As expected, the contact is distributed in the whole rear surface. At both sides of the layer we distinguish the silicon layer and the aluminium layer, on the top and behind it respectively.

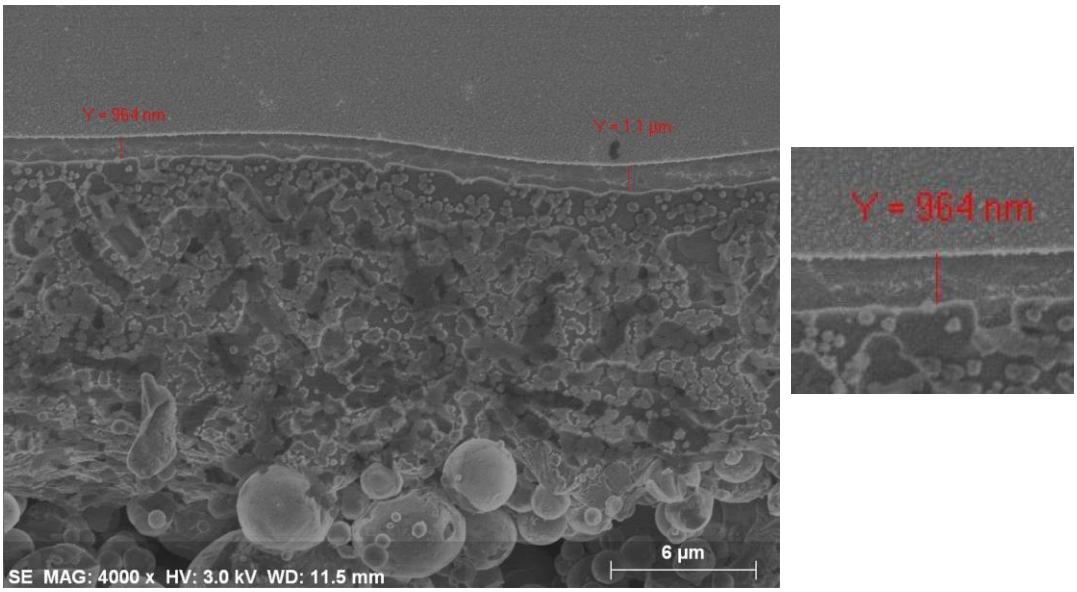

Figure 47. Al-BSF structure observed with SEM.

Al-BSF standard solar cells with soldering tabs

The same characterization techniques were applied for the solar cells processed with soldering tabs (*Iris-12, Iris-13, Only-26, Only-27*), in order to study their behavior and establish comparisons between these results and the ones obtained for *Only-25*.

➔ IV curve

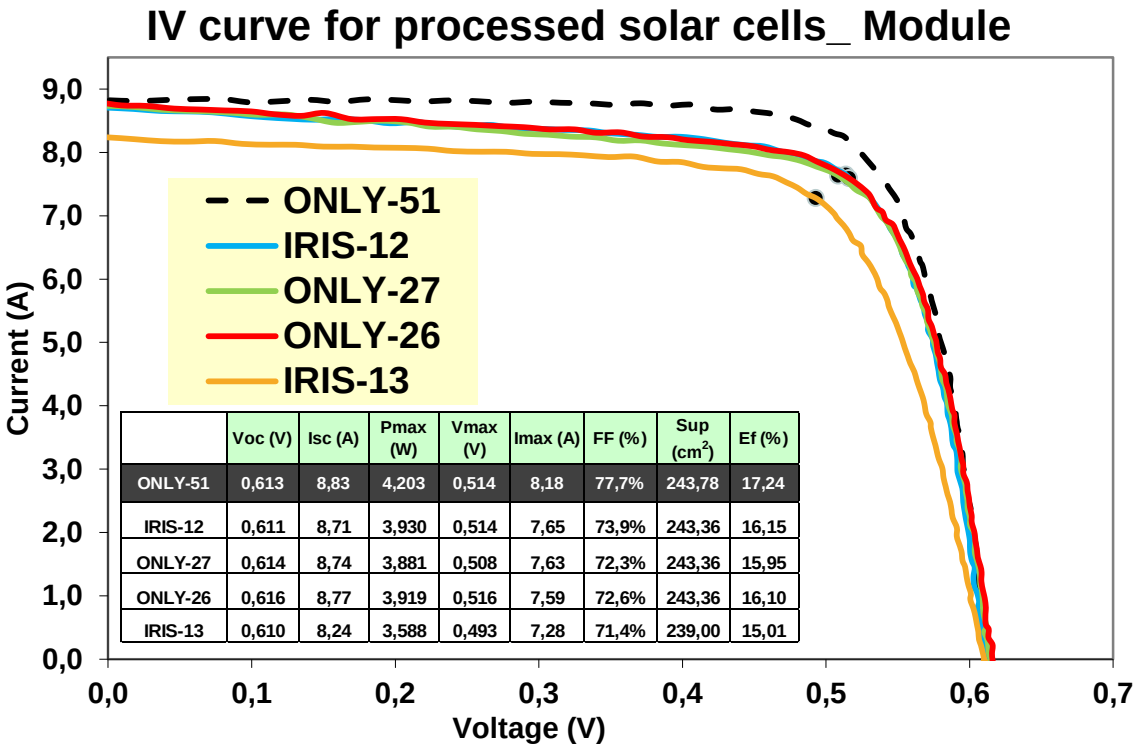

	Voc (V)	Isc (A)	Pmax (W)	Vmax (V)	Imax (A)	FF (%)	Sup (cm^2)	Ef (%)
ONLY-51	0,613	8,83	4,203	0,514	8,18	77,7%	243,78	17,24
IRIS-12	0,611	8,71	3,930	0,514	7,65	73,9%	243,36	16,15
ONLY-27	0,614	8,74	3,881	0,508	7,63	72,3%	243,36	15,95
ONLY-26	0,616	8,77	3,919	0,516	7,59	72,6%	243,36	16,10
IRIS-13	0,610	8,24	3,588	0,493	7,28	71,4%	239,00	15,01

Figure 48. IV curve of standard Al-BSF solar cell with soldering pads

In this case, the same problem of low value of parallel resistance was found (Figure 48). This lowering of the resistance caused an important decrease on the fill factor values (FF), and therefore, on the maximum power of the solar cell (P_{max}) and on the efficiency (Ef).

For all the processed solar cells, a lowering on the values of both the open-circuit voltage and short-circuit current were found. However regarding *Iris-13,* this lowering was a lot more evident, as can be observed on the represented IV curves.

Therefore, the problems found in the previous processing of standard Al-BSF solar cells without pads were not fixed.

➔ Electroluminescence (high polarity)

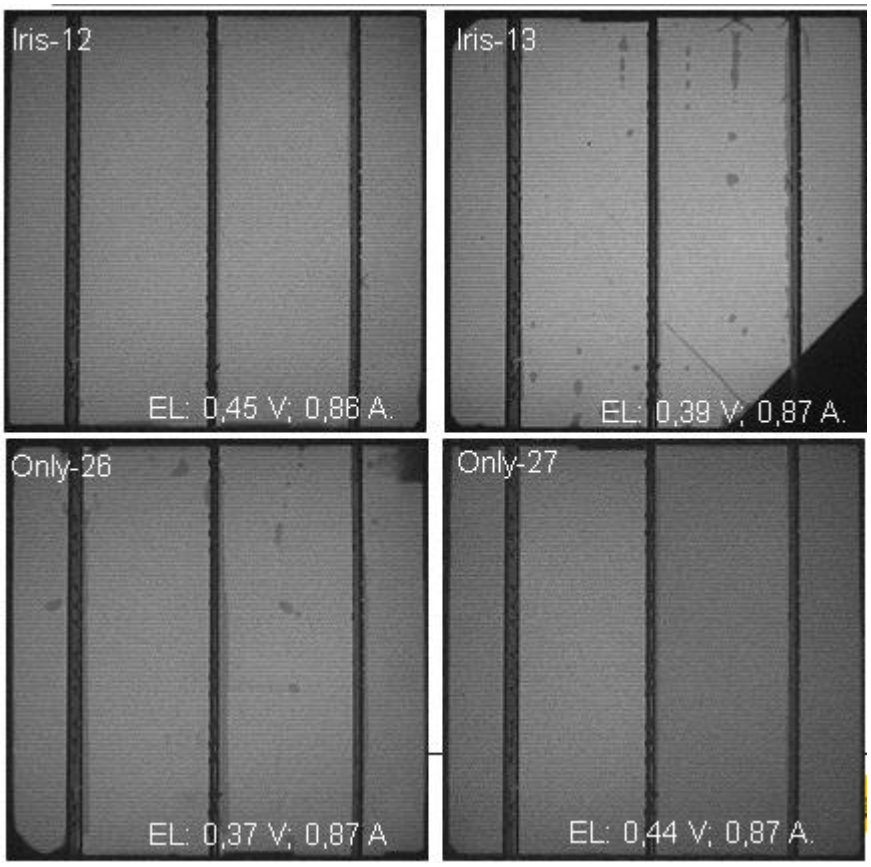

Figure 49. High-polarity electroluminescence results for the processed solar cells with soldering pads.

In high polarity electroluminescence, as it can be observed in **Figure 49**, *Iris-12* and *Only-27* are the cells that apparently show the best result. Even if they present a few small dark regions, which indicate the existence of cut fingers, the rest of the surface is correctly illuminated.

However, for *Only-26* and *Iris-13* things change. Both present some regions of cut fingers, bigger in the case of these two cells. In addition to this, over all the surface of the cells, small circle regions are appreciated. Because of the shape, they cannot be a representation of cut fingers. They correspond to some zones where aluminum did not fix to silicon correctly after firing and appear as dark spots.

A corner of solar cell *Iris-13* was broken during the process and that is why it appears dark in the high polarity electroluminescence test.

➔ Thermography

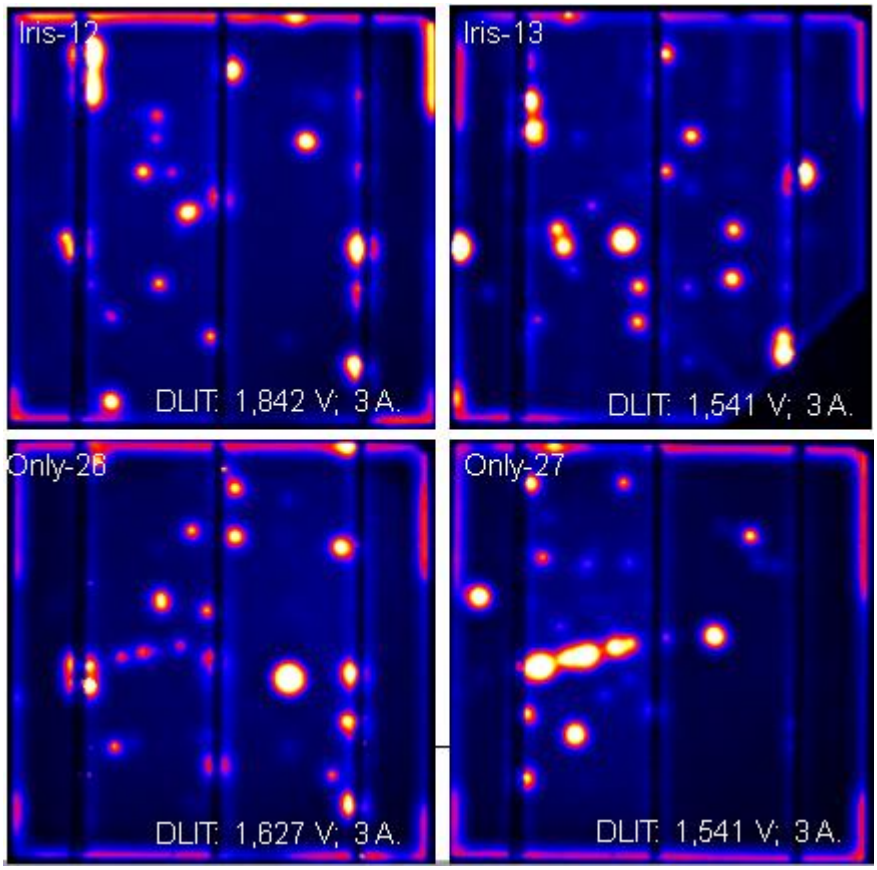

Figure 50. Thermography pictures of processed solar cells with soldering pads.

In the present thermography test, results do not change considerably from the case of solar cells without soldering pads, and therefore, problems are not solved. Lighted up areas are observed in all images from Figure 50. As explained before, this is due to both not enough edge isolation and contamination over the surface of the solar cells.

5.2.-PERC SOLAR CELL

5.2.1.-Fabrication process and design

As explained previously in section *3.5.- HIGH EFFICIENCY SOLAR CELL ARCHITECTURES: PERC*, the modification in the fabrication process of solar cells to go to PERC structure from Al-BSF structure consists on the addition of two new processes.

At this stage of the project, the objective was to perform experiments in order to find the optimal parameters to perform the back contact of this new architecture. The optimization of

the dielectric layers was not one of the purposes of the present work so the research was centered on the laser ablation for rear contact optimization.

As it was not clear which will give a better result, the design of the ablated areas to perform rear localized contacts was performed for both, lines and points. For each of the geometries, lines and points, four tests were carried out to find the best parameters:

- **Test 1**: In this experiment, laser parameters: current, mirror velocity and number of pulses were varied over dummy wafers to find process variable ranges able to ablate rear dielectric layer locally.
- **Test 2**: Complete solar cells were integrated varying laser parameters in the process variable ranges found in Test 1. Nine experiments in each solar cell were performed.
- **Test 3**: Complete solar cells were integrated varying distances between lines or points, keeping laser parameters fixed.
- **Test 4**: According with the results of Tests 2 and 3, complete solar cells were processed, using the best laser parameters found in Test 2 and the optimum distance found in Test 3 for each of the geometries.

5.2.1.1.- Rear dielectric laser ablation: Lines

The **first test** was to perform ablation with an infrared wavelength laser of some lines on a dummy wafer. The parameters used during this first experiment are collected in **Figure 51**.

Laser frequency = 20 kHz Mirror velocity = 800 mm/s Variable current (taking values 19, 20, 22 and 25 A)

Figure 51. Summary of parameters for laser ablation with lines (first test)

These patterns were then analyzed by optical microscopy (**Figure 52**) and the lines widths measured.

This first inspection was useful to fix a range of power that could be used to ablate rear passivation layer, considering that the optimal current, and hence laser power, would be inside this range.

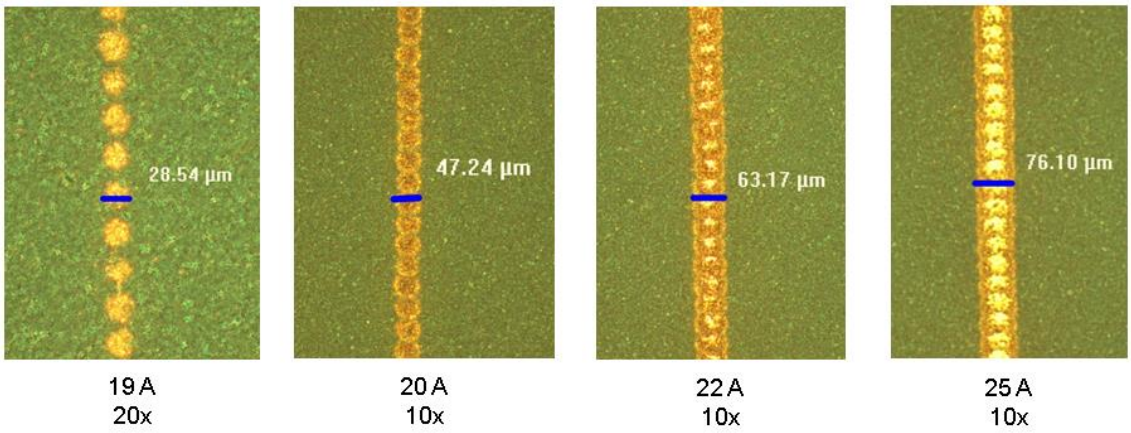

Figure 52. Inspection under optical microscopy of the areas ablated by lines.

From Figure 52 big differences could be observed on the marked lines depending on the current applied to the laser beam. In this case, as the velocity remained constant for the marking of all the lines, all lines had the same spot overlap. Hence, the difference was only due to distinct values of current applied. By first inspection, it seemed that a value of 19 A would lead to small isolated dots which do not overlap. The energy seemed to be too low to form a line. On the contrary, for a value of 25 A, a line could be clearly distinguished, with a bigger width. Line width varied from around 20 µm to 76 µm increasing laser current from 19 A to 25 A.

After these inspections, there already existed some parameters to start performing experiments and characterizing. Therefore, in the **second test**, it was decided to perform nine experiments varying laser current and overlap in each solar cell in order to, first verify that the contact was correctly formed after firing, and then look for performance differences among them.

Frequency was fixed and current and mirrors' velocity were varied to change both line width and spot overlap. The same geometry was maintained in all the cases.

To design the 9 experiments that were going to be performed, 3 different values of current were taken first: 20, 22 and 25 A. (The current value of 19 A was rejected in the initial test).

Taking into account that the relation between mirror velocity (v) and overlap (S) is given by the following formula:

$$S = 1 - \frac{v}{D\,f}$$

where,
D = spot diameter (m)
f = frequency (Hz)

Velocity was varied, taking 3 different values for fixing the spot overlap in 0.1, 0.27 and 0.5. This way, for a 0.1 overlap value the corresponding mirror velocity was 990 mm/s, while for 0.27 and 0.5 velocities of 800 and 550 mm/s respectively were assigned.

The designed nine experiments gave rise to nine differentiated regions, distributed in a solar cell the way expressed in Figure 53. That is, in squares of 46 mm x 46 mm each, and leaving a spare space of 6 mm between them.

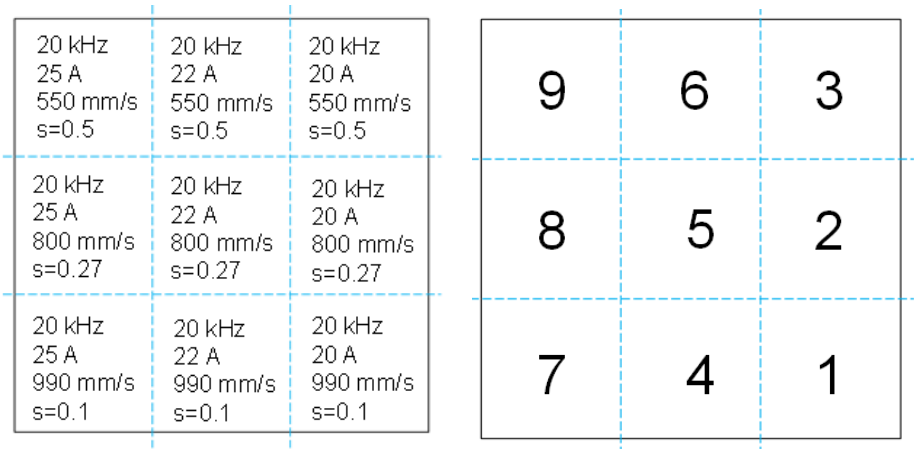

Figure 53. Representation of the front view of the location of the nine experiments for lines in a solar cell (left) and the nomenclature used (right)

With respect to the geometry, a typical value of line spacing was used (1 mm), and the laser ablated areas had the shape represented in Figure 54. The same spacing was repeated in all designed experiments. It is important to mention that the line direction of the rear localized line contacts was perpendicular to the frontal fingers direction.

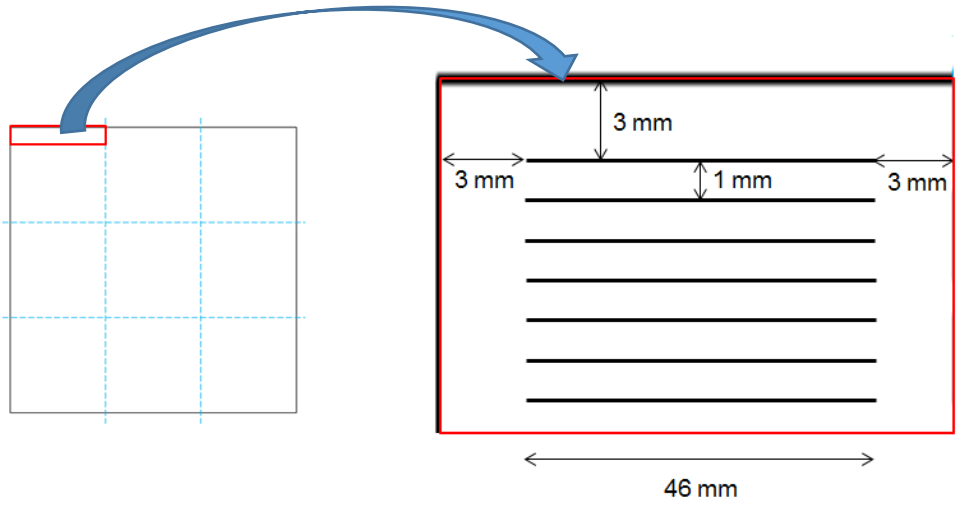

Figure 54. Schematic of the laser ablated areas for the case of lines.

For the laser ablation, the same nanosecond laser equipment as for the edge isolation process was used. The template was designed in the corresponding program, assigning the parameters specified before. Afterwards, optical microscopy was used for inspection of the differences in overlap (Figure 55) and for verification of the spacing (Figure 56).

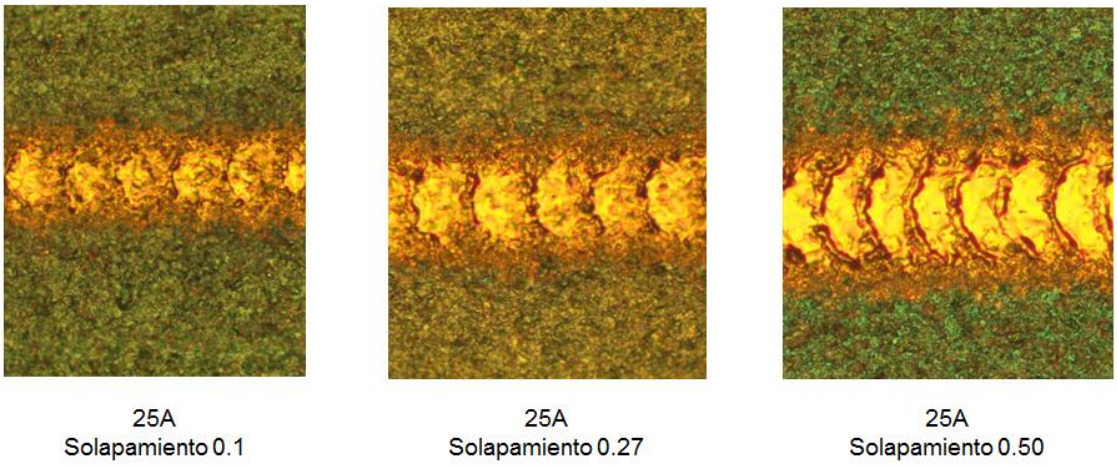

Figure 55. Representation of the different overlap values for the same current applied (25 A).

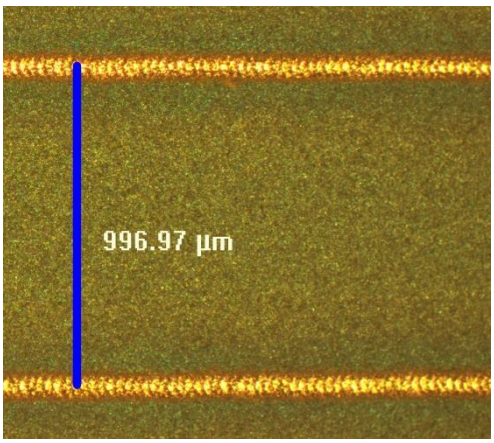

Figure 56. Line spacing observed by microscopic inspection.

With respect to the line width, as applied current increases, an increase on the line width could be observed from around 39 µm for 20 A to around 73 µm for a current of 25 A.

The **third test,** performed at the same time than the second one, was based on varying the spacing between lines keeping laser parameters' values constant for all experiments (Figure 57). These parameters were selected from the range of typical ones.

Laser frequency = 20 kHz Laser current = 22 A Mirror velocity = 990 mm/s (S = 0.1)

Figure 57. Summary of parameters for laser ablation with lines (third test)

The line spacing variation was performed according to the state of the art of PERC solar cells (See section *3.5.- HIGH EFFICIENCY SOLAR CELL ARCHITECTURES: PERC*).

The range of line spacing selected was from 0.5 to 2 mm, being this one the widest of the ones found in bibliography. Hence, this range was split into smaller distances so that 9 experiments of spacing variation were obtained.

A silicon solar cell rear side was laser ablated forming these experiments, as shown in Figure 58.

2 mm between lines	1.4375 mm between lines	0.875 mm between lines
1.8125 mm between lines	1.25 mm between lines	0.6875 mm between lines
1.625 mm between lines	1.0625 mm between lines	0.5 mm between lines

9	6	3
8	5	2
7	4	1

Figure 58. Representation of the front view of the line spacing chosen for each experiment (left) and the nomenclature used (right)

The ablation areas for each experiment had an approximate dimension of 46 x 46 mm, leaving between them a space of 6 mm, in which as openings were not made, contact was not supposed to exist.

After analyzing the results from the two previous tests of parameters and geometry variation, in the **fourth test**, the objective was to process a wafer using the optimal laser

parameters and spacing. From the results collected in the present document, it was extracted that the parameters that showed the best behavior were the ones summarized in **Figure 59**.

Laser frequency = 20 kHz Laser current = 22 A Mirror velocity = 800 mm/s (S = 0.27) Distance between lines = 1.4375 mm

Figure 59. Summary of optimal parameters for laser ablation with lines (fourth test)

The solar cells were processed and characterized afterwards, as occurred for the two previous designs. The results are analyzed in section *5.2.2.-Performance characterization.*

5.2.1.2.- Rear dielectric laser ablation: Points

For the case of points, the same testing procedure was applied, consisting of three tests and then the processing of entire solar cells with the optimal parameters found.

In the **first test**, laser areas in the form of points were ablated on the surface of a dummy wafer. The number of pulses applied per point was the only variable that was changed in a certain range to perform a scan. The rest of the variables were fixed to the values represented in **Figure 60**.

Laser frequency = 20 kHz Mirror velocity = 800 mm/s Laser current = 25 A Variable number of pulses per point (from 11 to 30 pulses per point)

Figure 60. Summary of parameters for laser ablation with points (first test)

Optical microscopy was used to inspect points and measure the diameter of the ablated area. In this case (**Figure 61**), remarkable differences could also be seen among the different values of pulses per point. When the number of pulses per point increased, the diameter of the point increased too, as expected. An application of less than 11 pulses per point was considered to be too low to remove the dielectric layer as it is shown on the dummy wafer.

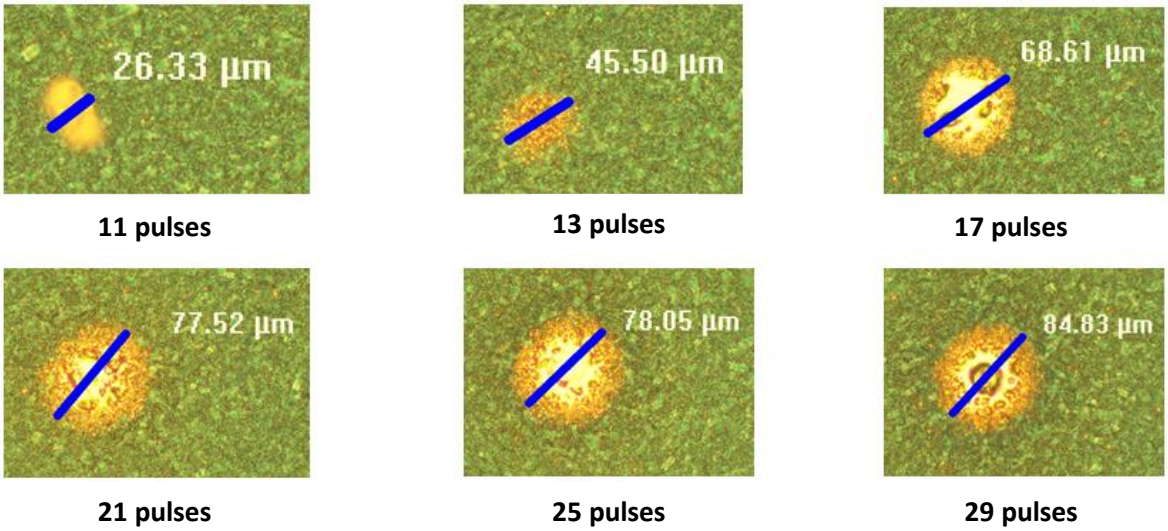

Figure 61. Inspection under optical microscopy of the areas ablated by points

The objective of the **second test** was to try different values of the laser ablation parameters. Frequency, mirrors' velocity and current value were fixed for all the performed experiments, while the number of pulses applied per point was varied. The range of variation of this parameter was from 13 to 29 pulses per point, but taking only the odd values and therefore, obtaining the nine experiments represented in Figure 62.

20 kHz 25 A 800 mm/s 29 pulses	20 kHz 25 A 800 mm/s 23 pulses	20 kHz 25 A 800 mm/s 17 pulses
20 kHz 25 A 800 mm/s 27 pulses	20 kHz 25 A 800 mm/s 21 pulses	20 kHz 25 A 800 mm/s 15 pulses
20 kHz 25 A 800 mm/s 25 pulses	20 kHz 25 A 800 mm/s 19 pulses	20 kHz 25 A 800 mm/s 13 pulses

9	6	3
8	5	2
7	4	1

Figure 62. Representation of the front view of the location of the nine experiments for points in a solar cell (left) and the nomenclature used (right)

A square geometry was chosen for these first tests, maintaining, as for the case of lines, the same spacing among points (Figure 63). In this case, the distance among points is 0.5 mm. An exclusion edge of 6 mm was left between experiments and of 3 mm around the border.

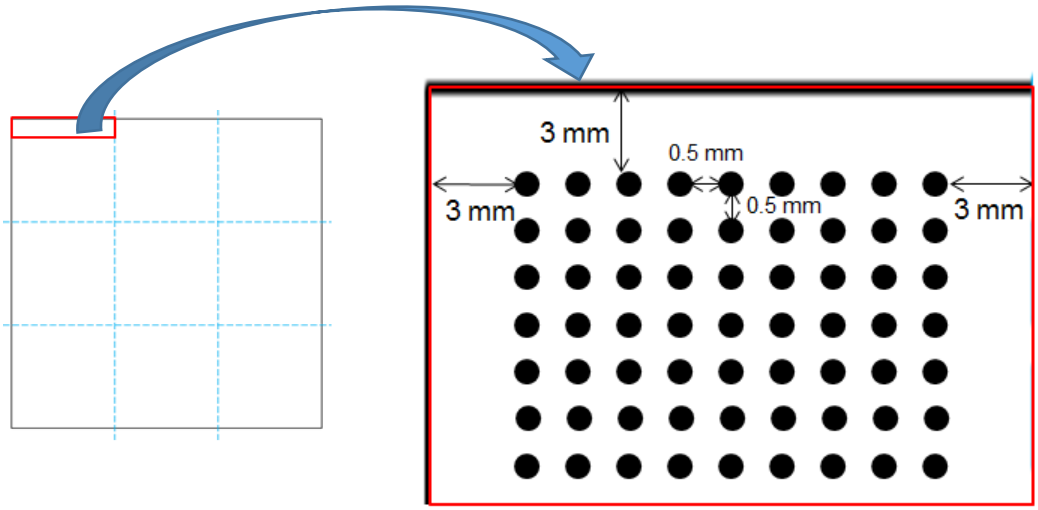

Figure 63. Schematic of the laser ablated areas for the case of points

The microscopic inspection posterior to laser ablation confirmed the spacing fixed between points, as can be extracted from Figure 64. As occurred in case of lines, the diameter of the points increased as did the number of pulses per point.

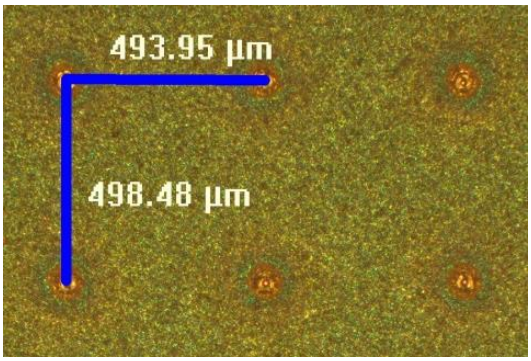

Figure 64. Points spacing observed by microscopic inspection

At the same time, other cells were processed for the **third step**, these ones containing experiments of variation of the distances among points. For the ablated area, typical parameters of laser current, mirror velocity, frequency and number of pulses per point were used. Despite the fact that these parameters may not be the optimal ones, the objective was to appreciate differences among opening distances. In this case, the chosen parameters to perform the point distance variation were the ones shown in Figure 65.

Laser frequency = 20 kHz
Laser current = 25 A
Mirror velocity = 800 mm/s
27 pulses per point

Figure 65. Summary of parameters for laser ablation with points (third test)

Openings separation distance range was chosen to be from 0.2 to 1 mm, choosing as in the case of lines the widest range of the ones found in bibliography. In order to get the desired nine experiments, the increase in distance between individual points from one to another experiment was 0.1 (Figure 66).

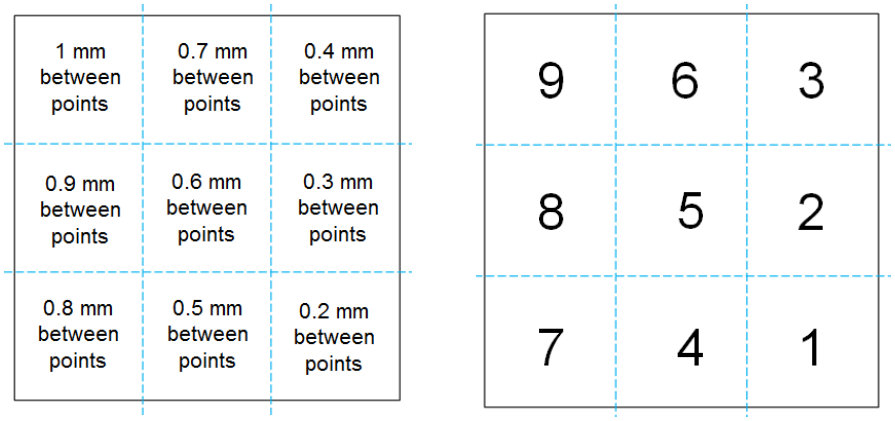

Figure 66. Representation in front view of the point spacing chosen for each experiment (left) and the nomenclature used

The ablation areas for each experiment had the same dimensions specified for the case of lines previously described.

After looking at the characterizations for second and third step tests in section *5.2.2.- Performance characterization*, the values of each of them that lead to the best result are selected to process entire solar cells. These values of laser ablation parameters and spacing were selected according to Figure 67.

Frequency = 20 kHz
Laser current = 25 A
Mirror velocity = 800 mm/s
17 pulses per point
Distance between points = 1 mm

Figure 67. Summary of parameters for laser ablation with points (fourth test)

5.2.1.3.- Back contact formation

Contact formation was the following step to laser ablation, since contacts are deposited and formed during screen printing and firing respectively. The procedure followed was the same for rear line or point contacts. That is why no distinctions are done in this section.

Front contacts were deposited using the same equipment and parameters mentioned in section *5.1.1.1.- Front contact formation* for standard solar cells. That is why the procedure is not developed in the present section.

However, back contact presents some differences with respect to the equipment used. It has the same shape as aluminium deposited on the whole rear surface, but the required metallization paste's properties differ a lot from the ones required for the cells that were processed for fixing the baseline.

The recommended paste to use for the metallization of this type of highly efficient solar cells is PV36A. Its characteristics are presented in detail in *APPENDIX V. PV36A METALLIZATION PASTE. DATA SHEET.*

At that point, the interesting parameters of the metallization paste were the ones related to the recommended screen type to use, summarized in **Table 4**.

	(I)	(II)
Mesh count (stainless steel)	380	400
Wire diameter (µm)	14	18
Emulsion thickness (µm)	10	10

Table 4. Summary of screen type suitable for PV36A metallization paste

The screen chosen had the specifications summarized in **Table 5**.

Irene	
Mesh (mesh/wire)	400
Wire diameter (um)	18
Emulsion thickness (um)	9
Angle (degree)	25

Table 5. Characteristics "Irene" screen

It can be observed that the mesh and wire diameter values for "Irene" screen coincide exactly with the specifications of the metallization paste and almost emulsion thickness value too. Hence, the screen is suitable for PV36A paste.

Summing up, the pastes and screens used for the complete metallization of this type of solar cells is the following (Figure 68).

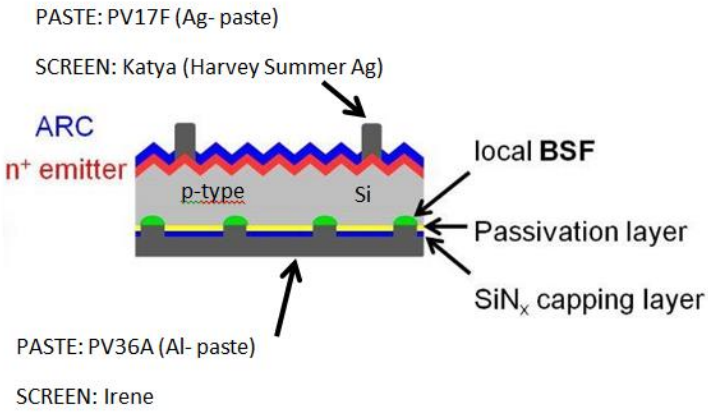

Figure 68. Representation of the screens and pastes used for processing PERC solar cells

5.2.2.-Performance characterization

The characterization was performed to all experiments of PERC solar cells. The tools used to characterize the nine small cells that derived from each wafer were IV curve measurement and electroluminescence. In order to study the morphology of the contact and to verify that local Al-BSF interfaces were formed, a sample was observed by using scanning electron microscopy (SEM).

PERC cells with line design

The wafers processed were *Only-54*, *Only-56* and *Ra-25.*

The cells were characterized to study the behavior of each experiment separately from the others, in order to establish differences among them.

Only-54 contained the nine experiments described in section *5.2.1.1.- Rear dielectric laser ablation: Lines*, in the position illustrated in Figure 53. The rear contacts design used was the one of parameters' (current and overlap) variation.

→ IV curve measurement

The IV curves of each small cell *Only-54* contains are represented.

It can be observed in Figure 69 that there are some small cells that reach higher values of open-circuit voltage and short-circuit current than others.

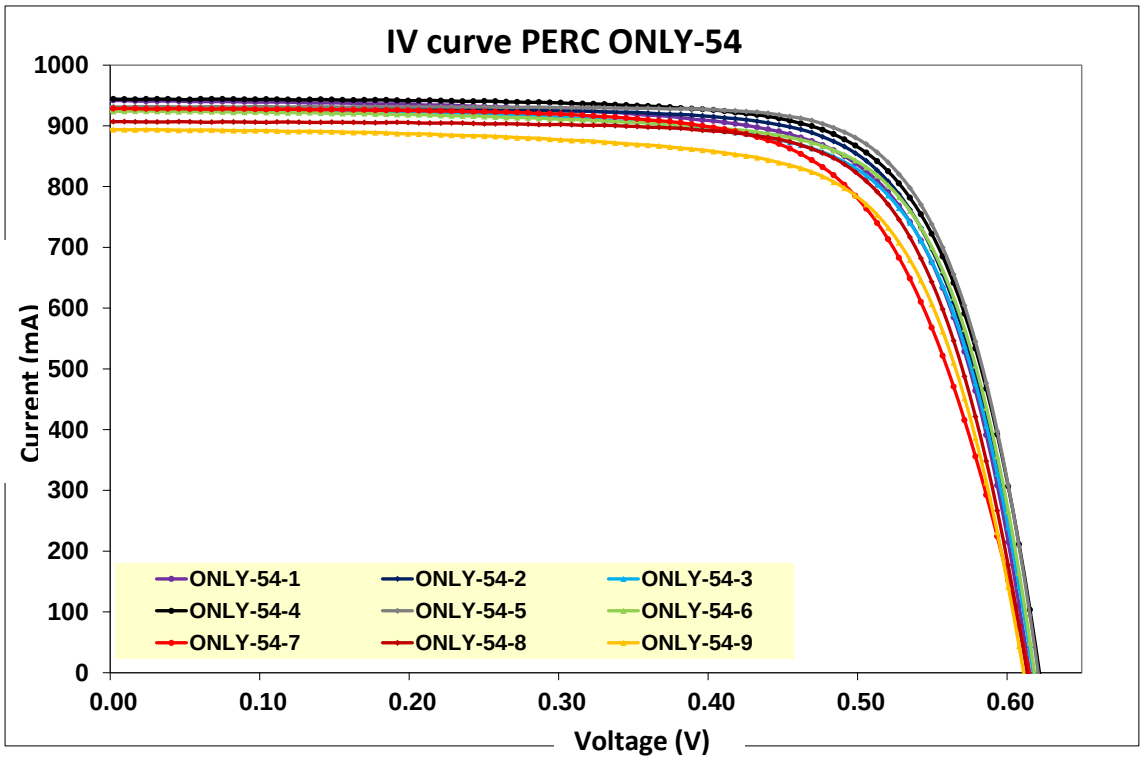

Figure 69. Representation of the IV curve of PERC Only-54 solar cell

In order to find the best electrical parameters, V_{oc} and R_s are the two parameters analyzed in detail. It is known that the best contact will be a compromise between less back surface recombination (higher V_{oc}) and so, lower laser ablation, and low series resistance and so, higher laser ablation.

Therefore, as observed in Table 6, for high values of laser current (25A), the values of open-circuit voltage and short-circuit current density tend to decrease (0.611-0.615 V and 32.8-33.7 mA/cm^2 respectively), showing a worse behavior. However, low current values (20A) also seem to make the open-circuit voltage slightly decrease. In Figure 70 it is graphically verified how the value of 22 A for current leads to the highest values of open-circuit voltage for the three overlaps.

	Voc (V)	Jsc (mA/cm^2)	Pmax (mW)	FF (%)	Área (cm^2)	Ef (%)
ONLY-54_1	0.615	35.5	418.0	72.2	26.52	15.76
ONLY-54_2	0.618	35.0	426.3	74.3	26.52	16.07
ONLY-54_3	0.617	35.4	414.0	72.1	26.27	15.76
ONLY-54_4	0.622	35.3	432.9	73.8	26.78	16.17
ONLY-54_5	0.621	34.8	440.0	76.1	26.78	16.43
ONLY-54_6	0.618	34.8	420.8	73.7	26.52	15.87
ONLY-54_7	0.615	33.7	396.6	69.5	27.56	14.39
ONLY-54_8	0.613	32.9	411.1	73.9	27.56	14.92
ONLY-54_9	0.611	32.8	391.8	71.7	27.30	14.35

9	6	3
8	5	2
7	4	1

Rp (Ωcm^2)		
2280	2348	2292
4443	7438	21064
3545	68985	1583
Rs (Ωcm^2)		
2.3	2.3	2.3
2.3	2.3	2.3
2.8	2.4	2.2

Table 6. Electrical parameters of PERC Only-54 solar cell

The fill factor value does not apparently follow any tendency, but it reaches its highest value (76.1 %) for experiment number 5.

With respect to the series resistance, similar values are observed for all the experiments, as illustrated in Figure 71 . The lowest value (2.2 Ω cm^2) is obtained for experiment number 1, followed closely by a value of 2.3 Ω cm^2 of experiments 2, 3, 5, 6, 8 and 9.

At this point of the project, getting a high value of efficiency is not the main goal so it is not a parameter in which we focus.

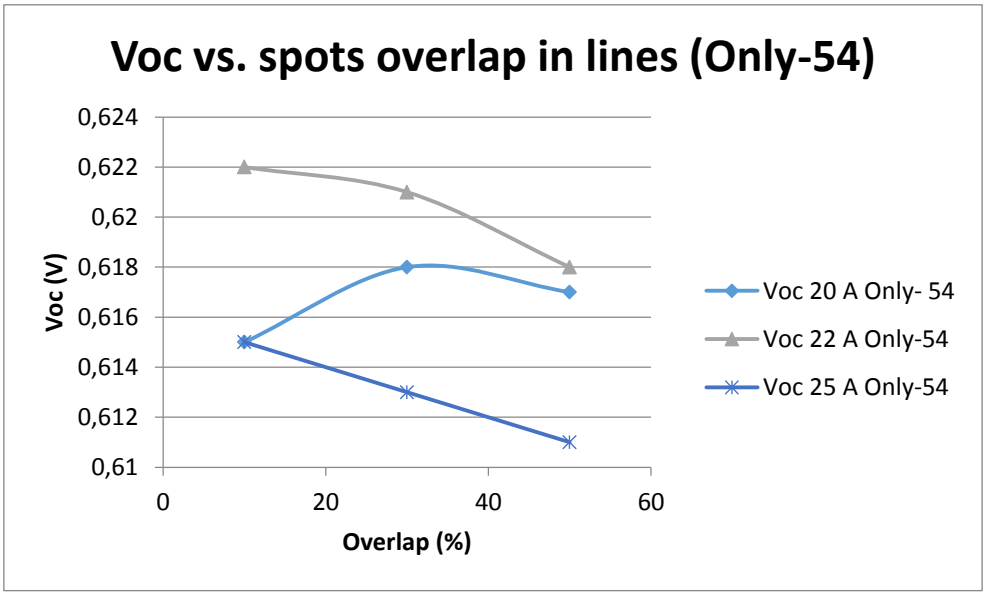

Figure 70. Graph representing open-circuit voltage versus laser spots overlap for lines and for different values of current

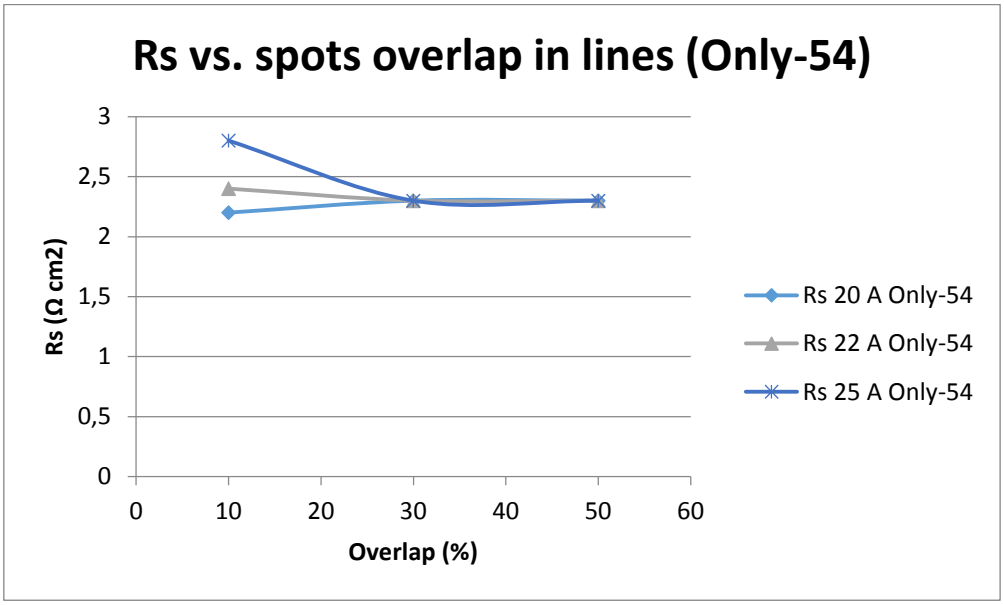

Figure 71. Graph representing series resistance versus laser spots overlap for lines and for different values of current

→ Electroluminescence

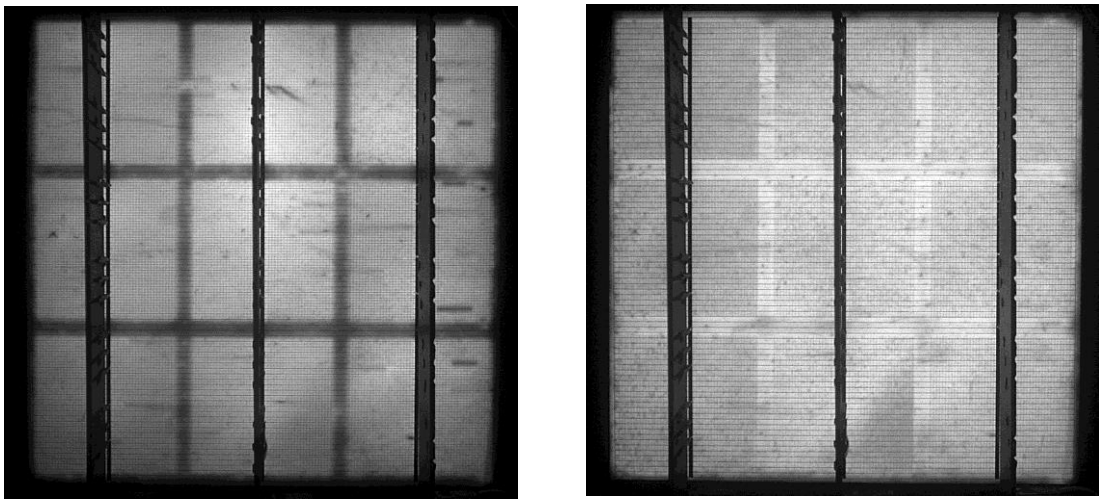

Figure 72. High polarity (left) and low polarity (right) electroluminescence test for PERC Only-54 solar cell

In high polarity electroluminescence picture of Figure 72, dark regions are appreciated corresponding to the areas in which no openings were made. Dark zones are indicators of high series resistance because of the absence of contact.

In low polarity electroluminescence, these regions appear brighter because it is where recombination velocity is lower and there exists a better passivation.

Screen-printing process was fulfilled correctly since no cut fingers are detected on the pictures.

→ SEM

By using SEM technology, the morphology of the rear contact can be studied.

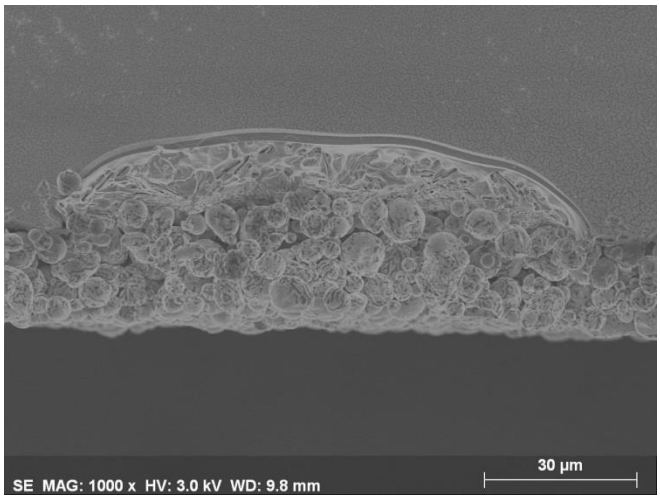

Figure 73. SEM image of the rear local Al-BSF contact in *Only-54*

As it is observed in Figure 73, aluminium penetrates in silicon a certain depth, and then between both layers, an interface Al-BSF is formed only where the dielectric layer has been ablated. This interface presents the same width in all the contact, but it does not exist on the areas that have not been laser ablated. Hence, the contact, as expected, is localized and the dielectric layer withstood the firing temperature and blocked aluminium to be in contact with silicon.

Now, regarding line spacing, ***Only-56*** contained the nine experiments developed in section *5.2.1.1.- Rear dielectric laser ablation: Lines*, in the position illustrated in Figure 58 and following the nomenclature represented in the same figure.

→ IV curve measurement

The IV curves designed in *Only-56* solar cell are represented in Figure 74.

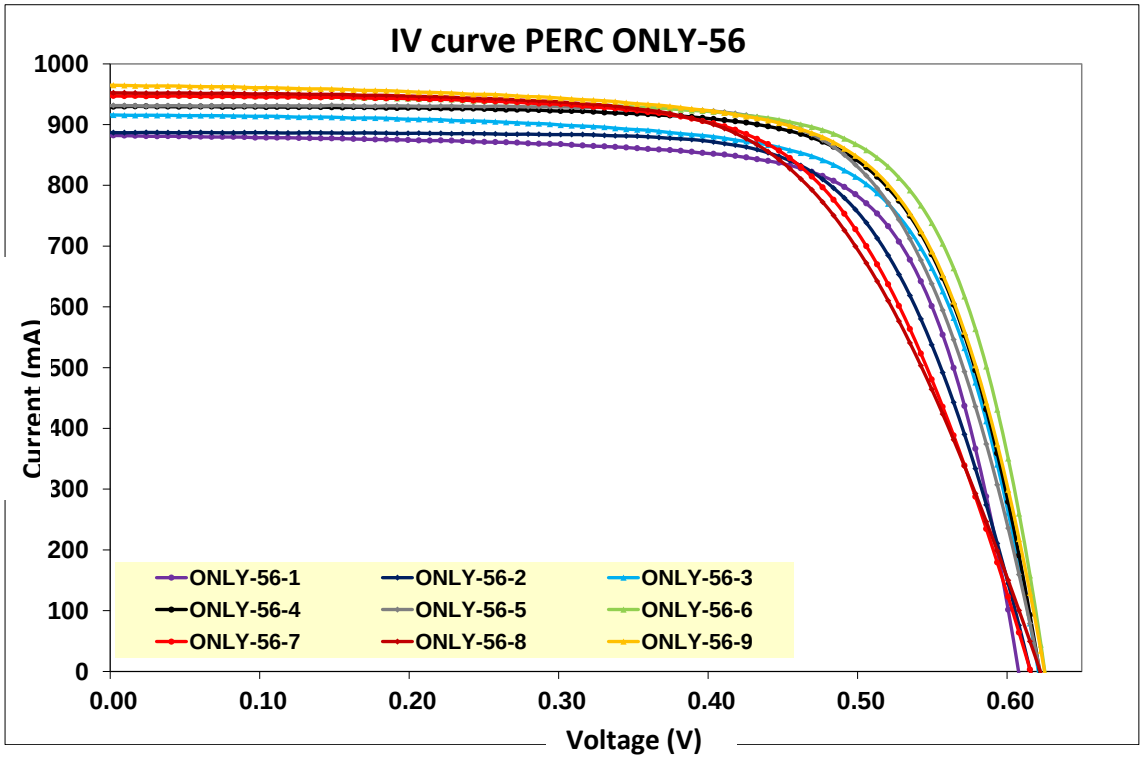

Figure 74. Representation of the IV curve of PERC Only-56 solar cell

As in the previous characterization, quantitative values of the electrical parameters, represented in Table 7, are used to establish comparisons among the different experiments.

	Voc (V)	Jsc (mA/cm^2)	Pmax (mW)	FF (%)	Área (cm^2)	Ef (%)
ONLY-56_1	0.608	33.3	391.7	73.1	26.52	14.77
ONLY-56_2	0.616	33.4	386.1	70.7	26.52	14.56
ONLY-56_3	0.621	34.9	405.9	71.4	26.27	15.46
ONLY-56_4	0.622	34.7	420.3	72.7	26.78	15.70
ONLY-56_5	0.622	34.8	417.9	72.1	26.78	15.60
ONLY-56_6	0.625	35.8	434.0	73.1	26.52	16.36
ONLY-56_7	0.616	34.4	384.1	65.9	27.56	13.94
ONLY-56_8	0.622	34.6	376.9	63.6	27.56	13.68
ONLY-56_9	0.625	35.3	423.1	70.2	27.30	15.50

9	6	3
8	5	2
7	4	1

Rp (Ωcm^2)		
1043	2209	2084
3371	8732	36792
2846	4429	916
Rs (Ωcm^2)		
2.7	2.5	2.6
4.1	2.9	3.1
3.5	2.6	2.1

Table 7. Electrical parameters of PERC Only-56 solar cell

From these results, it can be extracted that diminishing a lot the spacing between lines to a value lower than 1 mm increases recombination, since low values of open-circuit voltage such as 0.608 and 0.616 V are obtained (Figure 75). On the contrary, a large separation (of

nearly 2 mm between lines) seems to lead to an increase of the series resistance, reaching a value of 4.1 Ω cm^2 for experiment number 8 (Figure 76).

Experiment number 6 seems to be the one that leads to best results in overall. It presents a value of open-circuit voltage of 0.625 V, being the highest of the ones obtained and therefore indicating a reduction on the recombination in that small cell. In addition to this, the short-circuit current density attains a value of 35.8 mA/cm^2, which also constitutes a good result. With respect to the fill factor, a value of 73.1 % is reached. Series resistance is another parameter that needs to be considered. Experiment number 6 shows a value of 2.5 Ω cm^2. A lower and therefore better value is obtained for experiment number 1 but this one shows the worst results for open-circuit voltage and short-circuit current density parameters.

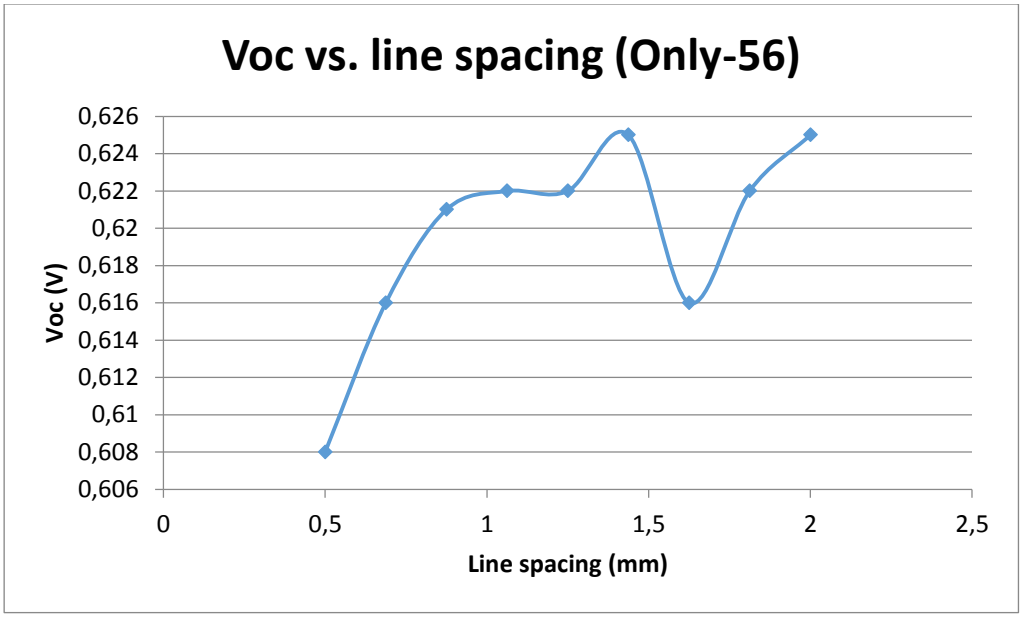

Figure 75. Graph representing open-circuit voltage versus line spacing

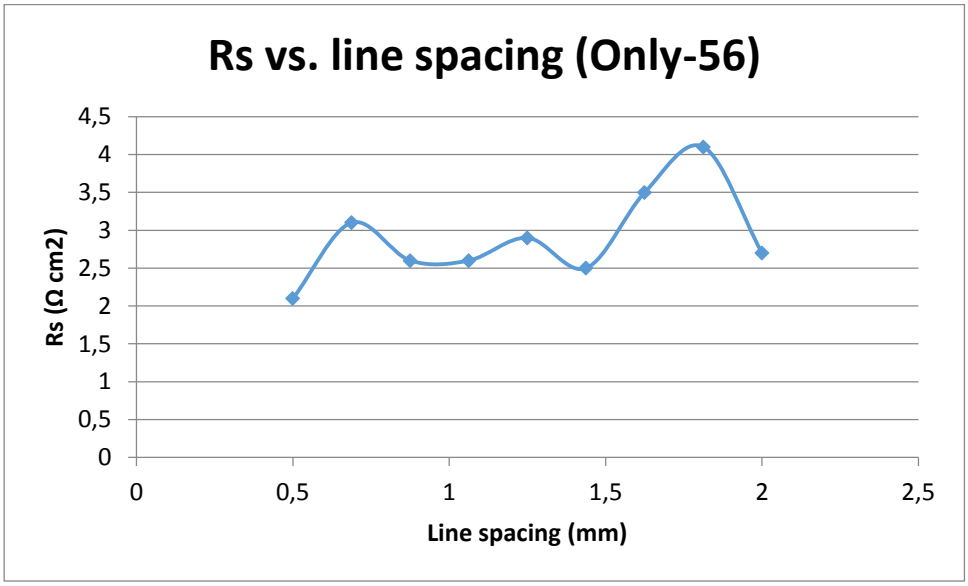

Figure 76. Graph representing series resistance versus line spacing

Cell ***Ra-25*** is processed as an entire cell unifying the best results obtained for *Only-54* and *Only-56*, summarized in **Figure 59**.

The characterization performed to this solar cell is the IV curve measurement.

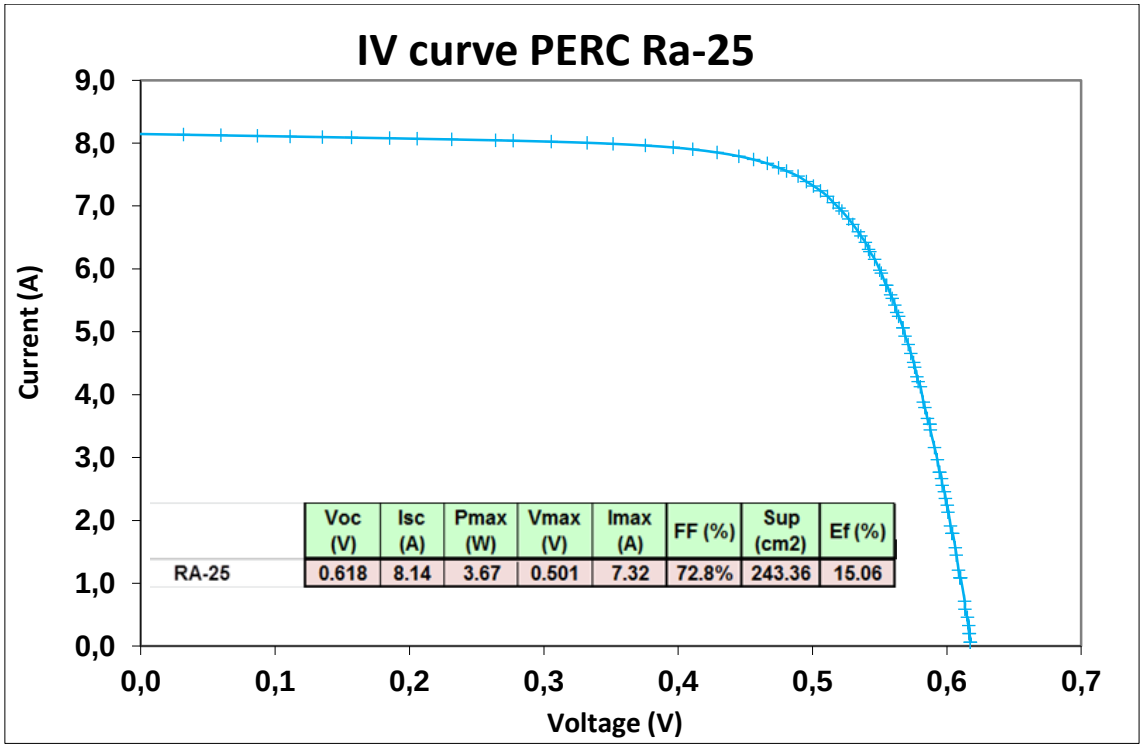

Figure 77. IV curve for Ra-25 PERC solar cell

In comparison with previous experiments, not higher values of V_{oc} and I_{sc} are shown in Figure 77. In fact, short-circuit current values are slightly lower than in previous experiments. Fill factor remains inside the range of results obtained before, which means that series resistance still takes high values.

In order to improve these results, whether laser damage was induced should be investigated, as well as passivation layers improved, since reduction on the recombination velocity is not attained.

PERC cell with points design

The wafers processed were *Only-55*, *Only-57* and *Ra-28.* As in the case of lines, the cells were characterized to study the behavior of each experiment separately from the others, in order to establish differences among them.

Cell ***Only-55*** contained the nine experiments described in section *5.2.1.2.- Rear dielectric laser ablation: Points*. In order to analyze the results it is important to know the position of each experiment on the rear side of the wafer and the nomenclature used to define them (Figure 62). The rear design was the one corresponding to parameters' variation.

→ IV curve measurement

As in the previous case, IV curves of each small cell were measured (Figure 78).

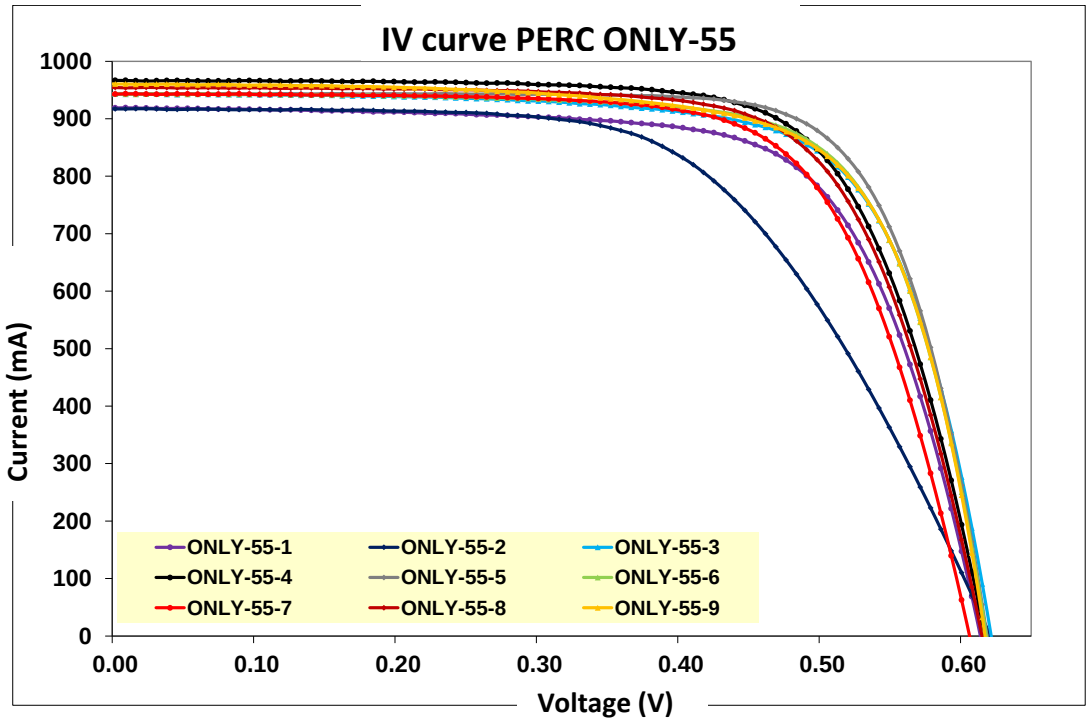

Figure 78. Representation of the IV curve of PERC Only-55 solar cell

In this case, a clear relationship between the number of pulses per point and the electrical parameters was not found (Table 8). Open-circuit voltage reaches its maximum value for experiments number 3 and number 2 (Figure 79), that is, for 17 and 15 pulses per point respectively.

	Voc (V)	Jsc (mA/cm^2)	Pmax (mW)	FF (%)	Área (cm^2)	Ef (%)
ONLY-55_1	0.614	34.6	394.8	70.0	26.52	14.89
ONLY-55_2	0.621	34.6	337.4	59.2	26.52	12.72
ONLY-55_3	0.622	35.9	421.1	71.8	26.27	16.03
ONLY-55_4	0.617	36.1	425.1	71.2	26.78	15.87
ONLY-55_5	0.619	35.2	438.6	75.1	26.78	16.38
ONLY-55_6	0.618	35.6	424.9	72.9	26.52	16.02
ONLY-55_7	0.606	34.2	400.2	70.0	27.56	14.52
ONLY-55_8	0.615	34.6	416.8	71.0	27.56	15.12
ONLY-55_9	0.617	35.2	422.9	71.3	27.30	15.49

9	6	3
8	5	2
7	4	1

Rp (Ωcm^2)		
2396	14523	2891
12894	7478	1779
3323	15950	1016
Rs (Ωcm^2)		
2.3	2.3	2.5
2.6	2.3	5.2
2.6	2.6	2.7

Table 8. Electrical parameters of PERC Only-55 solar cell

Experiment *Only-55_2* presents a high value of series resistance, which was necessarily caused by a problem during the fabrication process.

In solar cell number 5 is in which the highest value of fill factor is achieved (75.1 %). It is observed that experiments number 5, 6 and 9 are the ones that present the best behavior with respect to series resistance, as illustrated in Figure 80 and Table 8.

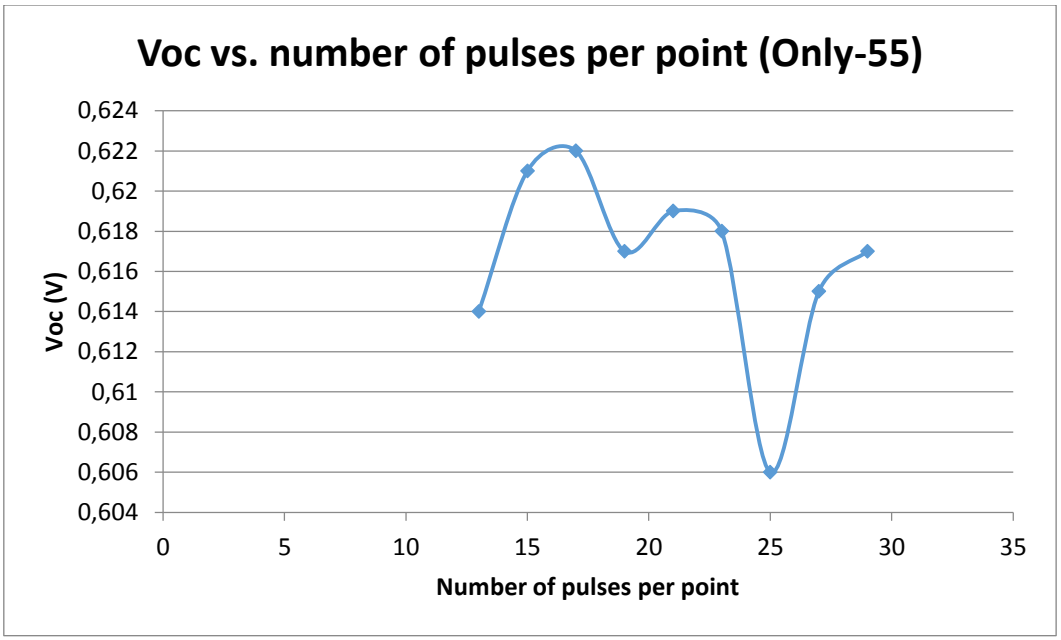

Figure 79. Graph representing open-circuit voltage versus the number of pulses per point applied

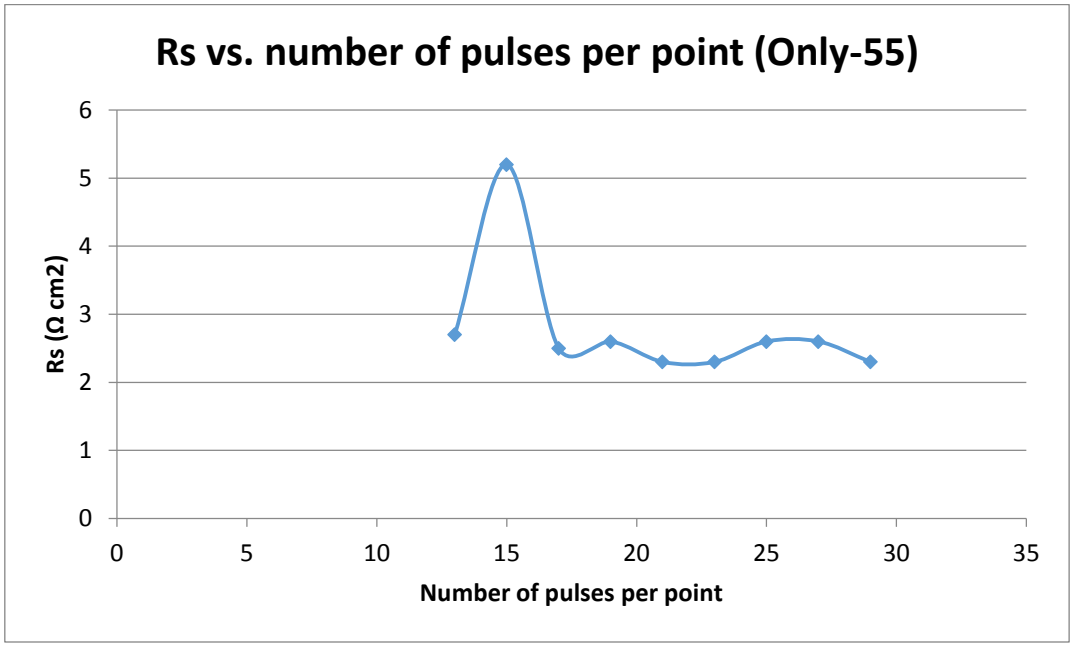

Figure 80. Graph representing series resistance versus number of pulses per point applied

The next characterization is performed to ***Only-57*** solar cell, where opening spacing is varied for point geometry. The cells were characterized to study the behavior of each experiment separately from the others, in order to establish differences among them.

The position of the experiments on the wafer and the nomenclature used for identifying them is represented in **Figure 66**.

→ IV curve measurement

The results from this test are represented in **Figure 81**, where a different IV curve is drawn for each of the small cells in which *Only-57* divides.

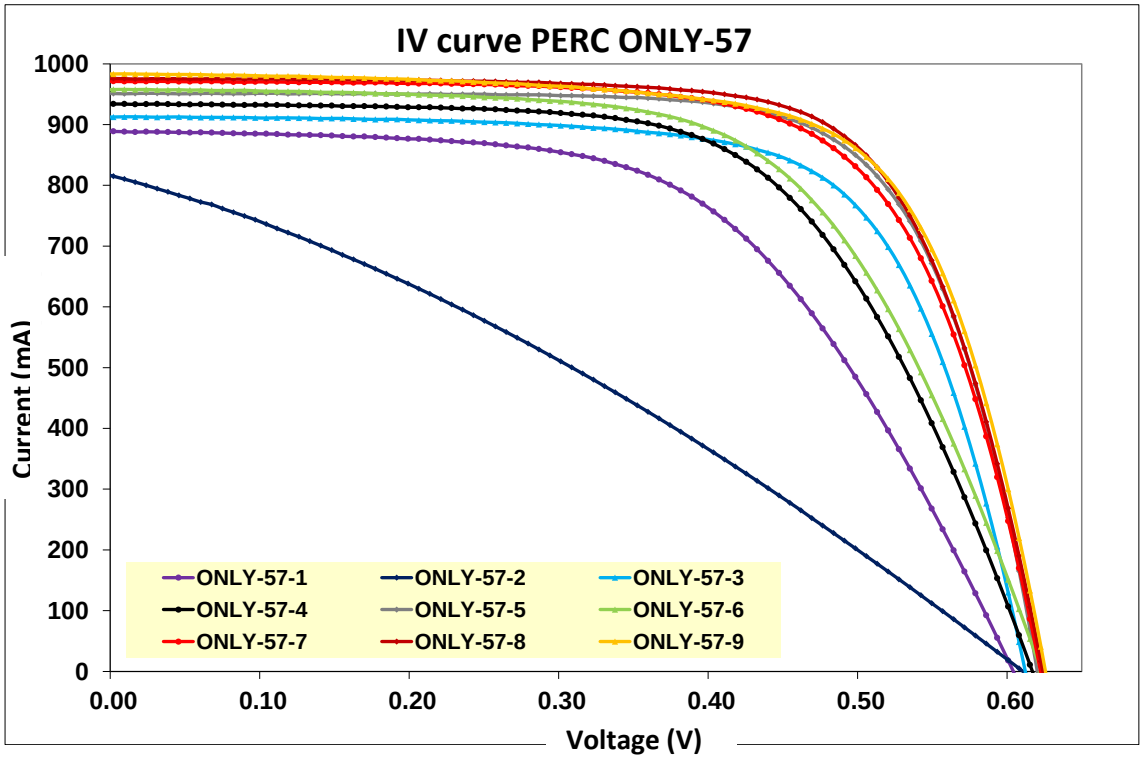

Figure 81. IV curve of PERC Only-57 solar cell

In Table 9 and at the same time illustrated in Figure 82, a clear increasing tendency of the value of open-circuit voltage can be observed as the opening spacing increases. Series resistance values seem to decrease in overall at the same time that V_{oc} increases, although it does not follow a clear tendency, as shown in Figure 83, but it seems that the increasing of the distance between points reduces recombination.

	Voc (V)	Jsc (mA/cm^2)	Pmax (mW)	FF (%)	Área (cm^2)	Ef (%)
ONLY-57_1	0.604	33.5	305.5	56.9	26.52	11.52
ONLY-57_2	0.611	30.8	155.3	31.1	26.52	5.85
ONLY-57_3	0.612	34.7	387.3	69.3	26.27	14.75
ONLY-57_4	0.617	34.9	357.6	62.1	26.78	13.35
ONLY-57_5	0.620	35.5	424.3	71.9	26.78	15.84
ONLY-57_6	0.623	36.1	369.9	62.0	26.52	13.95
ONLY-57_7	0.622	35.2	416.7	68.9	27.56	15.12
ONLY-57_8	0.624	35.4	432.6	71.0	27.56	15.70
ONLY-57_9	0.626	36.0	429.5	69.8	27.30	15.74

9	6	3
8	5	2
7	4	1

Rp (Ωcm^2)		
1133	1417	1691
5992	13266	50
5096	2723	916
Rs (Ωcm^2)		
2.8	4.2	2.7
2.8	2.5	14.6
2.8	4.3	5.3

Table 9. Electrical parameters of PERC Only-57 solar cell

For the short-circuit current density parameter, a similar tendency is observed despite the presence of some jumps in which high values are obtained in the middle of the spacing range.

The incorrect shape of the IV curve for experiment number 2 is due to a very low fill factor value (31.1 %). This lowering is not associated to the particular spacing of the experiment, but to an additional problem during the fabrication process.

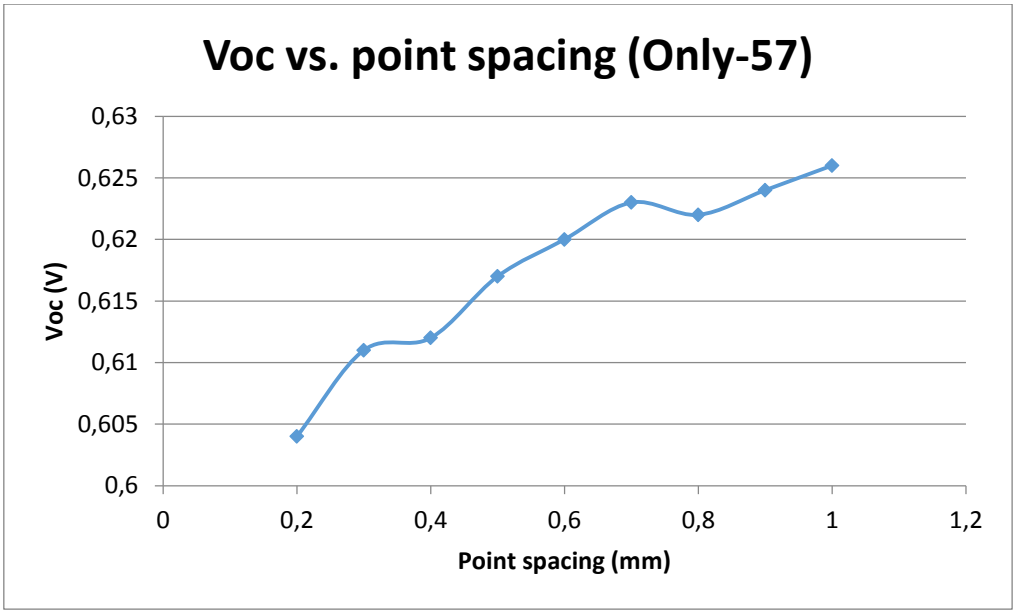

Figure 82. Graph representing open-circuit voltage versus point spacing

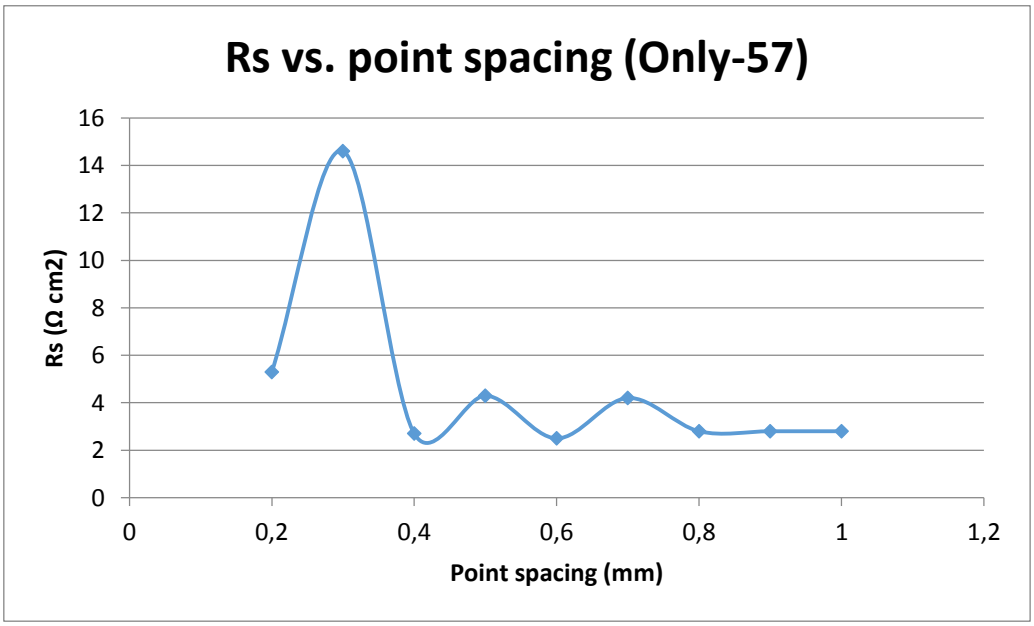

Figure 83. Graph representing series resistance versus line spacing

In the images from the electroluminescence test (Figure 84), it can be observed that front contacts were not correctly printed and therefore dark regions appear on the surface.

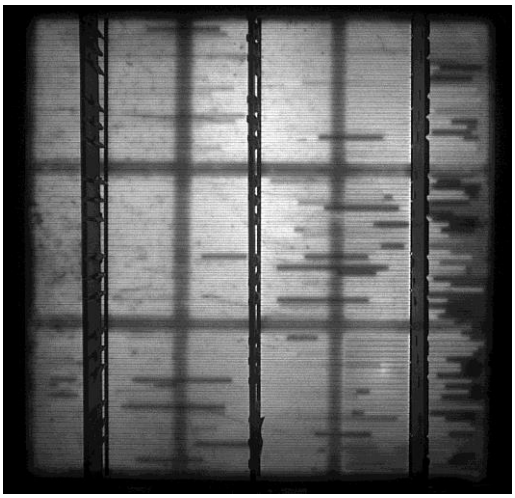

Figure 84. High polarity electroluminescence test for PERC Only-57 solar cell

These screen-printing defects have also an influence on the electrical parameters, increasing series resistance.

Ra-28 solar cell is processed as an entire cell unifying the best results obtained for *Only-55* and *Only-57,* which are summarized in Figure 67.

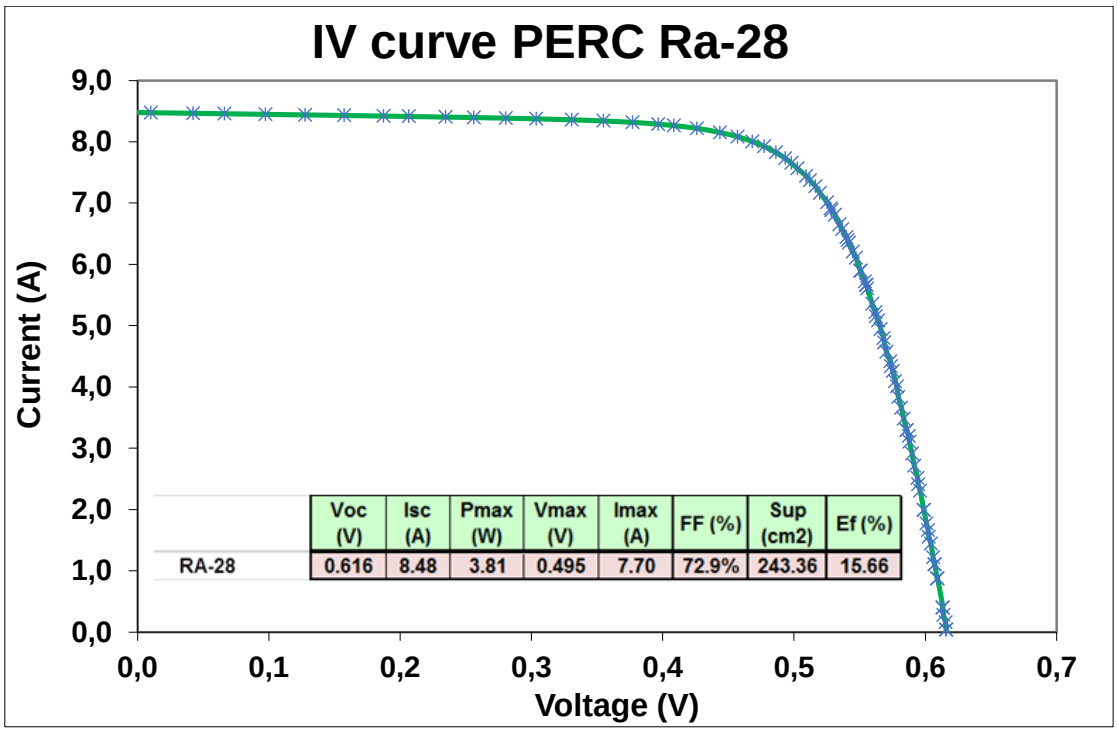

Figure 85. IV curve for Ra-28 PERC solar cell

The results obtained with the best parameters derived from the prior experiments (**Figure 85**) do not show the expected improvements. Open-circuit voltage values are similar to the ones obtained in the performed tests, and even slightly lower than some of them. With respect to short-circuit current values, they are neither improved compared to previous tests.

In order to improve these results, as occurred in the case of line design, whether laser damage was induced should be investigated, as well as passivation layers improved, since reduction on the recombination velocity is not attained.

6.- CONCLUSIONS

Crystalline silicon solar cells were processed in CENER according with Al-BSF architecture in order to establish a baseline. Moreover, as an improvement of this standard solar cell architecture, a high efficiency approximation, called PERC (Passivated Emitter and Rear Cell) was developed.

The main object of this FDP was the contact formation process, so different procedures were established to assure the quality of the contact. On this regard, screen printing process of front and back contacts was developed for all the experiments, based on the protocols and equipment available in CENER for standard Al-BSF solar cells. In addition, new developments were carried out in laser and screen printing processes to lead with the modifications of the fabrication route for PERC solar cells.

The main conclusions of this study can be summarized as follows:

1) The cleaning and operating procedure for screen printing process was improved in order to find the best and more efficient way to create front and back contacts. Instructions for any user that would need to make use of the system have been written, see *APPENDIX I. OPERATION PROTOCOL.*

2) Apart from this, in-depth knowledge was gained on different characterization techniques available in CENER i.e. I-V curve, thermography, spectral response and electroluminescence as well with auxiliary equipment as optical microscopy.

3) AL-BSF architecture

Operative Al-BSF solar cells were processed following standard process sequence available in CENER.

- In processed solar cells, *Only-25* and *Iris-08*, defects in contact formation were found: the first problem detected was that the fingers were not well-printed and some areas with no current collection appeared as shown in electroluminescence images. The second problem was that shunts related with metallic contamination were formed after screen printing.

  The solution to these problems was to stir harder Ag front screen printing paste in order to reduce viscosity and to let the paste flux through the finger openings of the screen more easily. Apart from this, the metallic contamination causing shunts was solved improving cleaning procedure tools used during screen printing process and avoiding any contact with the operator gloves during processing.

- Leaving aside these problems affecting series and shunt resistance and so fill factor, the rest of the parameters of the processed solar cells, I_{sc} and V_{oc}, were equivalent to

solar cells previously processed in CENER by the same route so the baseline was established.

- A modification of the process sequence of Al-BSF solar cells was made in order to obtain solar cells able to be soldered and form a module, solar cells *Iris-12*, *Iris-13*, *Only-26* and *Only-27*. The modification consists on introducing at the back contact of the solar cells a new screen printing step to define soldering pads. For this purpose, new pastes and screens were used to print in one step the Al back contact and in the following step the Ag-Al soldering pads.

  The screen printing process was successful also with this modification but some remaining issues emerged. These are that at the screen printing process sequence, depositing first Al back contact and then the Ag-Al soldering pads, was not adequate. Ag-Al paste did not fix onto the Al back contact properly and loss of material occurred at this zones. These delivered zones of high series resistance which degraded solar cell performance.

4) PERC architecture

Operative PERC solar cells were processed following a modified process sequence including a step for depositing a back passivation layer, the laser ablation to form local contacts at the openings, and back contact screen printing process with a new paste and screen.

- There were two geometries tested for the back contact of the PERC solar cells: lines and points, and a summary of the solar cells processed can be seen in the following table (**Figure 86**).

Geometry	Experiment 1: to find laser parameters ranges	Experiment 2: to find laser parameters ranges	Experiment 3: to find laser parameters ranges	Experiment 4: to find laser parameters ranges
Lines	Dummy silicon wafer	*Only-54*	*Only-56*	*Ra-25*
Points	Dummy silicon wafer	*Only-55*	*Only-57*	*Ra-28*

Figure 86. Summary of processed PERC solar cells

In order to find the best parameters, V_{oc} and R_s are the two parameters analyzed in detail. It is known that the best contact will be a compromise between less back surface recombination (higher V_{oc}) and so, lower laser ablation, and low series resistance and so, higher laser ablation.

- Regarding **lines structure**, the main findings are:
  - A laser current in the range between 19 A and 25 A is able to ablate, partially or totally, the dielectric layer for a frequency of 20 kHz and a mirror velocity of 800 m/s.
  - When varying laser current in the range of 20 A to 25 A and overlap in the range of 0.1 to 0.5 while keeping laser frequency at 20 kHz and distance between lines at 1 mm, the best compromise between high Voc and low Rs is found at around values of laser current of 22 A and 0.27 overlap (which corresponds to 800 mm/s mirror velocity).
  - When varying distance between lines and keeping laser frequency at 20 kHz and laser current at 22 A, the best compromise between high Voc and low Rs is found at around 1.4375 mm of line spacing.
  - With the optimal values of distance and laser parameters, a 156 mm x 156 mm solar cell has been processed. These optimal values are summarized in the following figure (Figure 87).

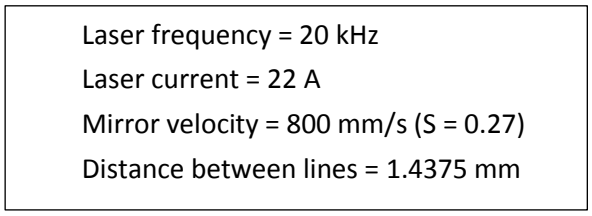

Figure 87. Summary of optimal parameters for lines laser ablation

- Regarding **points structure**, the main achievements are:
  - More than 11 pulses per point need to be applied to perform openings on the dielectric layer for a frequency of 20 kHz, a mirror velocity of 800 mm/s and a laser current of 25 A.
  - When modifying the number of pulses applied per point in the range from 13 to 29 pulses, keeping laser frequency at 20 kHz, laser current at 25 A, mirror velocity at 800 mm/s and point spacing at 0.5 mm, the best compromise between high Voc and low Rs is found at around 17 pulses per point.
  - When modifying distance between points and keeping frequency at 20 kHz, laser current at 25 A, mirror velocity at 800 mm/s and number of pulses per point at 27, the best compromise between high Voc and low Rs is found at around 1 mm.
  - With the optimal values of point distance and laser parameters, a 156 mm x 156 mm solar cell has been processed. These optimal values are summarized in the following figure.

Laser frequency = 20 kHz
Laser current = 25 A
Mirror velocity = 800 mm/s
17 pulses per point
Distance between points = 1 mm

Figure 88. Summary of optimal parameters for points laser ablation

7.- FUTURE LINES

Although the obtained results are not better than that of standard solar cells, the basis for the development of PERC solar cells has been established. Optimum parameters for the laser ablation and geometry design have been found and the processing of PERC solar cells attained.

Future lines are depicted here in order to continue the development of this solar cell technology:

- The geometry used for the series of experiments of points was a square geometry. Points can also take different dispositions to form ablated areas with triangular or hexagonal structures. Hence, experiments should be carried out to see whether better results are obtained with these geometries.
- Front and rear passivating layers need to be optimized in order to get a good passivating and anti-reflecting effect, which appears to be non-optimal on the experiments of the present Project.
- Research needs to be carried out to find the reasons for the increase in series resistance with respect to the cells processed according to Al-BSF structure.
- Tendencies regarding the best laser parameters and spacing have been observed. However, process repetitiveness needs to be checked in order to verify this tending.

8.- REFERENCES

[1] P. G. V. Sampaio, M.O. A. González, "Photovoltaic solar energy: Conceptual framework", *Renewable and Sustainable Energy Reviews,* 2017.

[2] "Best Research-Cell Efficiencies", NREL, 2017. [Online]. Available: https://www.nrel.gov/pv/assets/images/efficiency-chart.png. [Accessed: Jun 9, 2017]

[3] P. Wuerfel, "Physics of Solar Cells: from basic principles to advanced concepts", Book, Wieley-VCH Verlag GmbH&Co., 2009

[4] C. Honsberg, S. Bowden, "Photovoltaics: Devices, Systems, and Applications. Part 1: Photovoltaic devices", University of New South Wales, 1999.

[5] U. Wuerfel, A. Cuevas, P. Wuerfel, "Charge Carrier Separation in Solar Cells", IEEE Journal of Photovoltaics, Vol. 5, N. 1, 2015

[6] Micromaster Fraunhofer.

[7] J. Wu, X. Wang, G. Xing, "PERC Solar Cells and its Road to Industry", *Canadian Solar Inc.*, China.

[8] M. Hermle, "Silicon Solar Cells - Current production and future concepts", *Fraunhofer Institute for Solar Energy Systems ISE*, Brussels, 2017.

[9] T. Dullweber, J. Schmidt, "Industrial Silicon Solar Cells Applying the Passivated Emitter and Rear Cell (PERC) Concept - A review", *IEEE Journal of Photovoltaics*, vol. 6, Sep 2016.

[10] K. Wijekoon *et al.*, "Optimization of Rear Local Contacts on High Efficiency PERC Solar Cells Structures", *Hindawi Publishing Corporation*, International Journal of Photoenergy, Mar 2013.

[11] F. Colville, "Laser processing enables high-efficiency silicon-cell concepts", *Photovoltaics World*, USA, 2009.

[12] M. Gebhardt, T. Kiebling, M. Grimm, "Laser Contact Opening of High Efficient Solar Cells", *Laser Technik Journal*, 2014.

[13] H. Huang *et al.*, "20.8% industrial PERC solar cell: ALD Al_2O_3 rear Surface passivation, efficiency loss mechanisms analysis and roadmap to 24%", *Solar Energy Materials and Solar Cells,* vol. 161, Mar 2017, pp.14-30.

[14] R. Hendel, J. Liu, "Developments on laser drilling technology and ablation of dielectric lasers for c-Si cells, *Backcontact workshop*, Shangai, 2012.

[15] D.-H. Neuhaus and A. Münzer, "Industrial Silicon Wafer Solar Cells*", Hindawi Publishing Corporation,* vol.2007, ID 24521, Sep 2007.

[16] "Chapter 8: Diffusion", City University. [Online]. Available: http://personal.cityu.edu.hk/~appkchu/AP4120/8.PDF. [Accessed: Jun 12, 2017].

[17] L. J. Caballero, "Contact Definition in Industrial Silicon Solar Cell" in *Solar Energy*, Ed. Radu D Rugescu, Croatia: InTech, 2010, pp. 375-398 [Online]. Available: https://www.intechopen.com/books/solar-energy/contact-definition-in-industrial-silicon-solar-cells. [Accessed: Mar 16, 2017]

[18] S.R. Reddy, R. Prasad, A. Sharan, B. Prasad, "Development of Laser Edge Isolation Process for Industrial Solar Cells", *International Journal of Innovative Research in Science, Engineering and Technology,* vol. 2, Issue 10, 2013.

[19] S. M. Iftiquar *et al.*, "Fabrication of Crystalline Silicon Solar Cell with Emitter Diffusion, SiNx Surface Passivation and Screen Printing of Electrode", chapter 3, 2012.

APPENDIX I. OPERATION PROTOCOL

OPERATION PROTOCOL – SCREEN PRINTING

1) Clothing and protecting equipment needed to fulfill the screen-printing process:
   - **Lab coat.**
   - **Gloves.** Necessary to wear at any time 2 pairs of gloves: one of them of latex gloves (white color) and the other pair of nitrile gloves (blue color), or the other way around. It is recommended to change the outer pair whenever necessary since metallization pastes easily strain hands.
   - **Googles.** In order to protect eyes against the break of wafers, in particular multicrystalline wafers, which break into a high quantity of pieces that could cause serious damage.
   - **Two-filter mask.** To protect from pastes toxicity.
   - In case of wearing long hair, to tie it up.
   - **Over-sleeves.** To protect wrists and arms during cleaning of the used tools.

   Materials which are necessary to have inside the room where screen-printing is going to be done:

   - **Screen-printing manual.** In it all the steps to be followed to configure the program Compact 29 will be indicated.
   - **Nitrile gloves' box** to be able to change the wearing gloves by new ones when necessary.
   - **Insulating tape, scissors and cutter.** To open the paste jar and to close it again with new insulating tape once the process finished.
   - Piece of **removable transparence** to put it on one edge of the table.
   - **Pliers** to take the wafers and transport them. They should be always cleaned at the beginning of the process.
   - **Stirring bars.** Used to stir the paste inside the jar in order to homogenize it.
   - **Thermometer.** To control the temperature inside the room.
   - **Containers.** Where metallized wafers will be deposited.
   - **Paper roll** to protect tables and others.
   - **Wafers** to be metallized, having each of the corresponding identification. EACH TIME A MAXIMUM OF 5 WAFERS WILL BE SCREEN-PRINTED.
   - **Squeegees.** Different ones of silver and aluminium. Always necessary to use with the metallic bars.

- **Screen.** The one needed for the screen-printing process that is going to be performed.
- **Screws and "allen" keys** to screw the screen to the structure that fixes it.
- **Metallization paste.** Used in combination with the previously mentioned screen.
- **250-ml beaker.** Inside the furnace, to put the metallized wafers over them.

For the cleaning process:

- **IPA**. To clean the used screens, the stirring bars and other used tools. Quantities:
  - Washing bottle, filled ¾ of it approximately.
  - Big bottle with capacity for 5 L, full or nearly full.
- Special screen-printing cloths. They should not leave particles since they will be used for the screen cleaning.
- Solid wastes collecting bin. Blue color. It should be labeled and to it the wet papers of the cleaning will be thrown.
- Liquid wastes collecting bin. White color. Always correctly labeled and to it the contaminated IPA will be thrown.
- Funnel. To help throwing the liquid wastes.
- Chronometer. To measure the time the cells need to be inside the furnace.

2) Make the rest of the employees aware that screen-printing is going to be done in the lab and that they cannot go into the room.

3) Introduce the paste jar inside the room before starting acclimatization. The objective is that it gets to the room's temperature.

4) Turn on the drying furnace.
   - To 180 °C if the fulfilled process is aluminium screen-printing.
   - To 200 °C if the process is silver metallization.

   Make sure that there is nothing inside the furnace with exception of the 250-ml beakers, over which the solar cells will be posed to dry.

5) To acclimatize the room, for the temperature to be in the range of 20-25 °C (better to be near 25 °C). For turning on the conditioned air in hot position select in the device the position in which hot air goes out and fix intensity in the low level. Make sure that extractions are turned on.
   With respect to the extractions, initially the following need to be turned on:
   - Chemical bench extraction in the screen-printing room.
   - Chemical bench located out of the room.

6) Leave in a corner all the material used for the screen-printing of a different metal. It is convenient to maintain them separated and clean to avoid metallic contamination.

7) Leave each of the necessary objects in a different place so that the process execution is done in an easier way.
   - In the grey table located on the left of the machine leave the wafers that will be printed, inside a tray. Each wafer will be with its serviette, where the identification will be written.
   - In the table where the optical microscope is, a tray with a paste jar will be located, having covered the table with paper pieces to protect it. It will be the place where the paste jar will be opened, and where it will be stirred with the help of stirring bars to get the desired texture.
   - Over the chemical bench, and particularly on the right of the screen-printing machine (or where space for it is found), a tray it will be located where the serviettes corresponding to each cell will be left.
   - Also over the chemical bench, but in the opposite side, a tray will be located. This tray will be used for the cleaning of the used screen and should be the one corresponding to the metal that is being used. Each of them has written the name of the corresponding metal.
   - Leave the washing bottle and the IPA big bottle near the room or where the cleaning process is going to take place.

8) Once the room acclimatized, turn on the computer and follow the steps explained on the following lines to configure the correct screen-printing process.

   8.1. Open the program Compact 29.

   Click OK 3 times. Turn on “System Power” (equipment button) → OK.

   8.1. PRODUCT FILE PROCEDURES → Modify current product file: PLATA_SILIC.

   8.2.1 Print parameters (**Figure 89)**

   For metallization pastes Dupont PV17F and Al5132 and screen Harvey-Summer.

Print Parameters	Aluminio (Al)	Plata (Ag)
Foreward Speed	150mm/s	200mm/s (para Ag nuevas generaciones)
Reverse Speed	150mm/s	200mm/s
Front Pressure	16kg	16kg (antes 12kg)
Rear Pressure	16kg	16kg (antes 12kg)
Print Gap	1.3mm (antes1.5mm_año 2011)	1.3mm (antes1.5mm_año 2011)
Resto de puntos	X (no se tocan)	X (no se tocan)

Figure 89

SAVE, OK, CLOSE.

8.2.1 To take out the metallic structure from the machine. Open the upper tape and the lateral one. Screw the screen fixing the reverse side.

NOTE: The table can be slightly moved to center correctly the wafer with respect to the screen so it is not that important that the screen is exactly in that position.

Introduce the overall in the machine. The structure should be left in such a position that the measurements it has are read by the person working with the machine, as shown in Figure 90. Tighten the black roulettes. Close the covers.

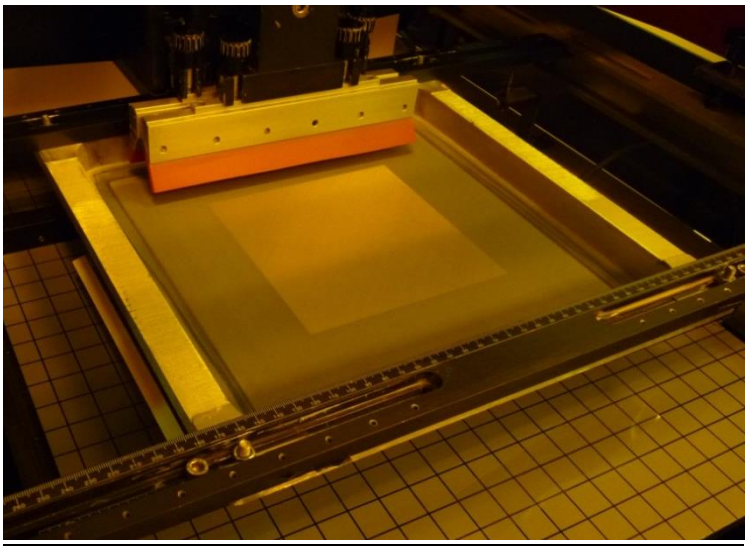

Figure 90

8.2.3 Print limits

REAR → The rear squeegee is screwed (the most separated screws in Figure 91Figure 92) → ADJUST BACKWARDS → STORE REAR LIMIT
FRONT → BACKWARDS (put the squeegee if necessary) → the front squeegee is fixed → ADJUST FORWARDS → STORE FRONT LIMIT → OK → Save new settings? YES
IMPORTANT: the used squeegees need to have always the metallic bars for the screen printing process to be correctly fulfilled.

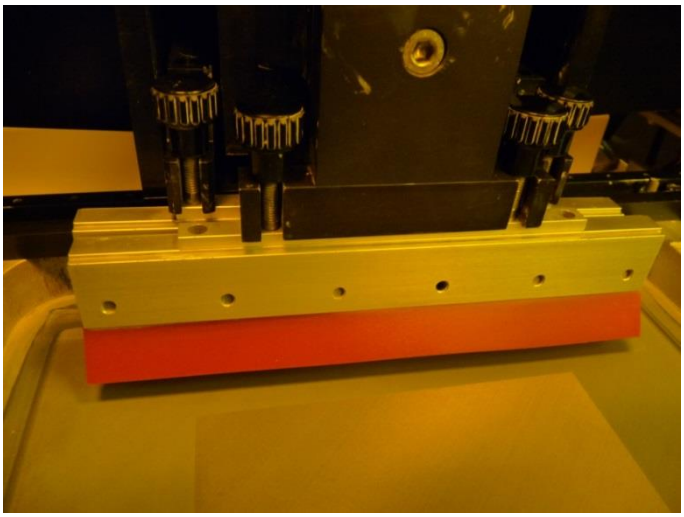

Figure 91

The sense of the squeegees should be the one shown in the following Figure 92.

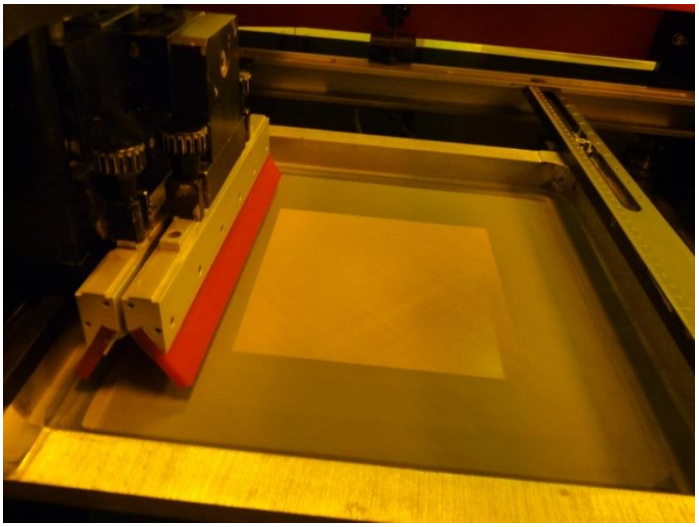

Figure 92

In the figure, the location of the screen with respect to the structure can be observed.

8.2.4 PCB on contact calibration

Introduce a wafer over the PCB (opening the cover by the black handle) → CONTINUE → Turn on vaccum tooling? NO → Coarse step? NO → Select FINE STEP
DIRECTION → TABLE UP (rise the PCB); TABLE DOWN if necessary → OK → YES

8.2.5 Squeege zero pressure calibration

Turn on vaccum tooling? → NO
REAR → With COARSE STEPS/ FINE STEPS, MOVE DOWN to the point when it touches → STORE POSITION
FRONT → With COARSE STEPS/FINE STEPS, MOVE DOWN to the point when it touches → STORE POSITION → OK
Save new settings? YES
CANCEL → CANCEL (to go back to the principal menu).

9) PRODUCTION in the principal menu.
   9.1. Prepare one acetate transparence and one moveable transparence piece, which will be located in the non-covered edge when vacuum is applied.
   9.2. Pulse the button RELEASE HEAD LATCHES. Fix the transparence in the table and apply vacuum. Close the machine cover that was opened.

NOTE: It is not necessary to use the transparence, the first test can be done on a dummy wafer cell.

9.3. Open the metallization paste and stir until it gets the correct texture.

9.4. Open the upper cover. Quit the front squeegee and add the paste, previously stirred, over the screen. For that process, the small transparent squeegee is used.
NOTE: 4 pieces of cello tape may not be necessary on the four corners of the wafer. Could be enough with a long cello tape piece on a non-covered edge and a moveable transparence piece on the other.

9.5. Fix the front squeegee.

9.6. Pulse PRINTING ENABLED and afterwards over the 2 yellow buttons of the machine (at the same time). This way, the first printing is performed.

9.7. Once the screen printing finished, pulse OPEN PRINT HEAD (RELEASE HEAD LATCHES), take the acetate away and leave it aside.

9.8. If the result of the screen printing process is correct, fix the wafer on the same position acetate was and with the help of the pliers. Fix 4 transparency pieces to cover the holes and the 4 cello tape pieces to fix over the 4 cut corners of the wafer. Apply vacuum.

9.9. ATTENTION → CONTINUE → CONTINUE → OK.

9.10. Pulse on the two yellow buttons at the same time to perform the first screen printing over the substrate.

9.11. In PRODUCTION menu, pulse on RELEASE HEAD LATCHES.

9.12. Quit vacuum, the transparency pieces and cello tape pieces. Take the substrate out of the machine and leave it in the containers previously mentioned.

9.13. Close the machine cover → OK → OK.

9.14. Follow steps from 9.8. to 9.13. with the rest of wafers.

10) When the whole process finished, send squeegees to rear (SEND CARRIER TO REAR) to open the upper cover and collect the excess of metallization paste again to the jar. For that, use the transparent squeegee.

11) Close the jar, fixing it correctly with insulating tape. Clean the outer part of the jar.

12) Take the structure where the screen is fixed out of the machine and separate the screen from the structure.

13) Turn in the general extraction of the lab.

14) Take the squeegees out from the machine.

15) Clean the screen before the metallization paste gets dry. For the process of cleaning, use warmed up IPA and paper. It is cleaned on both sides, rubbing with the paper until it does not get dirty. The squeegees also need to be cleaned. Wet papers go to the solid wastes collecting bin, while contaminated IPA is thrown to the liquid wastes collecting bin. THE CLEANING PROCESS IS PERFORMED AFTER THE SCREEN PRINTING OF ALL THE WAFERS (a maximum of 5).

16) Before starting the cleaning process or at the same time, the metallized wafers are transported to the drying furnace. Take the wafers with care from the tray with the help of pliers and leave them over the beakers inside the furnace. For the case of rear side screen printing, cells should be inside the furnace for 10 minutes at 180 °C. For the case of front side screen printing, cells will be inside also for 10 minutes at 200 °C.

17) Take the structure together with the screen out of the machine. Separate both.

18) Collect all the material use for the process and clean the room.
    - Clean the recipients where screens have been cleaned.
    - Eliminate metal rests on pliers or other used tools (as the trays used for taking the cells into the furnace).
    - Put the material used inside the boxes used for that purpose.
    - Take the solar cells out of the drying furnace when time ends, with the help of the pliers.
    - If other kind of screen printing is going to be done, put a different screen, the corresponding squeegees and perform another test on a transparency (instead of doing the following 3 steps).
    - If not, turn off the screen printing program:
      CLOSE → SHUTDOWN → YES → OK → OK → Open machine → Rise the upper cover → OK → Close machine → YES
    - Turn down the drying furnace.
    - Turn down all the extractions when the solar cells are out of the drying furnace (when they are taken out the evaporation of the solvents takes place).

APPENDIX II. PV17F METALLIZATION PASTE. DATA SHEET

DuPont™ Solamet® PV17F

photovoltaic metallization

Preliminary Technical Data Sheet

Product Description

DuPont™ Solamet® PV17F photovoltaic metallization front side paste is a highly conductive silver composition, part of the DuPont™ Solamet® PV17X family, designed to provide excellent efficiency, reliable soldered adhesion and low lay down. This paste may be cofired with back side (p-type) aluminum conductors such as DuPont™ Solamet® PV3XX and DuPont™ Solamet® PV5XX tabbing silvers. It is designed for rapid dry and very fast (spike) firing.

Product Benefits

- Improved efficiency over DuPont™ Solamet® PV16X family
- Designed to contact emitters with low phosphorous surface concentration (LDE cells)
- Optimized for low stress and high soldered adhesion
- Reduced junction damage
- Excellent solderability and consistent soldered adhesion
- Low lay down
- Fast drying and firing
- Excellent fine line capabilities
- Excellent ink transfer capability at fine line design
- High electrical conductivity after firing
- Cadmium free*

*Cadmium 'free' as used herein means that cadmium is not intentionally added to the product. Trace amounts however may be present.

Processing Summary

- **Application**
  Standard screen print process
- **Printing**
  Speed 6–10 in/sec (150–250 mm/sec)
- **Screen Type**
  325 mesh stainless steel preferred for >70µm open;
  290 or 400 mesh stainless steel preferred for ≤70µm

	(I)	(II)	(III)
Mesh (stainless steel)	290	325	400
Wire Diameter (µm)	20	23	18
Emulsion Thickness (µm)	20–25		
Mesh Angle (degrees)	22–30		

- **Drying**
  Vertical Dryer 170–230°C 10 minutes
  IR Belt Dryer 150–300°C 1 minute
  Flexible in accordance with industry practice. Actual settings to be determined by dryer type
- **Typical Line Resolution**
  50–100µm screen designed width
- **Soldering**
  Compatible with industry standard material and condition
  Flux type: non-clean, reactivity level L0/M0 (Standard: ANSI/J-STD-004)
  Ribbon: compatible with Pb contained and Pb free solder material, i.e. 60Sn/40Pb, 62Sn/36Pb/2Ag, 96.5Sn/3.5Ag

Table 1: Typical Physical Properties

Viscosity (Pa·s) (Brookfield HBT, 10 rpm SC4-14/6R utility cup and spindle, 25°C)	280–400
Solids (%) at 750°C	89.5–91
Fineness of Grind (4th/50%	≤16m/≤8m
Resistivity (m Ω/sq/10µm)	<5
Thinner	9450
Shelf Life (months)	6

All values reported here are results of experiments in our laboratories intended to illustrate product performance potential with a given experimental design. They are not intended to represent the product's specifications, details of which are available upon demand.

DUPONT®
The miracles of science™

Paste Preparation

The composition should be thoroughly mixed before use. This is best achieved by slow, gentle hand stirring with a clean burr-free spatula (flexible plastic) for 1–2 minutes. Jar rolling is NOT recommended, as this could change the rheology of the material. Care should be taken to avoid air entrapment.

Printing

Printing should be carried out in a clean, well-ventilated area. DuPont™ Solamet® PV17F photovoltaic composition, in its container, should be at ambient temperature prior to commencement of printing.

Firing

Solamet® PV17F is designed for rapid (spike) firing. Thermal budget above 600°C should be kept to minimum, ideally <8 seconds to ensure optimum electrical contact to the wafer. To get the best electrical performance, PV17F should be fired at a peak temperature around 30°C higher than for PV16X conductors.

See **Chart 1** for typical firing profile.

Actual furnace settings and belt speed will depend on the wafer thickness, texturing and emitter resistivity as these influence the temperature of the wafer during firing.

It is important that wafers are fired in a well ventilated furnace, with a continuous supply of clean filtered air. Airflow and extraction rates should be optimized to ensure that oxidizing conditions exist within the furnace firing chamber, especially when front and backside conductors are cofired.

Chart 1
Typical Firing Profile

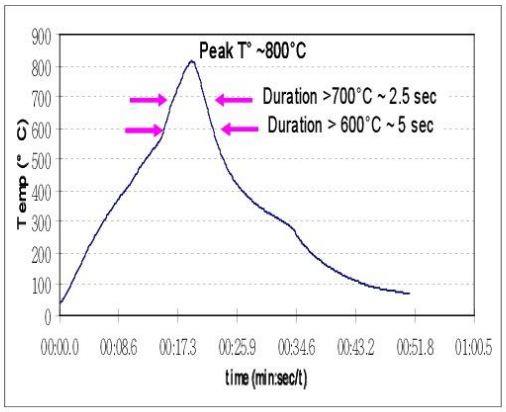

Thinner

Solamet® PV17F composition is optimized for screen printing and thinning is not normally required. Use the DuPont recommended thinner for slight adjustments to viscosity or to replace evaporation losses. The use of too much thinner or the use of a non recommended thinner may affect the rheological behavior of the material and its printing characteristics. Please refer to **Table 1**.

Storage and Shelf Life

Containers may be stored in a clean, stable environment at room temperature (between 5°C–25°C) with their lids tightly sealed. Storage in high temperature (>25°C) or in freezers (temperature <0°C) is NOT recommended as this could cause irreversible changes in the material.

Safety and Handling

For information on health and safety regulations please refer to the specific product MSDS.

For more information on DuPont™ Solamet® PV17F photovoltaic metallization or other DuPont Microcircuit Materials, please contact your local representative:

Americas
DuPont Microcircuit Materials
14 TW Alexander Drive
Research Triangle Park, NC 27709
USA
Tel +1 800 284 3382 (calls within USA)
Tel +1 919 248 5188 (calls outside USA)

Europe, Middle East & Africa
Du Pont (UK) Ltd
Coldharbour Lane
Bristol BS16 1QD
UK
Tel +44 117 931 3191

Asia
Du Pont Kubushiki Kaisha
Sanno Park Tower, 11-1
Nagata-cho, 2-chome
Chiyoda-ku, Tokyo, 100-611
Japan
Tel +81 3 5521 8650

DuPont Taiwan Limited
45, Hsing-pont Road
Taoyuan, 330
Taiwan
Tel +886 3 377 3616

DuPont China Holding Company Ltd
Bldg. 11, 399 Keyuan Road
Zhangjiang Hi-Tech Park
Pudong New District
Shanghai 201203
Tel +86 21 6386 6366 ext. 2202

DuPont Korea Inc.
3-5th Floor, Asia tower #726
Yeoksam-dong, Gangnam-gu
Seoul 135-719, Korea
Tel +82 10 6385 5399

E.I. DuPont India Private Limited
7th Floor, Tower C, DLF Cyber Greens
Sector-25A, DLF City, Phase-III
Gurgaon 122 002 Haryana, India
Tel +91 124 409 1818

Du Pont Company (Singapore) Pte Ltd
1 HarbourFront Place, #11-01
HarbourFront Tower One
Singapore 098633
Tel +65 6586 3022

http://mcm.dupont.com

The miracles of science™

APPENDIX III. Al5132 METALLIZATION PASTE. DATA SHEET

FERRO
ELECTRONIC MATERIALS
Delivering material advantages

Photovoltaic Materials

AL5132
Aluminum Conductor
Lead Free

Description: AL5132 aluminum conductor paste is a high open circuit voltage, low print weight conductor designed to form a p^+ doped layer when fired on p-doped silicon photovoltaic devices 160–200 microns thick. AL5132 accommodates variations in wafer surface texturization and other surface treatments to promote low distortion and a smooth surface. When properly processed on 150 mm x 150 mm wafers at 180 micron thickness, the material exhibits < 1.5 mm distortion. The material has been optimized to eliminate Al bead formation during the firing process. The product is lightly fritted using an environmentally friendly lead free glass composition and can be fired over a broad range of conditions including co-fire process techniques with front contact silver inks.

Target Physical Properties – Subject to Change	
	AL5132
Viscosity (Pa·s)[1]:	15.0–45.0
Dried Thickness (µm):	25–40
Fired Thickness (µm):	15–30
Wet Deposition (mg/cm^2):	4–6
Bowing for 180 micron wafer (mm):	< 1.5
Back Surface Field Thickness (µm):	6–10
Drying Profile[2]:	250–300 °C, < 60 seconds
Firing[2]:	810–940 °C, < 1–3 seconds
Recommended Thinner:	0804
Clean Up:	Isopropyl Alcohol (< 0.1% water)

All properties are target values and are not meant to represent product specifications.

Notes:
[1]Viscosity as measured on Brookfield model HBT cone/plate viscometer; 9.6 reciprocal seconds, 1.565° cone, 25°C.
[2] Recommended set points °C in infrared firing furnace.

Product Advantages:

- RoHS and WEEE compliant[3]
- Lead, cadmium and phthalate free[4]
- Exhibits < 1.5 mm camber on 150 mm x 150 mm wafers at 180 microns thickness
- Uniform BSF yields high electrical efficiency

www.ferro.com

FERRO
ELECTRONIC MATERIALS
Delivering material advantages

Photovoltaic Materials

AL5132
Aluminum Conductor Lead Free

Processing Recommendations

Printing: It is recommended that the paste temperature is between 20–25°C prior to printing, and it is advisable to control the ambient room temperature within ± 2°C to ensure consistent printing results. The printing area should be clean and adequately ventilated.

Screen: Screens with the following mesh/wire diameter/emulsion Thickness in µm is recommended: 200/40/5; 250/30/5; 280/35/5; and 325/23/10. Increase in mesh count decreases wet paste print weight and fired thickness.

Drying: The ink can be dried in an infrared or conventional dryer under a wide range of conditions. Inks are typically dried in an IR dryer with set points of 250–325°C in less than 60 seconds. If a convection dryer is used, set points of 130-170°C and a residence time of 9-11 minutes is recommended.

Firing: An infrared fast process furnace with three or more firing zones and belt speeds of > 200 inches per minute is highly recommended, although the product may be fired in a variety of furnaces with belt speeds > 120 inches per minute. Optimum firing conditions must be established by the customer based on the cell configuration, thickness, and manufacturing process. Peak set point temperatures between 830–940°C with a dwell time ranging from > 1 to 3 seconds above an actual (cell) temperature of 700°C is recommended.

Compatibility: Ferro has tested this material according to the recommended processing conditions described here, however, it is imperative that customers evaluate the material in their manufacturing process and conditions to ensure suitability for their intended use. Ferro technical personnel can help facilitate testing, and can assist with integration into customer manufacturing processes.

Thinning: Thinning is not recommended, since the paste is supplied at the correct viscosity for application. Contact your local Ferro Representative for appropriate solvent details should thinning become necessary to replace solvent lost through evaporation.

Transport, Paste Storage & Shelf Life: Climate controlled transport of the paste is required (5–30°C). The paste should be stored in tightly capped containers in a cool (20–30°C), dry and covered storage room away from direct sunlight. When properly stored, unopened material will have a shelf life up to 6 months.

Notes:
[3]EU Directive on Restriction of the use of Hazardous Substances (RoHS; 2002/95/EC and 2010/571/EU amendments) include exemptions for lead contained in the glass system of thick film materials used in electronic components. Customers need to verify that their applications fall within the RoHS exemptions, and and thus RoHS compliant. RoHS compliance results in exemption from WEEE (2002/96/EC). In anticipation of future amendments and more stringent environmental regulations, Ferro continues to expand its range of Lead Free[4] materials.
[4]Initial product composition was certified by a third party laboratory to be below the detection level for lead, cadmium and seven main phthalates in commerce today and, therefore, is considered to be lead, cadmium and phthalate free. Lead, cadmium and phthalates are not part of the formulation for this product. However, this conductor paste is not routinely analyzed for lead, cadmium and phthalate content. Lead, cadmium and phthalate content are not included in the product specification, are not included in Certificate of Test or Analysis, and are not the basis for any guarantee or warranty.

Rev.09/12

Vista, CA, USA +1 760-305-1000
Tsukuba, Japan +81 29-889-2144
Suzhou, China +86 512-62562258
Hanau, Germany +49 61-8159473

www.ferro.com

APPENDIX IV. PV52A METALLIZATION PASTE. DATA SHEET

DuPont™ Solamet® PV52A

Technical Data Sheet

Product Description

DuPont™ Solamet® PV52A photovoltaic metallization back side paste is a highly conductive solderable silver composition, developed to lower consumption yet providing excellent adhesion when used in conjunction with back side aluminum compositions. This paste may be co-fired with front side (n-type) silver conductors such as DuPont™ Solamet® PV17x, PV18x and with back side (p-type) aluminum conductors such as DuPont™ Solamet® PV3xx.

Product Benefit

- Excellent solderabililty
- High adhesion with ultra low consumption
- High conductivity
- Compatible with back side Al metallizations
- Co-fireable with front side silver and back side aluminum
- Good printing characteristics
- Lead and cadmium free*

*Cadmium 'free' as used herein means that cadmium is not an intentional ingredient in and is not intentionally added to the referenced product. Trace amounts however may be present.

Processing Summary

- **Application**
  Standard screen print process
- **Printing**
  Speed 6–8 in/sec (150–250 mm/sec)
- **Drying**
  Vertical Dryer 170 – 230°C 10 minutes
  Vertical Dryer 170–230°C 10 minutes
  IR Belt Dryer 220–270°C 30 seconds
  Flexible in accordance with industry practice. Actual settings to be determined by dryer type
- **Screen Type**
  150-280 mesh stainless steel with 5–15 µm emulsion
- **Typical Line Thickness**
  3–5µm
- **Soldering**
  Compatible with industry standard material and condition
  Flux type: non-clean, reactivity level L0/M0 (Standard: ANSI/J-STD-004)
  Ribbon: compatible with Pb contained and Pb free solder material, i.e. 60Sn/40Pb, 62Sn/36Pb/2Ag, 96.5Sn/3.5Ag

Table 1: Typical Physical Properties

Viscosity (Pa·s) (Brookfield HADV, SC4-14/6R @ 10 rpm, 25°C))	50–100
Solids (%) at 750°C	43–45
Fineness of Grind (4th/50%)	<12µm/<6µm
Thinner	9450
Shelf Life (months)	6

Paste Preparation

The composition should be thoroughly mixed before use. This is best achieved by slow, gentle hand stirring with a clean burr-free spatula (flexible plastic) for 0.5–1 minutes. Jar rolling is NOT recommended, as this could change the rheology of the material. Care should be taken to avoid air entrapment.

Printing

Printing should be carried out in a clean, well-ventilated area. DuPont™ Solamet® PV52A photovoltaic composition, in its container, should be at ambient temperature prior to commencement of printing.

Firing

Solamet® PV52A is designed for rapid (spike) firing. Thermal budget above 600°C should be kept to minimum, ideally <8 seconds to ensure optimum electrical contact to the wafer. See Chart 1 for typical firing profile. Actual furnace settings and belt speed will depend on the wafer thickness, texturing and emitter resistivity as these influence the temperature of the wafer during firing.

It is important that wafers are fired in a well ventilated furnace, with a continuous supply of clean filtered air.

Airflow and extraction rates should be optimized to ensure that oxidizing conditions exist within the furnace firing chamber, especially when front and backside conductors are co-fired.

DuPont™ Solamet® PV52A

Technical Data Sheet

Thinner

Solamet® PV52A composition is optimized for screen printing and thinning is not normally required. Use the DuPont recommended thinner for slight adjustments to viscosity or to replace evaporation losses. The use of too much thinner or the use of a non recommended thinner may affect the rheological behavior of the material and its printing characteristics. Please refer to Table 1.

Storage

Containers may be stored in a clean, stable environment at room temperature (between 5°C–25°C) with their lids tightly sealed. Storage in high temperature (>30°C) or in freezers (temperature <0°C) is NOT recommended as this could cause irreversible changes in the material.

Safety and Handling

For information on health and safety regulations please refer to the specific product MSDS.

Chart 1
Typical Firing Profile

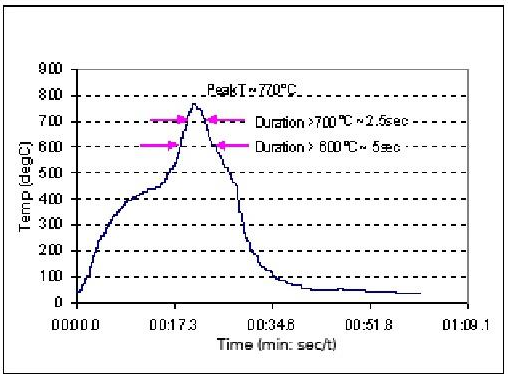

For more information on DuPont™ Solamet® PV52A or other DuPont Microcircuit Materials products, please contact your local representative:

Americas
DuPont Microcircuit Materials
14 T.W. Alexander Drive
Research Triangle Park, NC 27709
USA
Tel. +1800 284-3382 (calls within USA)
Tel. +1919 248 5188 (calls outside USA)

Europe, Middle East & Africa
Du Pont (U.K.) Limited
Coldharbour Lane
Bristol BS16 1QD
U.K.
Tel. +44-117-931-3191

Asia
DuPont Kabushiki Kaisha
MCM Technical Lab
DuPont Electronics Center
KSP R&D B213
2-1, Sakado 3-chom, Takatsu-ku,
Kawasaki-shi, Kanagawa, 213-0012
Japan
Tel +81 44 820 7575

DuPont Taiwan Ltd
45, Hsing-Pont Road,
Taoyuan, 330
Taiwan
Tel. +886-3-377-3616

DuPont China Holding Co. Ltd
Bldg 11, 399 Keyuan Rd., Zhangji Hi-Tech Park,
Pudong New District, Shanghai 201203
China
Tel. +86-21-6386-6366 ext.2202

DuPont Korea Inc.
3~5th Floor, Asia tower #726,
Yeoksam-dong, Gangnam-gu
Seoul 135-719, Korea
Tel. +82-10-6385-5399

E. I. DuPont India Private Limited
7th Floor, Tower C, DLF Cyber Greens,
Sector-25A, DLF City, Phase-III,
Gurgaon 122 002 Haryana, India
Tel. +91-124-4091818

Du Pont Company (Singapore) Pte Ltd
1 HarbourFront Place, #11-01
HarbourFront Tower One,
Singapore 098633
Tel. +65-6586-3022

http://mcm.dupont.com
http://photovoltaics.dupont.com

K-27391 09/13

APPENDIX V. PV36A METALLIZATION PASTE. DATA SHEET

DuPont™ Solamet® PV36A

Technical Data Sheet

Product Description

DuPont™ Solamet® PV36A photovoltaic paste is a high performance aluminum paste, part of the DuPont™ Solamet® 36x family, designed to provide excellent cell efficiency and low lay down on the PERC (Passivated Emitter Rear Cells) solar cell structure. This paste can be co-fired with DuPont™ Solamet® PV17x/18x front side metallization pastes and DuPont™ Solamet® PV56S tabbing silver. It is designed for rapid dry and very fast (spike) firing.

Product Benefits

- Excellent cell efficiency on the PERC structure*
- Low lay down
- Strong adhesion without damaging the passivation layer
- Strong hot water resistivity
- Good fired cosmetics (no bus bar discoloration, no pumping and low bowing)
- Compatible with the PERC structure cells with various rear-contact area formation processes, including laser ablation, laser firing, and etching paste
- Cadmium free**

*Solamet® PV36A delivers up to 1% cell efficiency improvement on the PERC structure, with 50% lay down compared to pastes for the conventional cell structure.
**Cadmium 'free' as used herein means that cadmium is not intentionally added to the product. Trace amounts however may be present.

Processing Summary

- **Application**
  Standard screen print process
- **Screen Type**

	(I)	(II)
Mesh count (stainless steel)	380	400
Wire diameter (µm)	14	18
Emulsion thickness (µm)	10	10

- **Printing**
  Speed 4–12 inch/sec (100–300 mm/sec)
- **Lay Down**
  0.8 g–1.2 g/6 inch wafer
- Thickness
  25 µm (after firing)
- **Drying**
  Vertical Dryer 170–230°C 10 minutes
  IR Belt Dryer 150–300°C 30 seconds

Flexible in accordance with industry practice. Actual settings to be determined by dryer type

Table 1: Typical Physical Properties

Fineness of Grind 4th Scratch 50% Point	</= 20 µm </= 10 µm
Viscosity (Pa·s) (Brookfield @ 10 rpm, 25°C)	20–65
Solids (%)	68.0–75.0
Thinner	8250
Shelf Life (months)	6

All values reported here are results of experiments in our laboratories intended to illustrate product performance potential with a given experimental design. They are not intended to represent the product's specifications, details of which are available upon demand.

Paste Preparation

The composition should be thoroughly mixed before use. This is best achieved by slow, gentle hand stirring with a clean burr-free spatula (flexible plastic) for 1–2 minutes. Jar rolling is NOT recommended, as this could change the rheology of the material. Care should be taken to avoid air entrapment.

Printing

Printing should be carried out in a clean, well-ventilated area. DuPont™ Solamet® PV36A photovoltaic composition, in its container, should be at ambient temperature prior to commencement of printing.

Firing

Solamet® PV36A is designed for rapid (spike) firing. Generally, Solamet® PV36A could be fired at the same firing profile as Al pastes for the conventional cell structure. the best firing peak temperature could be decreased (0 to -50°C) depending on types of cell structure including wafer thickness, texturing, emitter resistivity, and passivation structure.

See **Chart 1** for typical firing profile.

DuPont™ Solamet® PV36A

Technical Data Sheet

It is important that wafers are fired in a well ventilated furnace, with a continuous supply of clean filtered air. Airflow and extraction rates should be optimized to ensure that oxidizing conditions exist within the furnace firing chamber, especially when front and backside conductors are co-fired.

Thinner

DuPont™ Solamet® PV36A composition is optimized for screen printing and thinning is not normally required. Use the DuPont recommended thinner for slight adjustments to viscosity or to replace evaporation losses. The use of too much thinner or the use of a non recommended thinner may affect the rheological behavior of the material and its printing characteristics. Please refer to **Table 1**.

Storage

Containers may be stored in a clean, stable environment at room temperature (between 5°C–30°C) with their lids tightly sealed. Storage in high temperature (>30°C) or in freezers (temperature <0°C) is NOT recommended as this could cause irreversible changes in the material.

Safety and Handling

For information on health and safety regulations please refer to the specific product MSDS.

Chart 1
Typical Firing Profile

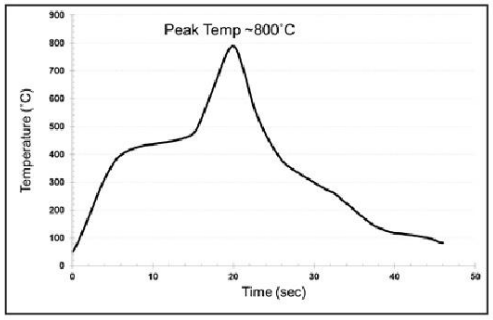

For more information on DuPont™ Solamet® PV36A or other DuPont Microcircuit Materials products, please contact your local representative:

Americas
DuPont Microcircuit Materials
14 T.W. Alexander Drive
Research Triangle Park, NC 27709
USA
Tel. +1800 284-3382 (calls within USA)
Tel. +1919 248 5188 (calls outside USA)

Europe, Middle East & Africa
Du Pont (U.K.) Limited
Coldharbour Lane
Bristol BS16 1QD
U.K.
Tel. +44-117-931-3191

Asia
DuPont Kabushiki Kaisha
MCM Technical Lab
DuPont Electronics Center
KSP R&D B213
2-1, Sakado 3-chom, Takatsu-ku,
Kawasaki-shi, Kanagawa, 213-0012
Japan
Tel +81 44 820 7575
DuPont Taiwan Ltd
45, Hsing-Pont Road,
Taoyuan, 330
Taiwan
Tel. +886-3-377-3616

DuPont China Holding Co. Ltd
Bldg 11, 399 Keyuan Rd., Zhangji Hi-Tech Park,
Pudong New District, Shanghai 201203
China
Tel. +86-21-6386-6366 ext.2202

DuPont Korea Inc.
3-5th Floor, Asia tower #726,
Yeoksam-dong, Gangnam-gu
Seoul 135-719, Korea
Tel. +82-10-6385-5399

E. I. DuPont India Private Limited
7th Floor, Tower C, DLF Cyber Greens,
Sector-25A, DLF City, Phase-III,
Gurgaon 122 002 Haryana, India
Tel. +91-124-4091818

Du Pont Company (Singapore) Pte Ltd
1 HarbourFront Place, #11-01
HarbourFront Tower One,
Singapore 098633
Tel. +65-6586-3022

http://mcm.dupont.com
http://photovoltaics.dupont.com

K-27812 01/14